
Article:
Niu, Shuangxia, Wang, Sigao and Zhao, Xing orcid.org/0000-0003-4000-0446 (2022) Overview of Stator Slot-opening Permanent Magnet Machines. IEEE Transactions on Transportation Electrification. ISSN 2332-7782

https://doi.org/10.1109/TTE.2022.3198438

Overview of Stator Slot-opening Permanent Magnet Machines

Shuangxia Niu, Sigao Wang*, and Xing Zhao

***Abstract*—In the past few decades, the stator permanent magnet (PM) machines have attracted much research attention because of their reliable rotor structure, high power density, wide speed range, and strong fault-tolerant ability. Among the recently proposed stator PM machine topologies, the stator slot-opening PM (SS-PM) machines are becoming increasingly popular because of their higher stator space utilization and robust rotor structure. According to the SS-PM magnetization direction, the SS-PM machines can be classified into three categories, namely, the tangentially magnetized stator slot-opening PM (TMSS-PM) machines, the radially magnetized stator slot-opening PM (RMSS-PM) machines, and the compound magnetized stator slot-opening PM (CMSS-PM) machines. The associated working principle and electromagnetic performance of different SS-PM machines can be diverse. Therefore, this paper gives an overview of SS-PM machines in terms of machine design, working principle, and machine performance. A qualitative performance evaluation and comparative study of SS-PM machines are presented, and the future challenges and potential opportunities in the SS-PM machine design are discussed.**

***Index Terms*—Finite element methods, permanent magnet machines, stator slot-opening PM.**

I. Introduction

The first permanent magnet (PM) machine can be traced back to 1821 when Michael Faraday discovered the electromagnetic rotations, and it is also dubbed as the first electric motor [1]. However, the electromagnetic performance of PM machines was dissatisfactory due to the poor magnetization ability of PM in the early stage [2]. In recent decades, the development of PM material brings with growing maximum magnetic energy product, which greatly improves the machine efficiency and power density, and has aroused increasing research interest in PM machines [3]. The PM machines can be classified into two types according to the location of PMs, namely, rotor PM machines, and stator PM machines. For rotor PM machines, there exist various non-negligible problems. For example, the centrifugal force limits the rotation speed, and also the associated output power of rotor PM machines [4]. Besides, due to the poor heat dissipation condition, the temperature rise in the rotor may cause demagnetization risk of the rotor PM [5].

To overcome these problems, stator PM machines have attracted much research interest as a promising alternative of rotor PM

This work was supported by the National Natural Science Foundation of China under Project 52077187 and in part by the Research Grant Council of the Hong Kong Government under Project PolyU 152143/18E and PolyU 152109/20E.

machines in recent decades. The first stator PM machine was proposed by Rauch and Johnson in 1955 [6]. The subsequent stator PM topologies, such as switched reluctance machine [7-10], doubly salient PM machine [11-14], flux switching PM machine [15-18], flux reversal PM machine [19-23], etc., inherit some merits of the first stator PM machine. These machines have a robust rotor structure as the rotor consists of silicon steel only. Besides, the PMs are assigned at the stator side of the machine, and the PMs do not suffer from centrifugal force and poor thermal condition, so higher rotation speed can be applied [24].

With the development of stator PM machines, the machines with stator slot-opening PM (SS-PM) design have become increasingly popular [25]. The area of slot-opening is relatively small in the practical designs of stator PM machines, especially in closed slot and semi-closed slot. The slot wedges are usually assigned at slot opening to hold the winding in place. However, although slot wedge is indispensable in terms of machine assembly, it has little contribution to the electromagnetic performance of the machine. Therefore, replacing slot wedge with PMs can improve the space utilization of the machine.

However, the design purpose of SS-PM machines and associated machine working principles can be diverse in different topologies. Some topologies adopt stator slot PMs as an extra excitation source to produce effective open-circuit back EMF and torque production [26]. In some topologies, the SS PMs are mainly used to relieve the stator core saturation to obtain an improved overload capability [27]. It is desired to give a comprehensive review of SS-PM machines in terms of machine topology and working principle.

In this paper, the SS-PM machines are classified into three categories according to the magnetization direction of SS PM, namely, tangential magnetized stator slot-opening PM (TMSS-PM) machines, radial magnetized stator slot-opening PM (RMSS-PM) machines, and compound magnetized stator slot-opening PM (CMSS-PM) machines. Then, for each category, the working principle is briefly introduced based on typical example structures. The further development of machine topology and electromagnetic performance are discussed. Finally, a comprehensive quantitative comparative study among typical machine examples is conducted. And the advantages and drawbacks of all machine categories are summarized based on the comparison results.

II. Machine Classification

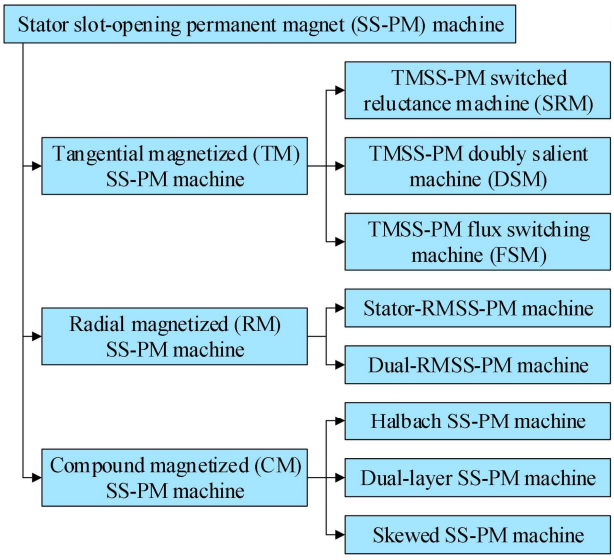

Fig. 1. Classification of SS-PM machines.

In recent decades, there are various SS-PM machines proposed. In this paper, these machines are classified as shown in Fig. 1. According to the magnetization direction of SS PM, there are three types of machines. The magnetization direction of PMs is along the circumferential direction in the TMSS-PM machine, the structure of which has been applied in switched reluctance machine (SRM) [28], doubly salient machine (DSM) [29], and flux switching machine (FSM) [30]. The magnetization direction of PMs is along the radial direction for RMSS-PM machines. There are also other compound PM magnetization direction arrangements, such as dual-layer PM, skewed PM, and Halbach array design. The following three sections discuss the above-mentioned three categories in detail, respectively.

III. Tangential magnetized SS-PM machines

A. TMSS-PM SRM

A traditional switch reluctance machine (SRM), as shown in Fig. 2(a), relies on the varying reluctance under different rotor pole positions to produce the reluctance torque [31]. It enjoys advantages like simple structure, low cost, and high reliability, due to that the stator and rotor consist of the iron core only [32]. SRMs are widely used in various industrial applications like electric vehicles (EV) [33] and aerospace [34]. Unlike the synchronous reluctance machines, SRM is driven by a unipolar trapezoidal wave current, as shown in Fig. 3. The armature windings are alternately switched on or off so that the salient pole rotor can be pulled to the corresponding position, and the reluctance torque is generated resultantly.

In traditional SRMs, the BH working range of the stator core is limited within only one quadrant because of the unipolar armature current [33]. It causes saturation in the stator core, especially at high current conditions, which limits the torque capacity of traditional SRMs. To overcome this problem, the idea of employing TMSS-PM design in SRMs was firstly proposed in [35-36], as

shown in Fig. 2(b). The basic flux path of the TMSS-PM SRM is presented in Fig. 4, where Φ_{SPM} and Φ_0 represent the flux from TMSS PMs and armature current, respectively. It should be noticed that the direction of Φ_0 is intentionally designed to be opposite with Φ_{SPM} in the stator core to relieve the core saturation. As shown in Fig. 5, before the introduction of Φ_{PM}, Φ_0 is biased in the stator core, hence suffering from easy saturation at high current conditions. The flux can be shifted away from the saturation line with the TMSS-PM design. As is shown in Fig. 6, the BH working range of the stator core is no longer limited within the first quadrant with the introduction of TMSS PMs. Thus, a higher current can be applied and the torque capability can be raised accordingly. It is validated by a comparative study between the traditional SRM and the TMSS-PM SRM, which shows that the TMSS-PM SRM has higher static torque versus different rotor pole positions and higher efficiency than traditional HRM under different speeds [35]. Besides, the introduction of TMSS PMs avoids the change in the reluctance of the magnetic circuit. Therefore, the TMSS-PM SRM still inherits the good flux regulation capability from traditional SRM topology.

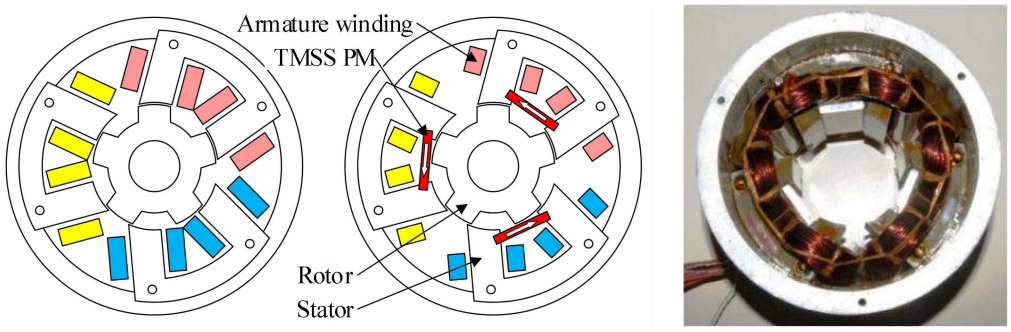

(a) (b) (c)

Fig. 2. The typical topologies for SRM. (a) Without TMSS PM [31]. (b) With TMSS PM [35]. (c) Prototype [35].

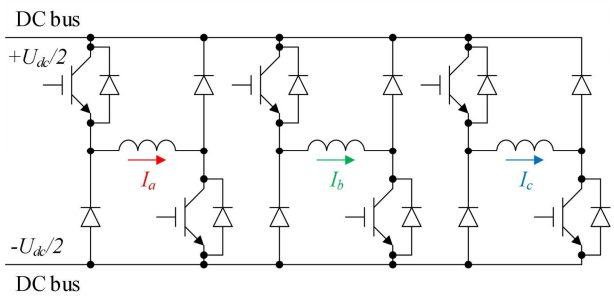

Fig. 3. The driving circuit of SRM.

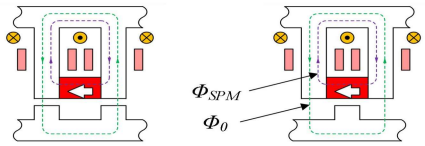

(a) (b)

Fig. 4. The basic flux path of TMSS-PM SRM. (a) Aligned position. (b) Unaligned position.

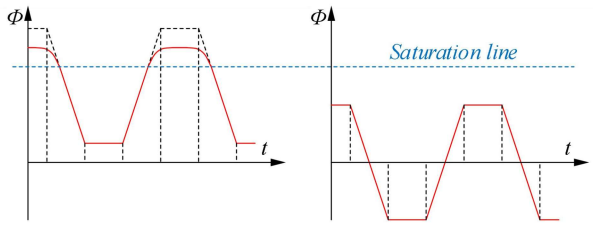

(a) (b)

Fig. 5. The schematic coil flux. (a) without TMSS PM. (b) With TMSS PM.

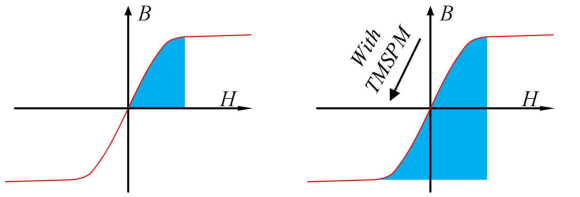

(a) (b)

Fig. 6. The BH working range of SRM. (a) Without TMSS PM. (b) With TMSS PM.

The latter development in the topology of TMSS-PM SRM is presented as shown in Fig.7-Fig.10. In Fig. 7(a), a modular stator hybrid excited SRM is proposed, and various slot pole combinations are discussed in [37]. The torque production of TMSS-SRM is 34% higher than the counterpart without TMSS-PM design. In Fig. 7(b), to better utilize the space at the rotor yoke, the topology is extended to the two-stator structure. The salient pole rotor is replaced by a group of iron segments, and the space inside the rotor is utilized by another stator. Although it is reported that the torque production is improved compared with single-stator structure [38], it brings more challenges in mechanical manufacturing.

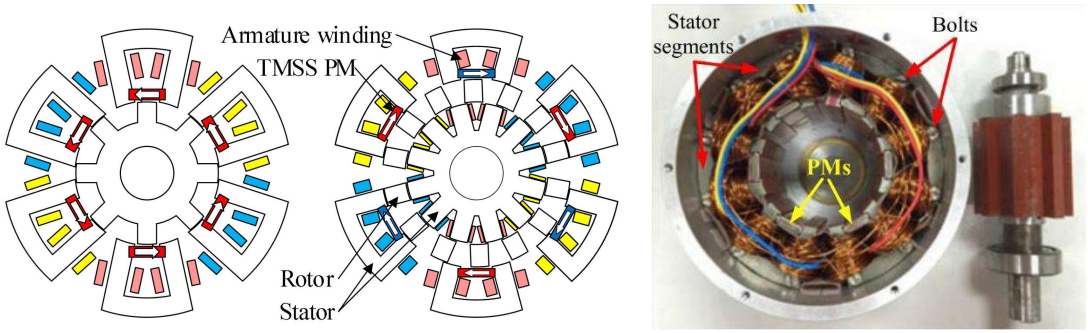

(a) (b) (c)

Fig. 7. The modular reluctance machine with TMSS PMs. (a) The typical single stator topology [37]. (b) The double stator topology [38]. (c) Prototype [37].

In the previous typical examples, all the stator core is separated and embedded in a light alloy enclosure. Another structure is shown in Fig. 8, in which the stator core is not separated so that a flux path for the low-pole-pair field can be provided. It is reported that the torque production is raised by 25% under the current density of 13A/mm^2 when compared with SRM without TMSS PM [39].

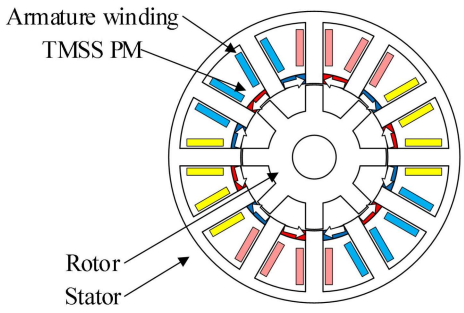

Fig. 8. The topology with joint stator core [39].

In [40-41], further innovation with the multi-tooth structure is developed, as shown in Fig. 9. The slot number can be designed to be much smaller than the rotor pole number with the introduction of the multi-tooth design. Under the same rotor pole number, the higher tooth split number is, the lower slot number can be designed so that the armature winding can be easier to be installed. However, one problem for SRMs with a high stator tooth split number is that only the neighboring poles of the stator can be relieved by the TMSS PMs. The saturation in stator poles far from PMs is yet to be relieved if the stator tooth is split into more than two poles. Another topology innovation lies in the rotor core design. In [42], the TMSS PMs are assigned at SRM with a segmental rotor as shown in Fig. 10. Further research points out that there is a 29% increase in average torque with the TMSS-PM design [43].

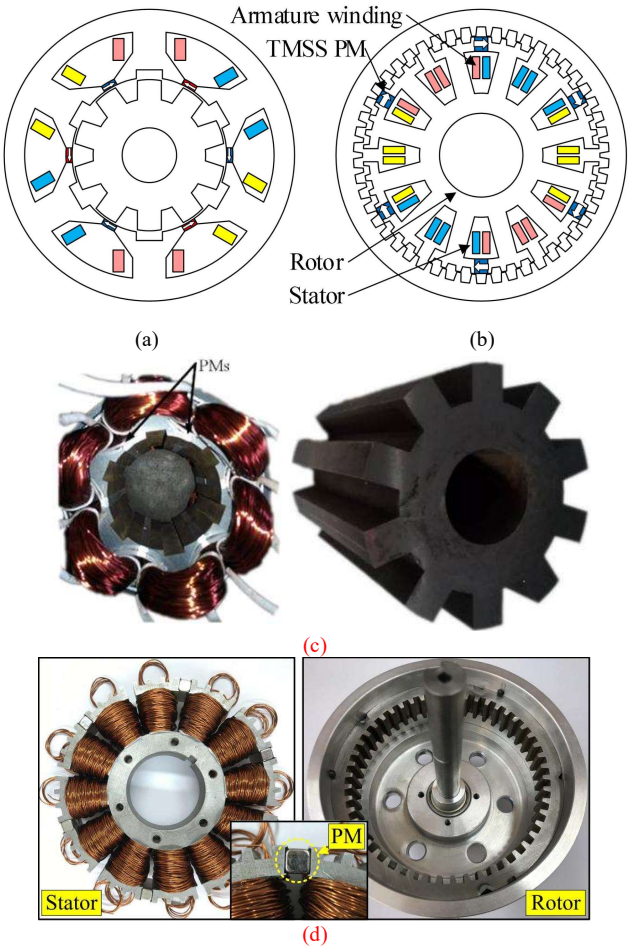

Fig. 9. The Multiple teeth topologies in TMSS-PM SRM. (a) The stator tooth split into two poles [40]. (b) The stator tooth split into four poles [41]. (c) Prototype [40]. (d) Prototype [41].

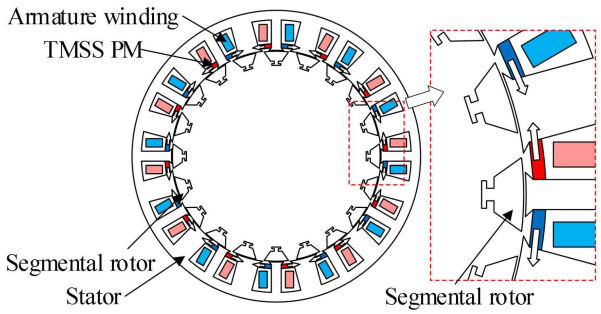

Fig. 10. The TMSS-PM SRM with segmental rotor topology [42].

B. TMSS-PM DSM

Despite various above-mentioned merits of SRM, SRMs suffer from relatively high torque ripple due to the half-cycle-conducting operation principle [44]. The double salient machine (DSM) is an alternative stator PM machine design to overcome this problem because some comparative studies have pointed out that the DSM has higher torque performance than SRM [45-46]. And therefore, TMSS-PM DSM design has attracted a lot of research interests [47-48].

The TMSS-PM DSM can be classified into the hybrid-excited type and PM-excited type according to different excitation sources. The hybrid-excited type has better flux regulation ability because of flexible excitation current, while the PM-excited type has higher torque density because PM has higher excitation ability than current. A detailed discussion of the two types is presented as follows.

1) Hybrid-Excited TMSS-PM DSM

For the hybrid-excited TMSS-PM DSM, in terms of machine topology, the rotor consists of the iron core only and all the stator windings and PMs are designed on the stator side. Hence it has similar mechanical robustness as TMSS-PM SRM. However, different from TMSS-PM SRM, there is one set of independent DC excitation windings in the hybrid-excited TMSS-PM DSM and the waveform of armature current is sinusoidal, rather than trapezoidal wave, which causes the difference in working principle and machine performance between these two kinds of machines.

The basic flux path of a typical hybrid-excited TMSS-PM DSM is presented in Fig. 11, in which Φ_{SPM} and Φ_{DC} represent the flux from TMSS PM and DC current, respectively. The machine relies on the vibration of Φ_{SPM} caused by the reluctance difference in rotor aligned/unaligned position to operate. As shown in Fig. 12, before the introduction of TMSS PMs, the maximum flux density may exceed the saturation point, especially at high current conditions. The flux waveform can be pulled down by the TMSS PMs from ΔB_1 to ΔB_2. Consequently, higher torque capacity can be obtained as the vibration range of ΔB_2 is larger than ΔB_1. Besides, the BH working range can be shifted to another quadrant, which means the stator core saturation effect can be relieved, and a higher DC current can be applied. Besides, with the introduction of TMSS PMs, the good flux regulation capability can be inherited as the magnetic circuit reluctance is not changed by TMSS PMs.

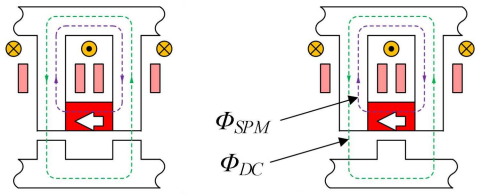

Fig. 11. The basic flux path of hybrid-excited TMSS-PM DSM. (a) Aligned position. (b) Unaligned position.

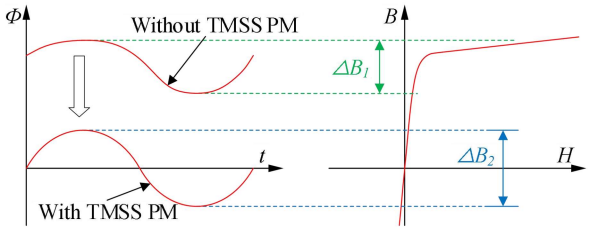

Fig. 12. The change of BH working range of TMSS-PM DSM.

There are various TMSS-PM DSM topologies proposed in recent decades, and the development in topology is discussed as follows. The variable flux machine (VFM) is one of the promising candidates in the DSM family [49], and a typical example for TMSS-PM DSM is presented as in Fig. 13(a) [50]. The DC excitation coils and the corresponding TMSS-PMs are assigned in every stator slot with alternate polarity. A comparative study shows that compared with the traditional VFM without TMSS PM, the torque capacity can be improved by 18% under the same copper loss [51].

Further study on slot/pole combination of the typical VFM is investigated in [52]. It is reported that the slot/pole combination of 12/14 and 12/10 have higher average torque than that of 12/11 and 12/13, but also have higher torque ripple because of the third harmonics [52].

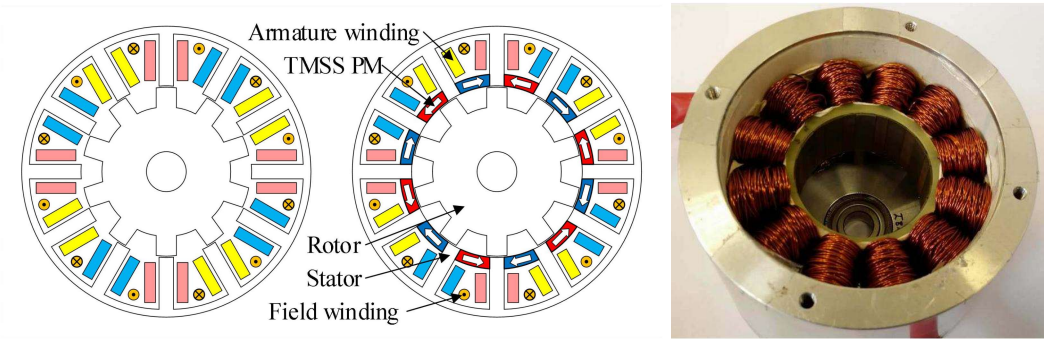

Fig. 13. The topologies of DSM. (a) Without TMSS PM [50]. (b) With TMSS PM [51]. (c) Prototype [51].

There are other machine topologies with different DC coils and TMSS PM arrangements. As shown in Fig. 14, the machine topology with TMSS PM and DC coils assigned in every other slot is presented [53]. The copper loss from DC current and the use of PM material can be reduced nearly by half, compared with typical TMSS-PM DSM. But the equivalent magnetomotive force (MMF) in every stator tooth is also reduced. Therefore, the back EMF and associated torque production are reduced, accordingly. Further development in topology design can be found in Fig. 15 [54-55], where the AC and DC coils are arranged in separated slots.

It is reported that compared with the typical VFM with DC coils and TMSS PMs in every slot, it has almost 50% higher average torque, in spite of higher torque ripple and larger iron losses [56].

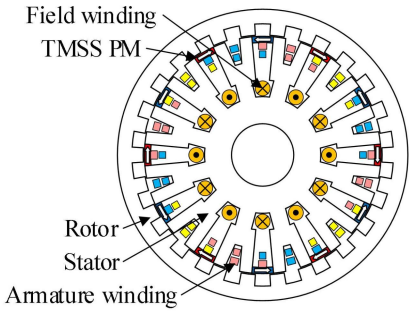

Fig. 14. The TMSS-PM DSM with DC coils across two stator tooth [53].

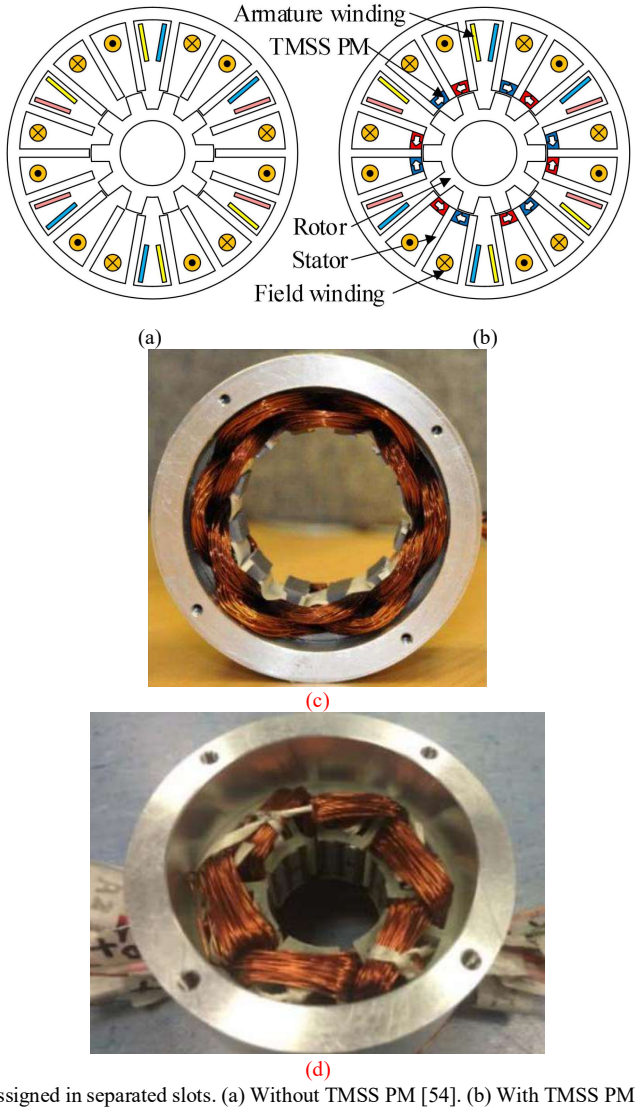

Fig. 15. The DSM with DC and AC coils assigned in separated slots. (a) Without TMSS PM [54]. (b) With TMSS PM [55]. (c) Prototype [54]. (d) Prototype [55].

The TMSS-PM DSM with multi-tooth design is another research topic as it can effectively reduce the stator slot number under the same rotor pole number. It brings relatively lower copper loss and lower manufacturing difficulty. A special winding configuration for multi-tooth TMSS-PM DSM is proposed and analyzed in [57], and a typical example of the special winding

configuration is presented in Fig. 16(a) [58]. It can minimize the torque ripple with the reconstructed magnetic paths. Similar to other TMSS-PM DSMs, in the multi-tooth design, the TMSS PMs can also bring higher torque production due to the relieving-DC-saturation effect. Compared with the traditional DSM structures [59], the hybrid-excited TMSS-PM DSM has higher torque production under the same overall size and current density, especially at high load current conditions. It is reported that the torque production is 82.5% higher under the current density of 6A/mm^2 and 134% higher under the current density of 24A/mm^2[58]. However, one drawback of the combination of TMSS-PM and multi-tooth design is that only the neighboring poles of the stator can be relieved, while the other stator poles in the middle are not relieved.

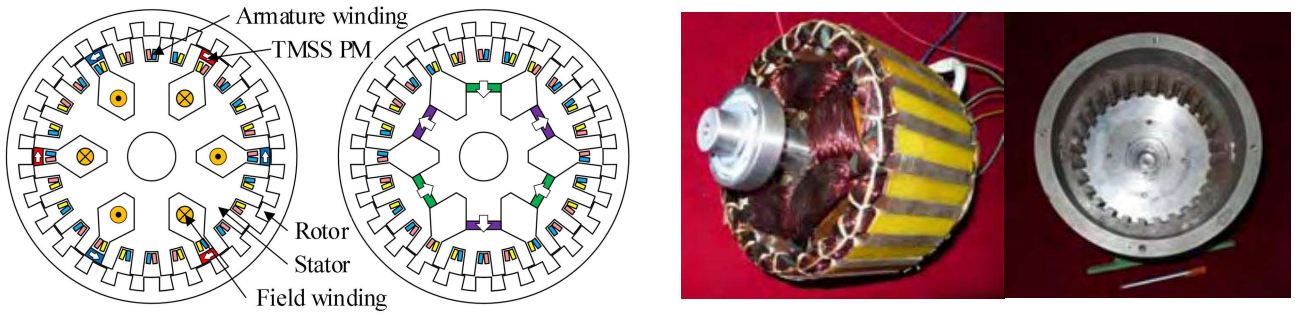

(a) (b) (c)

Fig. 16. The multi-tooth topology of DSM (a) With TMSS PM [58]. (b) Without TMSS PM [59]. (c) Prototype [59].

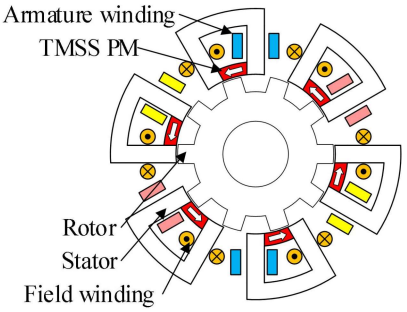

(a)

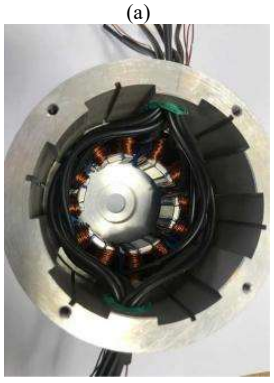

(b)

Fig. 17. The TMSS-PM DSM with modular topology [62]. (a) Topology. (b) Prototype.

Modular design is another popular research topic, in which the stator yoke is separated to facilitate manufacturing, assembling, and transportation [60-61]. A typical example of modular TMSS-PM DSM is proposed in [62] and shown in Fig. 17. The flux changes in the horseshoe-shaped stator core with the changing rotor positions, based on which the modular TMSS-PM DSM can

work. However, one drawback of this topology is that the leakage flux when the rotor is at the unaligned position with the stator tooth leads to a large torque ripple. To solve this problem, the torque ripple of modular TMSS-PM DSM can be reduced when combined with complementary rotor topology. One typical example with complementary rotor topology is presented in [63], where TMSS PMs are used to a DSM with a claw-shaped modular stator and complementary magnetic circuit, which is shown in Fig. 18. The complementary rotor provides a commutative flux path for the DC field so that the leakage flux and associated torque ripple can be reduced. The torque ripple is reduced from 15.49% to 7.05% with the complementary magnetic circuit. Besides, the relieve-DC-saturation effect in the stator core improves overload capability by 41.6% at rated current excitation [63]. The complementary topology is further applied on linear machines. In [64], TMSS PMs are used in a tubular linear motor with the complementary magnetic circuit, as shown in Fig. 19. The detent force can be suppressed to as low as 2.65% thanks to the complementary structure and eliminated leakage flux. The overload capacity is improved by TMSS PMs with stator core saturation relieved.

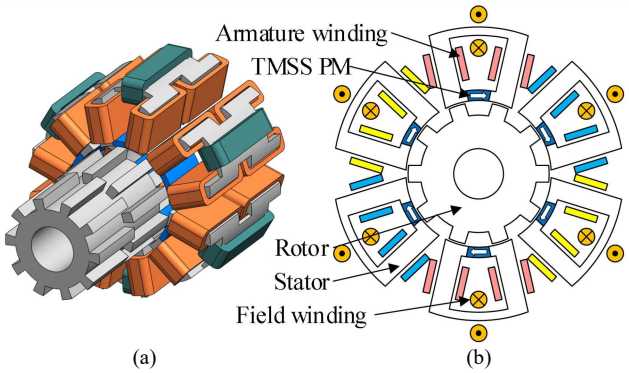

Fig. 18. The Configuration of claw-shaped modular stator TMSS-PM DSM [63]. (a) The three-dimensional model. (b) The cross section.

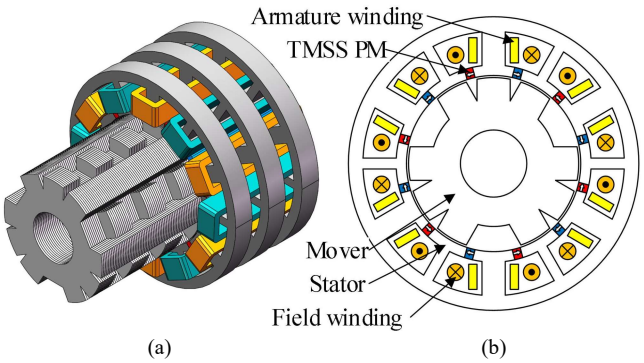

Fig. 19. The tubular motor with TMSS PM and complementary magnetic circuit [64]. (a) The three-dimensional model. (b) The cross section.

In the above-discussed TMSS-PM DSM topologies, the rotor consists of the iron core only. However, the PM can be designed between the rotor teeth to form consequent pole topology to further improve the torque density. As the introduction of rotor PM does not change the reluctance of the rotor magnetic circuit, the working principle of TMSS PMs and DC coils is kept unchanged. In [65-66], the TMSS-PM machine is used together with rotor PMs, as is shown in Fig. 20. A comparative study between two machines with/without rotor PM is presented in [67]. With the extra torque production from rotor PMs, the machine has higher

torque but a relatively smaller speed range.

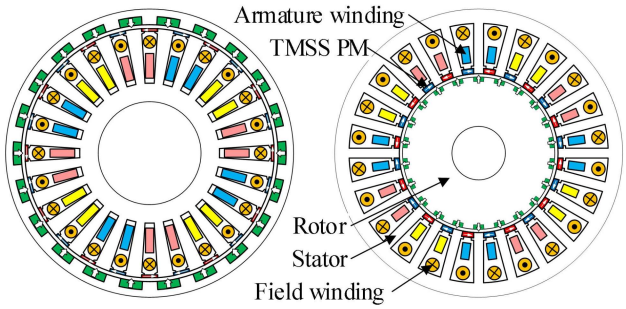

(a) (b)

Fig. 20. The TMSS-PM topologies with rotor PM. (a) The outer rotor structure [65]. (b) The inner rotor structure [66].

The above machines employ DC coils for excitation, but the copper loss can be reduced when AC and DC coils are combined into one armature winding with the zero-sequence current, which is also called DC-biased current. One typical example machine topology is presented in Fig. 21. When the armature current is sinusoidal with a biased current, the torque density can be enhanced by about 20% under relatively high current density [68].

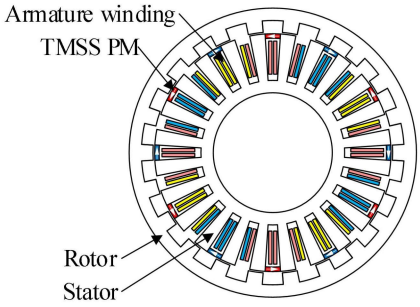

Fig. 21. The typical TMSS-PM DSM with zero-sequence current [68].

There are various driving circuits and associated control strategies proposed for the DC-biased machines in recent decades. The driving circuit [69-73] and the control diagram [71-72][74-75] are presented in Fig. 22 - Fig. 23, respectively. In [69], there are two three-phase armature windings with opposite DC-biased current. The neutral points of two groups of three-phase winding are connected to provide a path for zero-sequence current. In [70], the open-winding circuit is used and connected to two individual three-phase inverters. The DC biased current flows from one converter to the other through the armature winding.

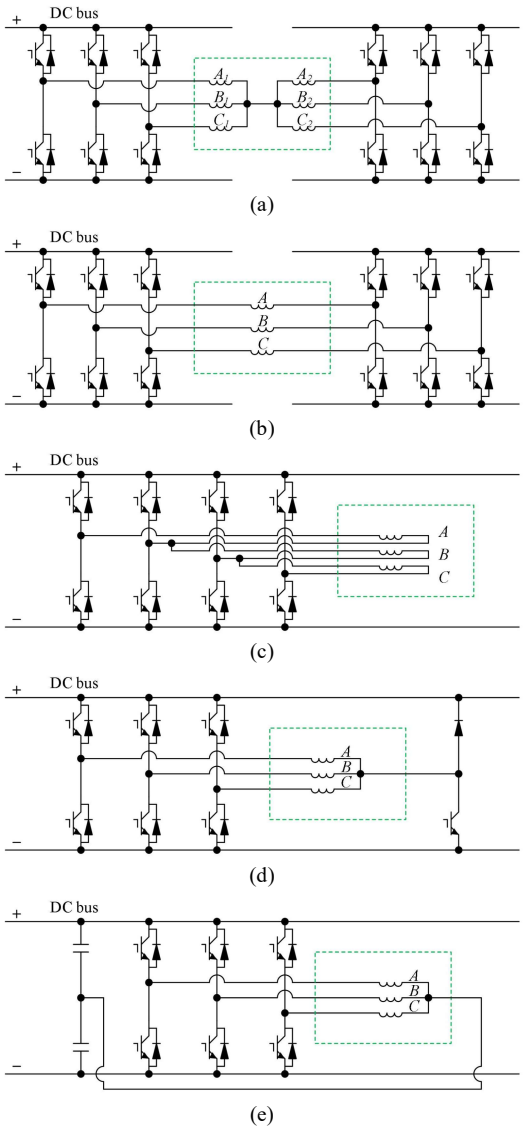

Fig. 22. Driving circuits of TMSS-PM machines with DC-biased current. (a) Dual three-phase configuration [69]. (b) Open-winding configuration [70]. (c) Three-phase four-leg configuration [71]. (d) Four-leg configuration with asymmetrical neutral leg [72]. (e) Configuration with neutral point connected to the DC bus midpoint [73].

To reduce the number of power devices, in [71], a three-phase four-leg configuration is proposed. Compared with the traditional open-winding topology, it reduces the power devices by one-third. Further, in [72], another three-phase four-leg configuration is proposed. An asymmetrical neutral leg is used, through which the DC biased current can flow in both directions. And the power device number is further reduced. In [73], the neutral point of three-phase winding is connected to the midpoint of the DC bus capacitors through the ground so that a circuit path for zero-sequence current can be formed.

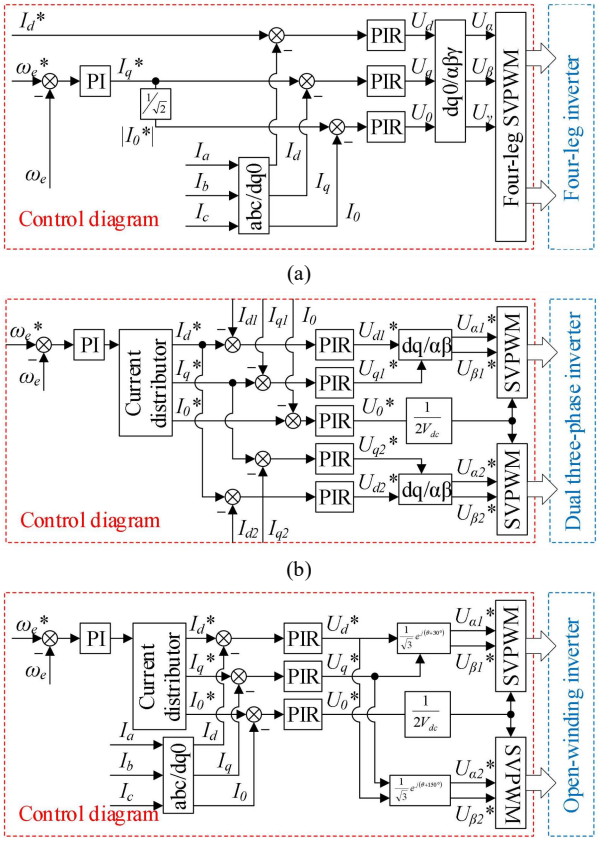

Fig. 23. Control diagram of TMSS-PM machines with DC-biased current. (a) For three-phase four-leg configurations [71-72]. (b) For dual three-phase windings [74-75]. (c) For open winding [74-75].

2) PM-Excited TMSS-PM DSM

The following part gives an introduction to the PM-excited TMSS-PM DSM, whose basic flux path is shown in Fig. 24. Φ_{SPM} and Φ_{YPM} represent the flux form slot-opening PM and yoke PM, respectively. As is shown in Fig. 25, when the rotor is at the aligned position, Φ_{YPM} is at maximum value, but Φ_{SPM} is at the minimum value (in absolute value). When the rotor is at the unaligned position, Φ_{SPM} is at maximum value, but Φ_{YPM} is at minimum value. However, Φ_{SPM} and Φ_{YPM} have opposite directions in the stator tooth. Therefore, Φ_{SPM} is in phase with Φ_{YPM} and both of them can contribute to torque production.

The key topology difference between PM-excited and hybrid-excited TMSS-PM DSM lies in whether the TMSS PM is short-circuited in magnetic flux circuit. For the hybrid-excited TMSS-PM DSM, the TMSS-PM is short-circuited by the stator yoke. Therefore, the torque contribution of TMSS PMs is less significant, especially at low current conditions. By contrast, for the PM-excited TMSS-PM DSM, the TMSS PMs are parallel excited with the yoke PM, and the torque contribution of TMSS PM is significant in both high and low current conditions.

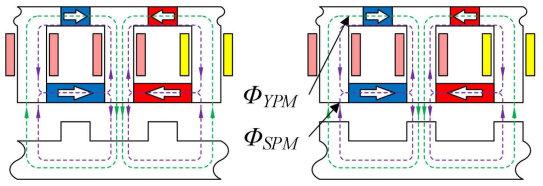

Fig. 24. The basic flux path of PM-excited TMSS-PM DSM. (a) Unaligned position. (b) Aligned position.

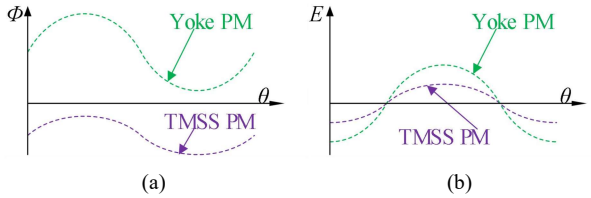

Fig. 25. Schematic coil flux and back EMF of PM-excited TMSS-PM DSM. (a) Coil flux. (b) Back EMF.

Based on the above basic topology, the typical PM-excited TMSS-PM DSM structure can be generated as shown in Fig. 26 [76]. The working principle of the typical PM-excited TMSS-PM DSM structure can also be explained from the perspective of air-gap flux modulation theory. As is shown in Fig. 24, it is obvious that the yoke PM and the TMSS PM have the same air-gap magnetomotive force (MMF) waveform. Thus the introduction of TMSS PM can improve the amplitude of air-gap MMF of the DSM. The air gap flux density from the stator PM (B_{PM}) can be expressed as:

$$B_{PM}(\theta,t)=\sum_{i=1}^{+\infty}\sum_{j=-\infty}^{+\infty}B_{S(i,j)}cos\left[\left(iN_p+jN_r\right)\theta-jN_r\omega_{me}t\right] \tag{1}$$

where θ is the mechanical angular position, $B_{PM}(\theta,t)$ is the air gap flux from TMSS PM and yoke PM, ω_{me} is the rotor mechanical speed, $B_{S(i,j)}$ is the amplitude of air-gap field harmonic, N_r is the rotor teeth number, and the N_p is the pole pair number of the excitation field. In this typical structure, N_p should satisfy:

$$N_p=N_s/2 \tag{2}$$

where N_s is the stator slot number. Based on (1), the order number, and rotation speed of each air gap field harmonics can be summarized as:

$$\begin{cases}\theta_{(i,j)}=\left|iN_p+jN_r\right| \\ \omega_{(i,j)}=\dfrac{jN_r\omega_{me}}{\left|iN_p+jN_r\right|}\end{cases} \tag{3}$$

To obtain a higher gearing ratio, the main working harmonic is selected as the case when $i=1$, $j=-1$. The other harmonics with $j=\pm1$ are also working harmonics, but their contribution is relatively smaller. Therefore, the armature winding pole pair number (P_{aw}) should be designed according to the main working harmonic order as the following equation:

$$P_{aw}=\left|N_{slot}-N_r\right| \tag{4}$$

However, the typical structure suffers from a high torque ripple due to the leakage flux when the rotor is at the unaligned position. To solve this problem, the complementary rotor structure can be combined in PM-excited DSM as shown in Fig. 27 [77-78]. The flux from all PMs can either go through the outer or inner air gap so that the leakage flux can be largely reduced.

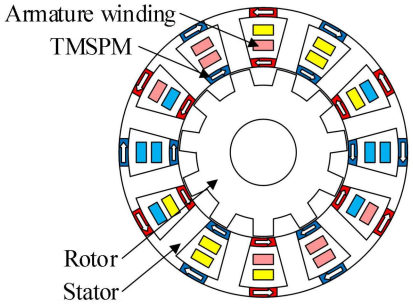

Fig. 26. The typical topology of the PM-excited TMSS-PM DSM.[76]

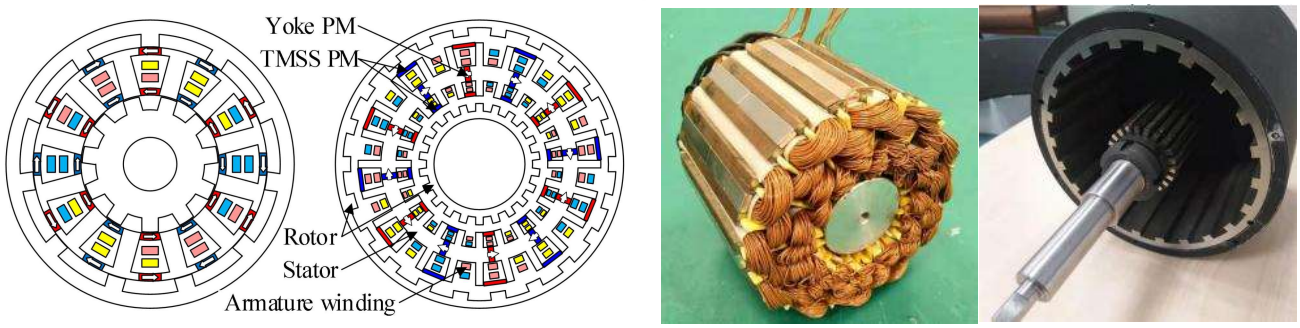

(a) (b) (c)

Fig. 27. The PM-excited TMSS-PM DSMs with complementary rotor structure. (a) Without yoke PM [77]. (b) With yoke PM [78]. (c) Prototype [78].

C. *TMSS-PM FSM*

TMSS-PM flux switching machine (FSM) is an alternate solution as the phase flux-linkage waveform is bipolar [79]. The FSM inherits various advantages from the stator PM machine. For example, due to the simplicity and robustness of the rotor structure, a very high rotor speed can be applied. Moreover, as all the windings and PMs are assigned at the stator side, most of the heat produced by copper and iron loss can be effectively dissipated [80]. Therefore, FSM has wide industrial applications, such as wind power generation [81-82], railway traction [83-85], electric vehicle, and hybrid electric vehicle [86-89].

The basic flux path of the FSM with TMSS PMs is presented in Fig. 28, where Φ_{SPM} and Φ_0 are the fluxes from TMSS PMs and field excitation coil (FEC) current, respectively [90]. The TMSS-PM FSM can be considered as a traditional FSM with PM partly replaced by a series of FEC slots. The cost from PM material can be reduced and the flux regulation ability can be improved. Φ_{SPM} and Φ_0 are combined under flux enhancing region, while they have reverse polarity under flux weakening region. Therefore, the flux can be easily regulated by the flexible FEC current and a wide speed range can be achieved.

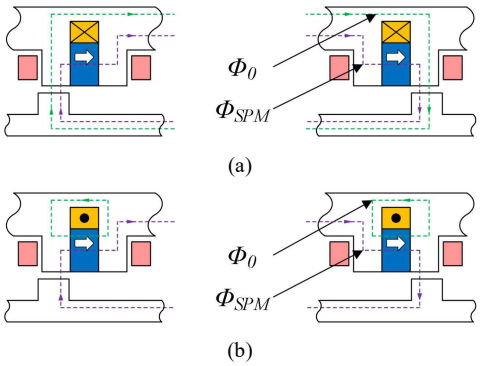

Fig. 28. The Basic flux path of TMSS-PM FSM [90]. (a) Flux enhancing. (b) Flux weakening.

Based on the basic flux path, the two typical structures of TMSS-PM FSM are presented in Fig. 29 [91-92]. The recent research in the topology of TMSS-PM FSM is discussed as follows.

In [93], the comparison between TMSS-PM FSMs with/without iron flux bridge is investigated. The high excitation current utilization ratio can be achieved with the iron flux bridge, while a high PM utilization ratio can be achieved without the iron flux bridge. This is because the iron flux can provide the flux from FEC current with a low reluctance flux path. However, if the iron flux bridge is designed to be too wide, the flux of TMSS PM would be shorted-circuited in the magnetic circuit. Therefore, the trade-off should be considered when designing the iron flux bridge.

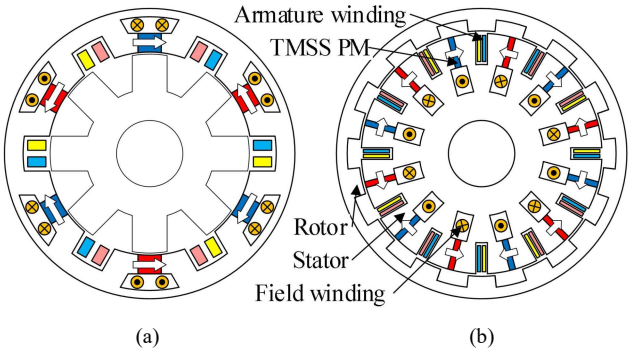

Fig. 29. The typical structure of TMSS-PM FSM. (a) The inner rotor structure [91]. (b) The outer rotor structure [92].

In terms of TMSS-PM FSMs with iron flux bridge, in [94], the influence of topology arrangement of the iron bridge and FEC coils is investigated. Compared with the FSM without the iron flux bridge, the introduction of the iron flux bridge can effectively increase the field coil excitation and associated flux regulation ability at the cost of slightly reduced torque [94]. As is shown in Fig. 30, there are three types of iron flux bridge arrangements of FSM. Under the same bridge width, the excitation level in Fig. 30(c) is the lowest as the leakage goes through both bridges. The highest torque capacity can be achieved when the iron bridge is assigned over the FEC slot among the three iron bridge topologies.

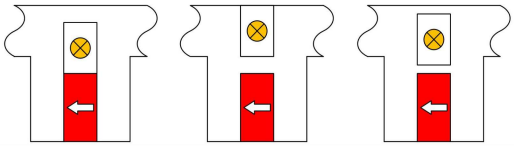

Fig. 30. The different iron flux bridge arrangement topologies [94]. (a) Over the FEC slot. (b) Below the FEC slot. (c) In both sides.

In terms of TMSS-PM FSM without iron flux bridge, in [95], a comparative study about the relative location of FEC coils and PM is conducted. As is shown in Fig. 31, there are three types of topology arrangements of FEC coils. The PM-middle topology has the lowest flux regulation ability as the flux in armature winding is enhanced by positive field current (PFC) but weakened by negative field current (NFC). The PM-top machine can only realize the flux weakening function because of the saturation in the stator core. The PM-bottom topology has the highest magnet utilization and the strongest flux-regulation ability [95].

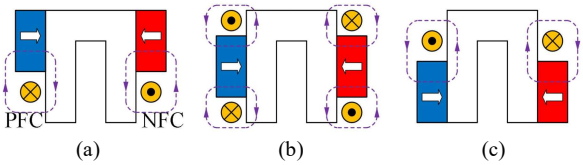

Fig. 31. The Different PM arrangement topologies [95]. (a) PM-top. (b) PM-middle. (c) PM-bottom.

To reduce the cogging torque and torque ripple of TMSS-PM FSM is another hot research topic [96-97]. There are various design methods for cogging torque minimization, such as rotor skewing, variable rotor arcs, and segmented rotor [98-100]. In [101], several methods are investigated and compared, it is concluded that the rotor skewing method has the best overall electromagnetic performance among all methods.

IV. Radially Magnetized SS-PM Machines

This section gives a review of the recent topology development of RMSS-PM machines. The magnetization direction of RMSS PM is along the radial direction, and therefore the flux from RMSS PM can go through the air gap directly. Under flux modulation effect, the flux from RMSS PMs can generate the air gap field harmonics with the interaction between the MMF of RMSS PM and rotor permeance. And some air gap field harmonics can be utilized as the working harmonics.

From the location of PM arrangement, the RMSS-PM machines can be divided into stator-PM and dual-PM machines. For the stator-PM design, the rotor consists of the iron core only, which brings low cost, and high mechanical robustness. For the dual-PM design, the PMs are assigned at both stator and rotor sides. The rotor PM can provide additional torque production. However, the rotor PM brings more severe saturation in the neighboring teeth and suffers from poor heat dissipation condition than rotor PM. The following parts discuss the two types of machine topology, respectively.

A. Stator-RMSS-PM machine

The basic flux path of an RMSS-PM machine with stator-PM design is presented in Fig. 32, where N_s, N_r, and P_{aw} are the stator

slot number, rotor teeth number, and winding pole pair number, respectively. The air gap flux from stator PM (B_{SPM}) can be expressed as:

$$B_{SPM}(\theta,t)=\sum_{n=1}^{+\infty}\sum_{k=-\infty}^{+\infty}B_{S(n,k)}cos\left[(nN_s+kN_r)\theta-kN_r\omega_{me}t\right] \tag{5}$$

where θ represents the mechanical angular position, $B_{SPM}(\theta,t)$ is the air gap flux from stator PM, ω_{me} is the rotor mechanical speed. Based on (5), the order number, and rotation speed of each air gap field harmonics can be summarized as:

$$\begin{cases}\theta_{(n,k)}=\left|nN_s+kN_r\right| \\ \omega_{(n,k)}=\dfrac{kN_r\omega_{me}}{\left|nN_s+kN_r\right|}\end{cases} \tag{6}$$

The open-circuit back EMF ($E_{(n,k)}$) produced by each field harmonics can be expressed as:

$$E_{(n,k)}=\frac{4.44DLT_{ph}}{60}\left(B_{(n,k)}k_{w(n,k)}\omega_{(n,k)}\right) \tag{7}$$

where D is the diameter of the air gap circumference, L is the stack length, T_{ph} is the number of turns, and $k_{w(n,k)}$ is the corresponding winding factor. The torque production is in direct proportion to the back EMF if stator core saturation is ignored. In order to get a higher torque capacity, a higher rotation speed ($\omega_{(n,k)}$) is required. According to (6), $\omega_{(n,k)}$ is inversely proportional to the harmonic order. Therefore, the main working harmonic is selected as the case when $n=1$, $k=-1$. The other harmonics with $k=\pm1$ are also working harmonics, but their contribution is relatively smaller. Therefore, P_{aw} should be designed according to the main working harmonic order as the following equation:

$$P_{aw}=\left|N_{slot}-N_r\right| \tag{8}$$

To give a more intuitive understanding of the flux modulation effect, the schematic flux distribution of a typical RMSS-PM machine is presented in Fig. 33. When the rotor tooth is at the aligned position with the stator tooth, the PM is short-circuited in the neighboring teeth. When the rotor tooth is at the unaligned position, the flux of RMSS PM is upwards through the rotor tooth, and the magnetic path is completed through the tooth at the aligned position.

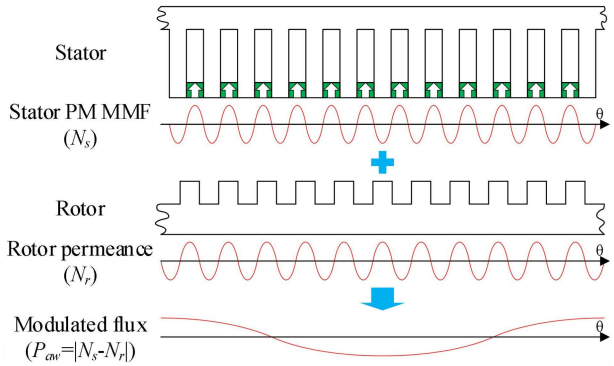

Fig. 32. The Basic modulation principle of RMSS-PM machine.

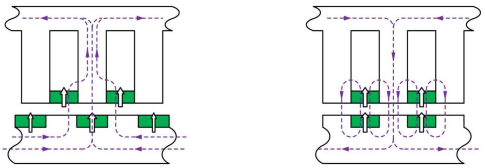

Fig. 33. The schematic flux path. (a) Unaligned position. (b) Aligned position.

Based on the above basic flux path, a typical stator-PM machine with RMSS PMs is presented in Fig. 34 [102]. In this case, N_s=12 and N_r=11, and therefore, P_{aw} should be designed as 1. In Fig. 35, the DC field winding is combined with RMSS PMs, so that the flux can be easily regulated by the flexible DC current. Although the DC current and RMSS PMs have different working harmonic orders in the air gap, both can be utilized by the single-layer winding configuration [103].

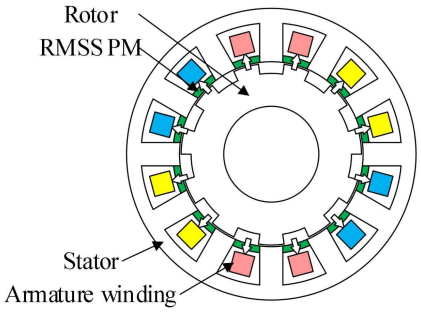

Fig. 34. The typical stator-PM machine with RMSS PM [102].

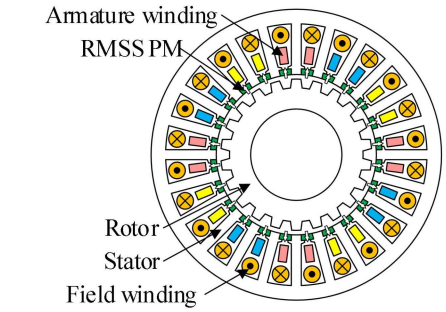

(a)

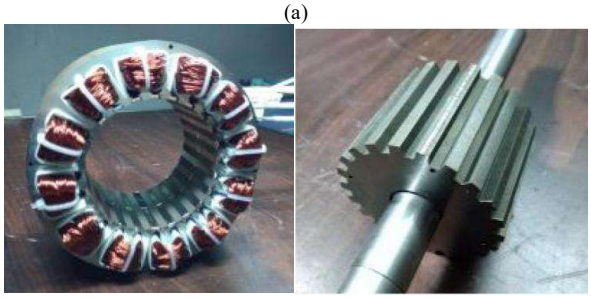

(b)

Fig. 35. The hybrid-excited structure with RMSS PM [103]. (a) Topology. (b) Prototype.

B. Dual-RMSS-PM machine

The name "dual-PM" refers to the topology when the PMs are assigned on both stator and rotor sides. The dual-RMSS-PM machine structure is developed from the stator-RMSS-PM topology by assigning a group of additional PM at rotor slots. The

torque capacity can be improved because the air gap flux modulated by the rotor PM has the same order as those of RMSS PMs. The air gap flux from rotor PM (B_{RPM}) can be expressed as:

$$B_{RPM}(\theta,t)=\sum_{p=1}^{+\infty}\sum_{q=-\infty}^{+\infty}B_{S(p,q)}cos\left[\left(qN_s+pN_r\right)\theta-pN_r\omega_{me}t\right] \tag{9}$$

Eq. (9) has a very similar form with (5), and therefore, the main working harmonic of rotor PMs is the same as that of RMSS PMs. The main working harmonic is corresponding to the case when p=1 and q=-1. The schematic flux distribution of a typical dual-PM machine is presented in Fig. 36. When the rotor tooth is at the unaligned position with the stator tooth, the flux from rotor PMs and RMSS PMs are upwards and combined through the rotor tooth. When the rotor tooth is at the aligned position, the RMSS PMs and rotor PMs are short-circuited in the neighboring teeth.

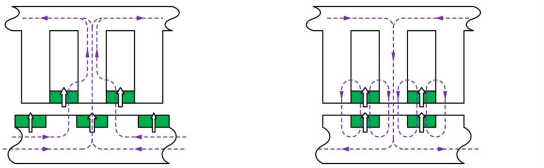

(a) (b)

Fig. 36. The schematic flux path of dual RMSS-PM Machine. (a) Unaligned position. (b) Aligned position.

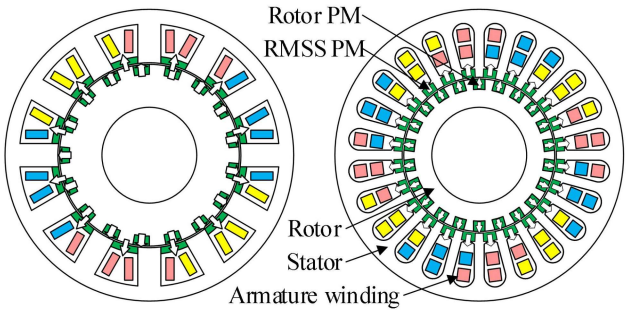

(a) (b)

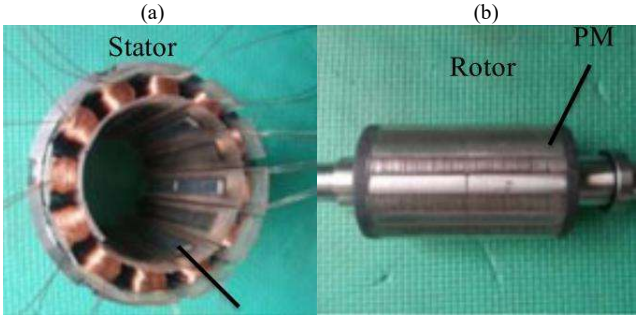

(c)

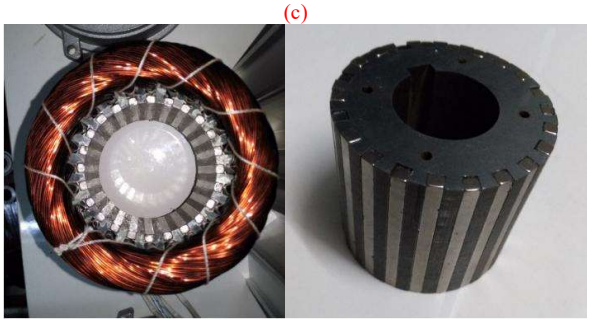

(d)

Fig. 37. The typical dual-PM structure. (a) Without pole shoe [104]. (b) With pole shoes [105]. (c) Prototype [104]. (d) Prototype [105].

Based on the above basic working principle, a typical dual-PM machine is presented in Fig. 37(a) [104]. The torque can be generated by both RMSS PMs and rotor PMs. One drawback of this topology is that the flux path of RMSS PMs has a relatively high reluctance because of the low permeability in the marked area in Fig. 38(a). To solve this problem, as is shown in Fig. 38(b), the pole shoe can be used in the RMSS-PM machine. In [105], a typical example is shown in Fig. 37(b). However, another drawback of this topology still remains that the end winding is relatively long due to the distributed winding configuration. According to (6), $\omega_{(n,k)}$ is in direct proportional to gearing ratio (k_{Gear}), which is defined as:

$$k_{Gear} = \frac{N_r}{P_{aw}} \tag{10}$$

To obtain higher k_{Gear} and associated torque capacity, N_r is usually designed to be much higher than P_{aw}. It implies that N_s is designed to be much higher than P_{aw}, which leads to a long end coil. To overcome this problem, the multi-tooth design can be used to reduce the slot number and end coil length under the same k_{Gear}.

$$P_{aw} = \left| n_{spl} N_s - N_r \right| \tag{11}$$

where n_{spl} is the split number of stator teeth. The stator tooth is split into several parts so that relatively low N_s can be obtained. A typical structure for multi-tooth design is presented in Fig. 39 [106]. Each stator tooth is split into 3 parts, and thus, there are only 9 stator slots with a 27-pole-pair rotor. The concentrated winding configuration can be adopted so that the end coil length is reduced. However, the torque production is lower than single-tooth design due to relatively lower winding factor.

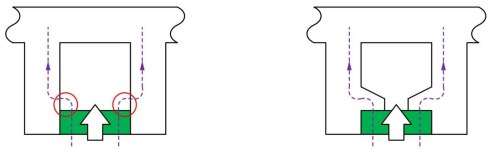

Fig. 38. Flux path. (a) Without pole shoe. (b) With pole shoes.

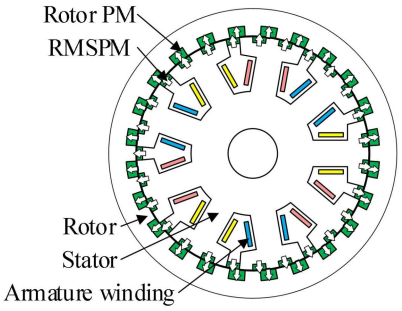

Fig. 39. The typical multi-tooth RMSS-PM machine [106].

V. Compound Magnetized SS-PM Machines

Apart from TMSS PMs and RMSS PMs, there are other SPM machines with different magnetization designs in recent decades, such as the Halbach array design, dual-layer PM design, and skewed PM design. The following parts give a review of these compound PM magnetized SS-PM machines.

A. Halbach SS-PM machine

The basic flux path of the machine with Halbach array structure is presented in Fig. 40(a). The Halbach array arrangement can be seen as an RMSS PM replaced by two TMSS PMs on both sides. The two TMSS PMs in a slot opening have opposite directions so that the flux can be concentrated to the stator tooth. It has a similar principle with the stator-PM machine with RMSS PMs in the last Section from the perspective of air gap flux modulation. Therefore, they share the same armature winding design. Replacing the RMSS PM with the Halbach PM array does not change the reluctance in the magnetic circuit, and therefore, the rotor PM can be used and combined with the Halbach array as presented in Fig. 40(b).

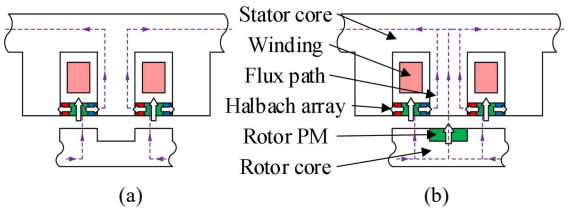

Fig. 40. The basic flux path of two typical machines with Halbach array PM. (a) The stator-PM structure. (b) The dual-PM structure.

Based on the basic flux path, two typical topologies with Halbach array PM are presented in Fig. 41 [107-108]. They can be seen as two Vernier machines whose RMSS PMs are partly replaced by the TMSS PMs. In terms of the comparison between the two typical examples, the additional rotor PM can contribute to the torque production under flux modulation effect as discussed in the last part. Therefore, in spite of the higher difficulty in manufacturing, a higher torque density can be obtained.

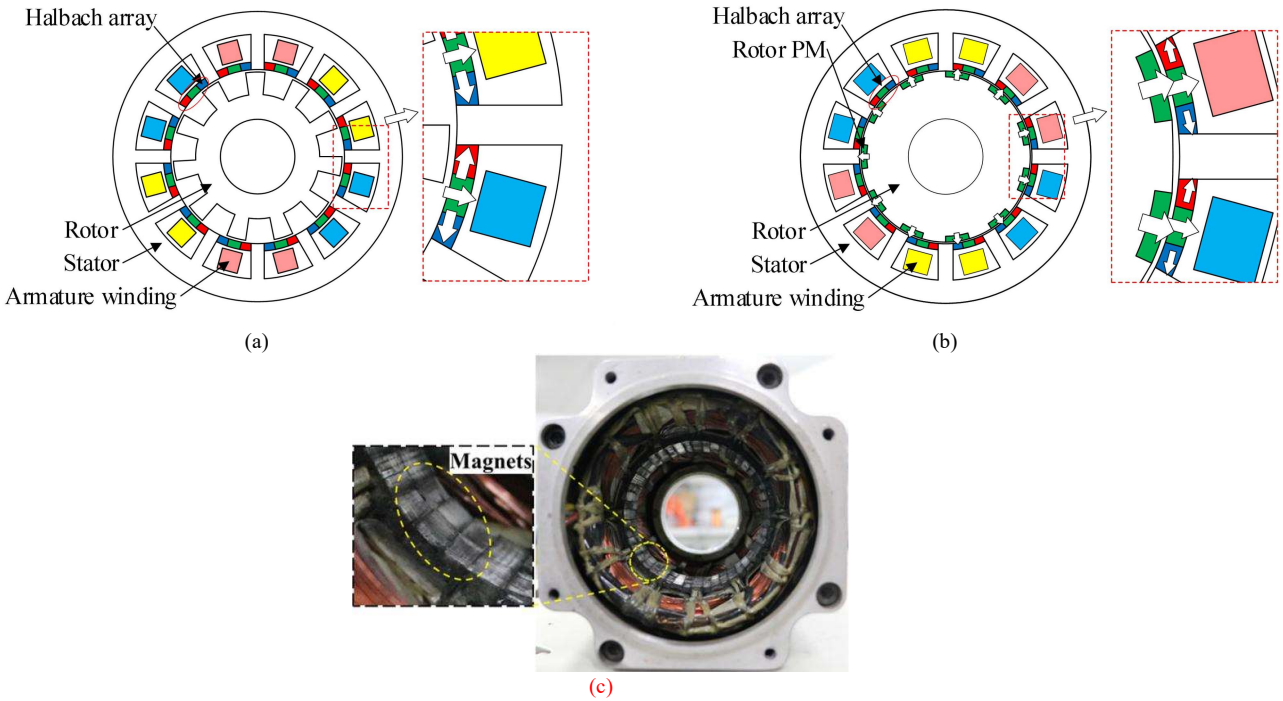

Fig. 41. The typical SPM machines with Halbach array. (a) The stator-PM structure [107]. (b) The dual-PM structure [108]. (c) Prototype [107].

B. Dual-layer SS-PM and skewed SS-PM machine

As analyzed in previous sections, the RMSS PMs can be used to generate the air gap field working harmonics and associated torque production under flux modulation effect. The TMSS PMs can be used to relieve the stator saturation when combined with DC excitation current so that a wide flux regulation range can be achieved. Therefore, when both TMSS PMs and RMSS PMs are used, torque and flux regulation ability promotion can be achieved.

Based on the above idea, the dual-layer PM structure, as another promising design for SPM machines, is presented in Fig. 42. Both TMSS PMs and RMSS PMs are used, and the torque promotion can be achieved by RMSS PMs under flux modulation effect, while flux regulation ability can be improved by TMSS PMs with relieving-DC-saturation effect [109]. However, the two-layer PM structure brings difficulty in manufacture. To solve this problem, in [110], the dual-layer TMSS PMs and RMSS PMs are replaced by skewed PM. As shown in Fig. 43, the skewed PM has both tangential and radial magnetization components, and therefore it has a similar working principle with the dual-layer PM structure, but lower mechanical manufacturing difficulty.

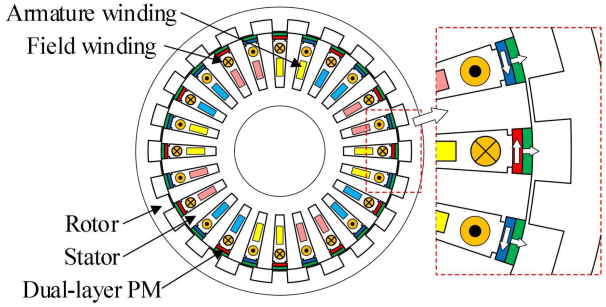

Fig. 42. The typical dual-layer PM machine [109].

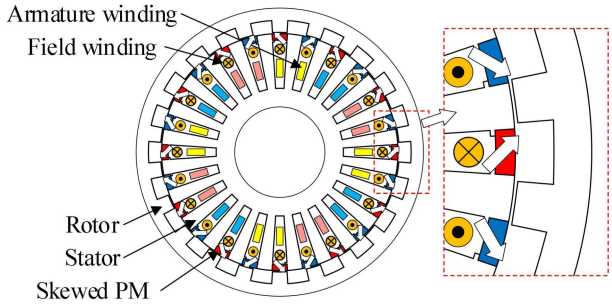

Fig. 43. The typical skewed magnetized PM machine [110].

VI. Comprehensive comparative study

A. Machine optimization

To this date, no paper has been published comparing the machine performance of the above SS-PM machines. To provide a comprehensive comparison among the above SS-PM machine categories, a comparative study is carried out in this paper. For each SS-PM machine category, the topology with corresponding basic flux path is selected as the typical structure for comparison, which are listed in Fig. 44-45. For a fair comparison, the maximum diameter, stack length, air gap length, estimated slot filling factor, rated copper loss, slot number, and rotor pole number (shown in Table 1). The other dimensional parameters are optimized by the Genetic Algorithm with the aim of maximizing average rated torque and minimizing the torque ripple.

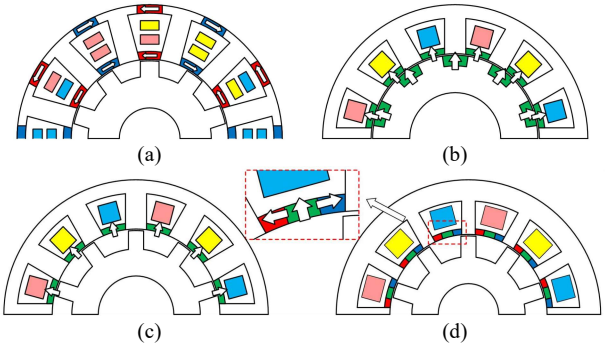

Fig. 44. The PM-excited machines. (a) TMSS-PM DSM.[76] (b) Dual-RMSS-PM machine [105]. (c) Stator-RMSS-PM machine [102]. (d) Halbach SS-PM machine [107].

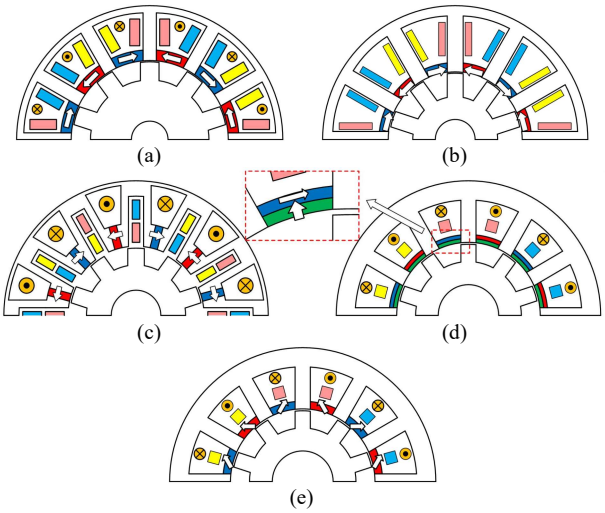

Fig. 45. The hybrid-excited machines. (a) TMSS-PM DSM [51]. (b) TMSS-PM SRM [39]. (c) TMSS-PM FSM [91]. (d) Dual-layer SS-PM machine [109]. (e) Skewed SS-PM machine [110].

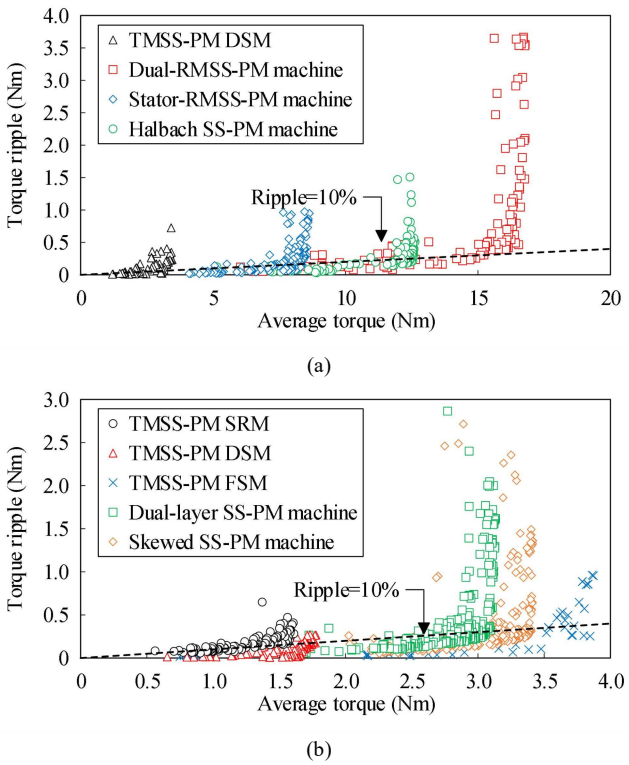

Fig. 46. The Pareto frontier of each generation in Genetic Algorithm. (a) PM-excited machines. (b) Hybrid-excited machines.

Table 1
Common design parameters.

Item	Unit	Value
Maximum diameter	mm	100
Stack length	mm	50
Air gap length,	mm	0.5
Estimated slot filling factor	/	0.5
Rated copper loss	W	50
Slot number	/	12
Rotor pole number	/	10
Speed	rpm	2000

B. Machine performance evaluation

The detailed performances of the optimal machines are presented in this part. The Pareto frontier of multi-objective optimization in every generation is presented in Fig. 46 for each machine. Taking the torque ripple less than 10% as the essential condition, the design with the highest average torque is selected as the optimal design. Based on the optimal designs, the machine performance of each model is summarized in Table 2 and Table 3. In general, the PM-excited machines have relatively poorer flux regulation ability due to the fixed PM excitation. By contrast, the other hybrid-excited machines have relatively better controllability due to the flexible current excitation [111-112]. Therefore, the PM-excited and hybrid-excited machines are discussed separately in the following parts. To give a better comparison between the SS-PM machine and the existing rotor PM machine (IPMs, PMa-SynRMs), the torque densities of IPM and PMa-SynRM are quoted, which are 27.70 and 24.87 kN/m^3, respectively [113-114]. The torque density of different SS-PM machines can be distinct. Some SS-PM machines have relatively low torque density while others have high torque density. The dual-RMSS-PM machine has a higher torque density than the IPM and

PMa-SynRM because the torque of the Dual-RMSS-PM machine is contributed by both SS PM and rotor PM. The Stator-RMSS-PM machine and Halbach SS-PM machine have comparable torque density with the IPM and PMa-SynRM. However, a relatively higher rotor speed can be applied in the Stator-RMSS-PM machine and Halbach SS-PM machine because the rotor consists of the iron core only. Therefore, they are very promising candidates for high power density applications.

Table 2
Electromagnetic performances of PM-excited SS-PM machines

Topology	TMSS-PM DSM	Stator-RMSS-PM machine	Dual-RMSS-PM machine	Halbach SS-PM machine
Torque density (kNm/m^3)	8.71	21.85	42.68	32.14
Torque ripple (%)	10.26	9.90	8.92	4.06
PM volume (m^3)	3.07×10^{-5}	2.22×10^{-5}	3.62×10^{-5}	4.31×10^{-5}
Torque per PM usage (kNm/m^3)	111.53	387.31	463.42	292.69
Iron loss (W)	6.10	48.18	53.40	45.81
Copper loss (W)	50	50	50	50
power factor	0.839	0.429	0.709	0.647
Efficiency (%)	92.74	94.82	97.14	96.50

Table 3
Electromagnetic performances of hybrid-excited SS-PM machines

Topology	TMSS-PM SRM	TMSS-PM DSM	TMSS-PM FSM	Dual-layer SS-PM machine	Skewed SS-PM machine
Torque density (kNm/m^3)	3.89	4.52	9.78	7.76	8.65
Torque ripple (%)	10.36	10.09	6.90	9.28	9.97
PM volume (m^3)	1.29×10^{-5}	1.04×10^{-5}	3.12×10^{-5}	2.71×10^{-5}	2.58×10^{-5}
Torque per PM usage (kNm/m^3)	118.49	171.25	123.16	112.55	131.80
Iron loss (W)	31.10	16.17	20.18	15.29	18.37
Copper loss (W)	50	50	50	50	50
power factor	/	0.496	0.935	0.779	0.822
Efficiency (%)	79.77	84.88	91.98	90.72	91.23

1) Rated and maximum short-duration torque-speed characteristics

In this part, the torque-speed characteristics of the 9 machines are predicted. The DC voltage supply of PM-excited machines is set to be 350V while the supply is 100V for hybrid-excited machines. As the induced voltage is in direct proportion to the number of turns of armature winding, for a fair comparison, the number of turns of armature winding is determined by the following equation.

$$N_t = \begin{cases} \dfrac{A_{slot} k_{sff}}{A_{cond}}, \text{for single-layer winding} \\ \dfrac{A_{slot} k_{sff}}{2 A_{cond}}, \text{for double-layer winding} \end{cases}$$

where N_t is the number of turns, A_{slot} is the slot area, k_{sff} is the slot filling factor (estimated to be 0.5), A_{cond} is the conductor area (assumed to be 2 mm^2). The rated copper loss of all machines is set to be 50W, and the copper losses assigned to AC and DC current are set to be the same. For the maximum short-duration condition, according to the design experience, the current density can be tripled. Therefore, the copper loss can be set to be 9 times of rated value if the coil resistance is assumed to be unchanged. Thus, the copper loss of maximum short-duration condition is set to be 450W for all machines. The torque-speed characteristics are presented in Fig. 47 and Fig. 48.

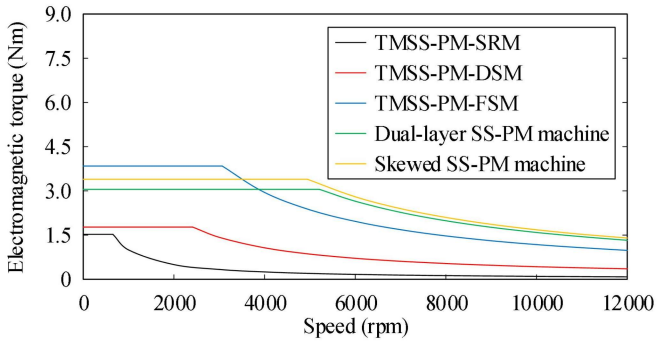

(a)

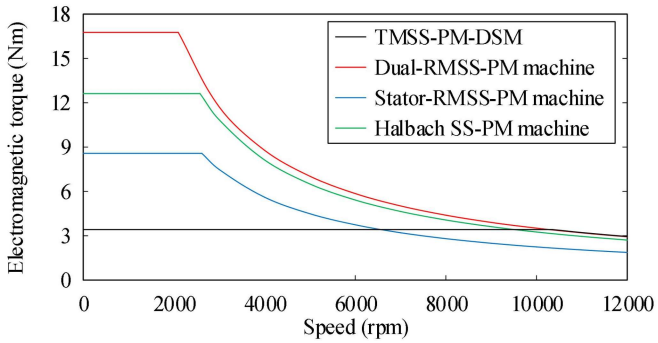

(b)

Fig. 47. Predicted torque-speed characteristics under rated current. (a) Hybrid-excited machines. (b) PM-excited machines.

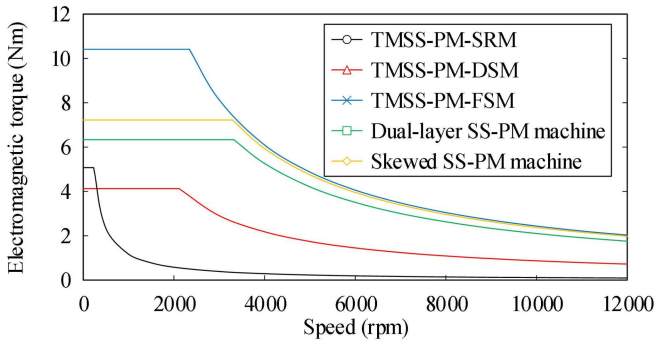

(a)

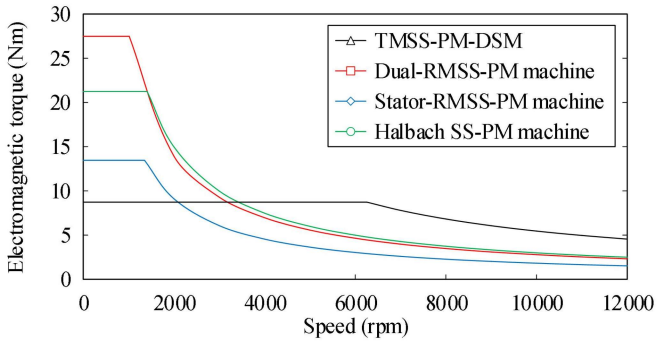

(b)

Fig. 48. Predicted maximum short-duration torque-speed characteristics. (a) Hybrid-excited machines. (b) PM-excited machines.

2) Rated and maximum short-duration torque-speed characteristics

This part evaluates the core loss and the associated efficiency under rated and short-duration conditions. The rated and short-duration copper losses are set to be 50W and 450 W, respectively. As is presented in Fig. 49 and Fig. 50, among the hybrid-excited machines, the TMSS-PM SRM, which is driven by trapezoidal wave current, has much higher core loss than the other machines. This is mainly because the vibration of flux in the stator tooth of TMSS-PM SRM can be very rapid when the driving current is at rising edge or falling edge. In terms of PM-excited machines, the TMSS-PM DSM has a significantly lower core loss than the other machines.

As is presented in Fig. 51 and Fig. 52, generally speaking, the efficiency increases as rotation speed at the low-speed region, but declines as the speed at the high-speed region for most machines. All machines show relatively lower efficiency when the copper loss is increased from the rated value to the short-duration value. In hybrid-excited machines, the TMSS-PM FSM has the highest efficiency over a wide speed range because of the highest torque production. By contrast, the efficiency of TMSS-PM SRM is not satisfying, especially at the high-speed region, because of the lowest torque and high iron loss. In PM-excited machines, TMSS-PM DSM has the lowest efficiency because of the lowest torque production, but the efficiency in the high-speed region exceeds the others because of the lowest iron loss.

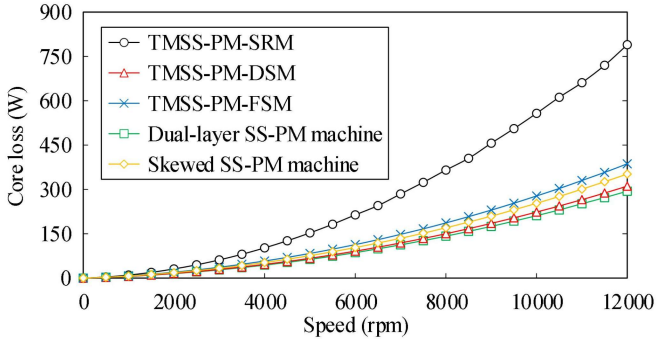

(a)

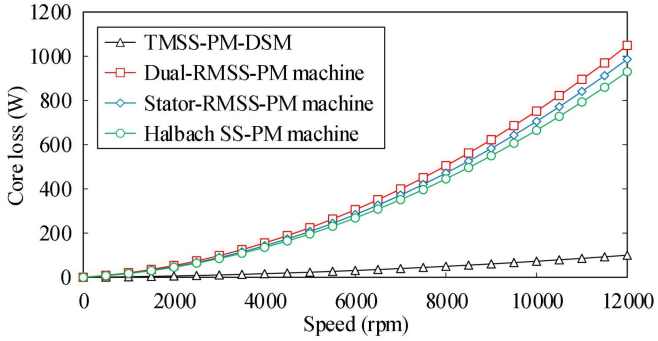

(b)

Fig. 49. Core loss under rated current. (a) Hybrid-excited machines. (b) PM-excited machines.

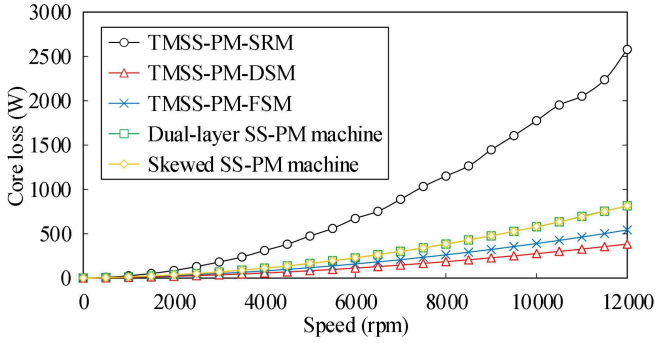

(a)

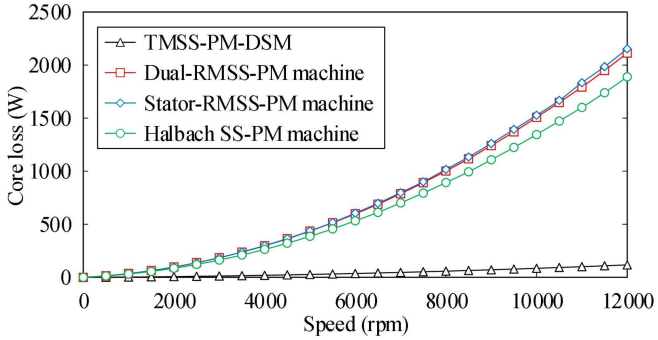

(b)

Fig. 50. Core loss under short-duration current. (a) Hybrid-excited machines. (b) PM-excited machines.

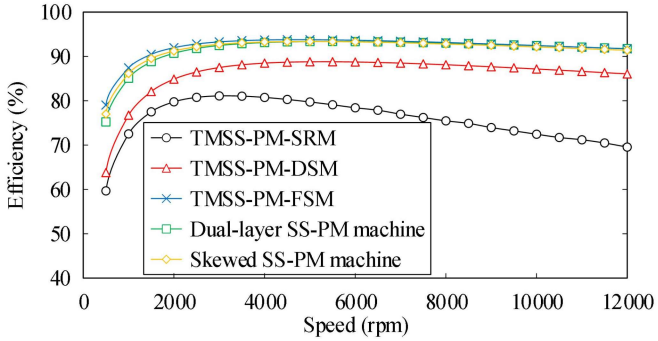

(a)

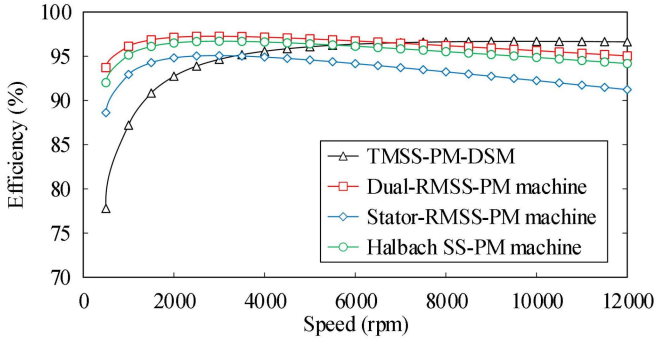

(b)

Fig. 51. Efficiency under rated current. (a) Hybrid-excited machines. (b) PM-excited machines.

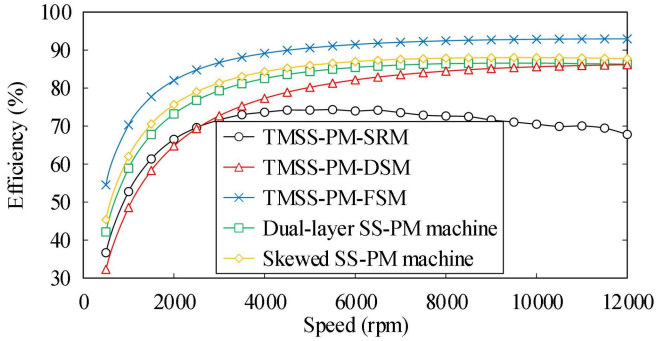

(a)

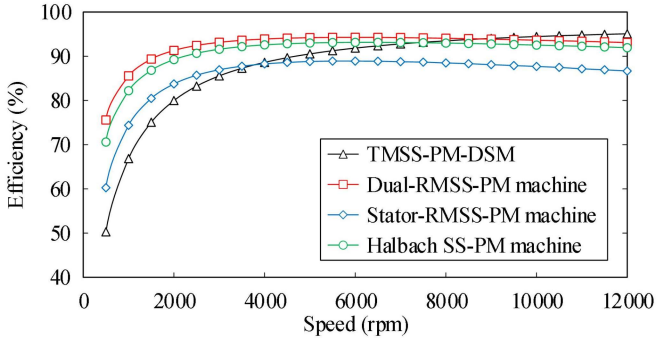

(b)

Fig. 52. Efficiency under short-duration current. (a) Hybrid-excited machines. (b) PM-excited machines.

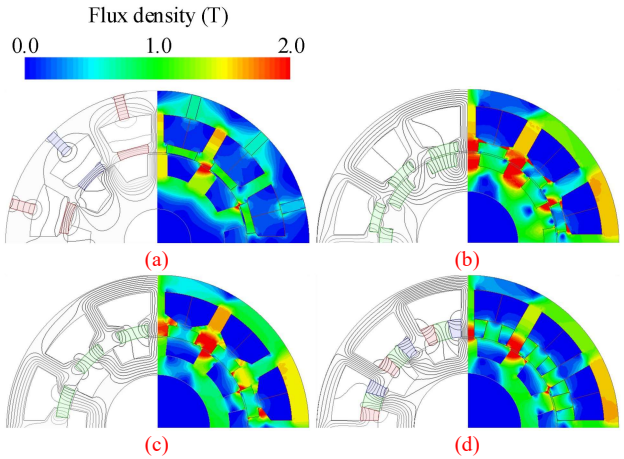

Fig. 53. Flux density distribution at rated current. (a) TMSS-PM DSM. (b) Dual-RMSS-PM machine. (c) Stator-RMSS-PM machine. (d) Halbach SS-PM machine.

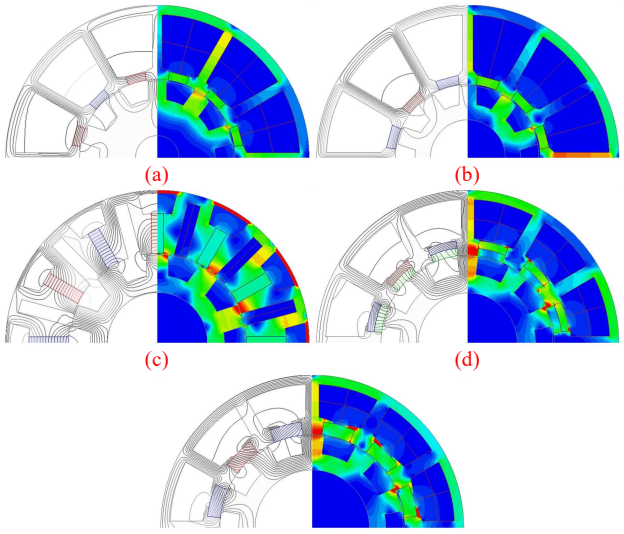

Fig. 54. Flux density distribution under short-duration current. (a) TMSS-PM DSM. (b) TMSS-PM SRM. (c) TMSS-PM FSM. (d) Dual-layer SS-PM machine. (e) Skewed SS-PM machine.

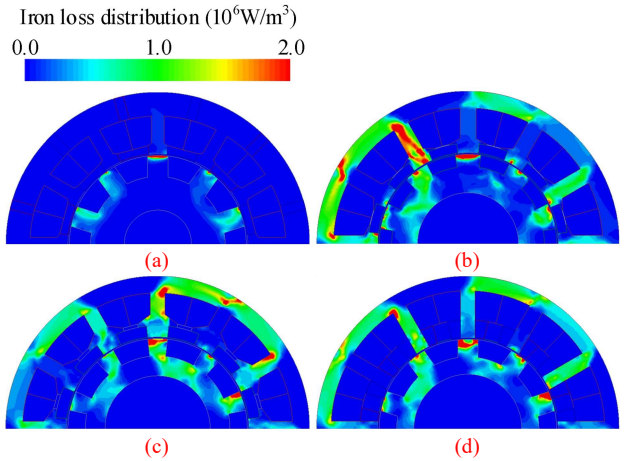

Fig. 55. Iron loss distribution at rated current. (a) TMSS-PM DSM. (b) Dual-RMSS-PM machine. (c) Stator-RMSS-PM machine. (d) Halbach SS-PM machine.

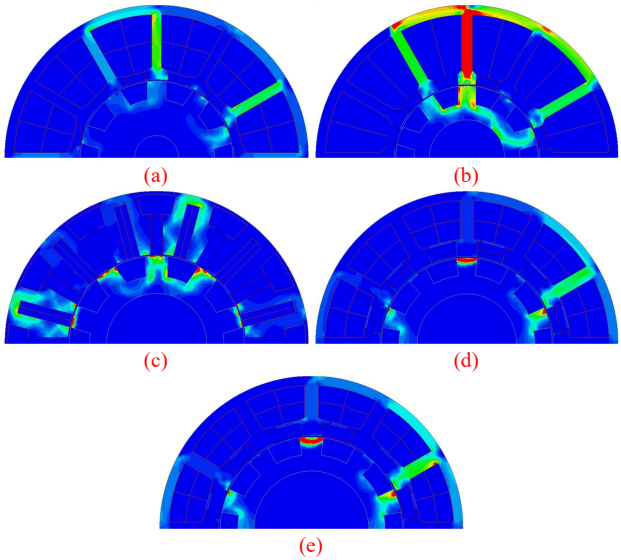

Fig. 56. Iron loss distribution under short-duration current. (a) TMSS-PM DSM [51]. (b) TMSS-PM SRM [39]. (c) TMSS-PM FSM [91]. (d) Dual-layer SS-PM machine [109]. (e) Skewed SS-PM machine [110].

The flux density distribution and the iron loss distribution under rated current of each optimized machine in Fig. 53-Fig.56. As is shown in Tables 2 and 3, it can be found that the dual-RMSS-PM machine, stator-RMSS-PM machine, and Halbach SS-PM machine have significantly higher iron loss than the other machines. This is because they do not have TMSS PM for stator core saturation relieving. By contrast, the stator core of hybrid-excited SS-PM machines can be relieved, and thus lower iron loss can be obtained. However, as is analyzed in Section III, the TMSS PM can only relive the stator core saturation, therefore, the iron loss in the rotor of the TMSS-PM machine is still very high. The iron loss in the stator core is much lower than those of the dual-RMSS-PM machine, stator-RMSS-PM machine, and Halbach SS-PM machine. This can be validated by the iron loss distribution. The only exception is the TMSS-PM SRM (shown in Fig. 56(b)), where the iron loss is still high even with the relieving-DC-saturation effect of TMSS-PM. The reason is that the TMSS-PM SRM is driven by trapezoid current. There is a rapid change in the armature current when the rotor tooth passes by the corresponding stator tooth. Such rapid change in current brings a rapid change in the stator tooth and associated high iron loss. Therefore, a relatively higher iron loss can be found in TMSS-PM SRM.

3) Power factor

The power factors under various excitation conditions for 9 machines are presented in Fig. 57. In hybrid-excited machines, the TMSS-PM FSM has the highest power factor. The TMSS-PM SRM is not included in this part because of its trapezoid driving current. In PM-excited machines, the dual-RMSS-PM machine, stator-RMSS-PM machine, and Halbach SS-PM machine, which are Vernier machines, show a very low power factor under all current excitation. This is a common disadvantage of the Vernier machine.

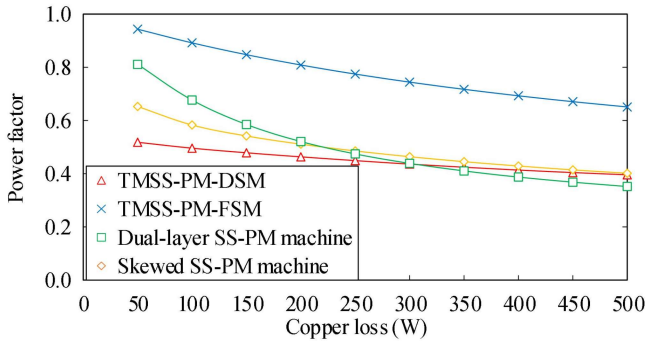

(a)

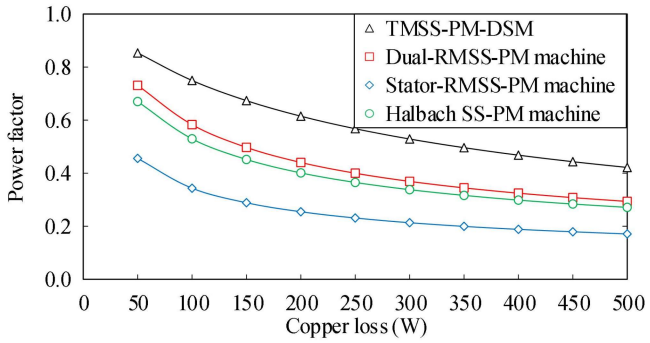

(b)

Fig. 57. Power factor under various current excitation. (a) Hybrid-excited machines. (b) PM-excited machines.

4) Structure robustness and manufacturing complexity

In terms of rotor mechanical robustness, most machines enjoy simple structure and high rotor mechanical robustness because no PMs are assigned on the rotor side. Therefore, a higher rotor speed can be applied to these machines to obtain a high output power. However, there is an exception (Dual-RMSS-PM machine) among these machines. The PMs are designed on both rotor and stator sides, and therefore, the rotor PM suffers from centrifugal force and poor heat dissipation conditions.

In terms of stator core mechanical robustness, the iron core of TMSS-PM DSM is separated into pieces by the yoke PMs. However, in practical manufacturing, the iron core bridges (whose thickness is usually set as 1mm) are usually designed beside the yoke PM to integrate the stator core into one piece. The purpose of integrating the stator cores is to improve the assembly precision of the stator core. However, these narrow iron core bridges lead to leakage flux. Another problem is that the strength of the iron bridge may not be reliable when stamping the iron core. Although using electrical discharge machining (EDM) is another approach to manufacturing the iron core, it may lead to a long time and associated high cost. A similar problem can also be found in TMSS-PM FSM because the iron bridges are also used. Nevertheless, as is reviewed in Part C of Section III, the iron bridges can be designed wider than those of TMSS-PM DSM. Therefore, TMSS-PM FSM has lower manufacturing difficulty than TMSS-PM DSM in terms of stator iron bridges.

As for the stator core of the other machines, they are similar to that of conventional rotor-PM open-slot synchronous machines. The main difference lies in the structure of the slot open. In conventional design, the slot wedges are usually assigned at the slot

opens to hold the windings in place. The slot wedge is indispensable in practical manufacturing but has little contribution in the electromagnetic field. In the SS-PM machines, the SS PMs can be used to replace the slot wedge, which improves the space utilization factor. However, the mechanical strength of PM material is poorer than the conventional slot wedge material (such as plastic), which increase the difficulty in manufacturing.

In terms of PM mechanical robustness, the Halbach SS-PM machine has the highest manufacturing difficulty, because the repelling forces among the PM pieces are very strong. The PM pieces are likely to fracture by the repelling force from the other PM during the manufacturing process. A similar problem can be found in dual-layer SS-PM machines as TMSS PM and RMSS PM are assigned at the same slot open. Using skewed-magnetized SS PM is a good solution to replace the dual-layer SS PM. As for the other RMSS PM machines, although there is repelling force when adhering PMs to the stator core, the repelling force is much lower than that of Halbach SS-PM machines. By contrast, there is little repelling force when adhering PMs of TMSS-PM DSM, TMSS-PM SRM, and TMSS-PM FSM to the stator core, because the SS PM is short-circuited by the stator yoke in the magnetic circuit. Therefore, TMSS-PM DSM, TMSS-PM SRM, and TMSS-PM FSM have the highest PM mechanical robustness.

5) Power-electronics drive and control complexity.

The above-mentioned machines can be classified into three types according to the driving circuit and control method. The first type is the TMSS-PM SRM, where the trapezoid current is applied in the armature winding to drive the machine. Therefore, the TMSS-PM SRM has the simplest control complexity. The second type includes the TMSS-PM DSM, Dual-RMSS-PM machine, Stator-RMSS-PM machine, and Halbach SS-PM machine. The driving circuit and control model is the same as that of conventional rotor-PM machines. The third type includes TMSS-PM DSM, TMSS-PM FSM, Dual-layer SS-PM machine, and skewed SS-PM machine. Apart from the three-phase armature winding, there is an additional DC field winding in these machines. The purpose of the DC field winding is to flexibly regulate the flux of the machine so that a wide speed range can be applied. However, the additional DC field winding increases the complexity of the driving circuit and control methods.

6) Demagnetization risk

The demagnetization risk of the PM material mainly results from high temperature. For the stator-PM machines, as is discussed in Part B of Section VI, it is pointed out in several publications that the stator PMs have the better cooling condition than the rotor PMs. Therefore, the SS PM has a lower demagnetization risk than the conventional rotor-PM machines in terms of thermal condition. Among the above 9 typical SS-PM machines, the dual-RMSS-PM machine may face higher PM temperature under the same cooling condition, because the PMs are designed on both stator and rotor sides.

C. Discussions and summary

1) PM-Excited Machines

For two RMSS-PM machines, the dual-RMSS-PM machine shows almost twice of torque density than the stator-RMSS-PM

machine, due to the additional rotor PM. Besides, the torque per PM usage of the dual-RMSS-PM machine is also higher. This is because the working harmonic of stator PM is the modulated field, while both modulated and unmodulated fields of rotor PM can be used as working harmonics. Therefore, the rotor PM is more efficient than stator PM. The power factor and efficiency are another key concerns for RMSS-PM machines because they largely determine the inverter capacity. Thanks to the additional rotor PM, the dual-RMSS-PM machine enjoys a higher power factor and efficiency. In spite of the above advantages, the introduction of rotor PM may cause other challenges like centrifugal force, assembly difficulty, heat dissipation, and associated demagnetization risk [115-118].

For the Halbach SS-PM machine, the Halbach array can be regarded as the RMSS PM partly replaced by two TMSS PMs. Therefore, the Halbach SS-PM machine has a similar machine structure and modulation principle with the stator-RMSS-PM machine. The Halbach SS-PM machine has higher torque density, power factor, and efficiency than the stator-RMSS-PM machine because the flux is concentrated to the stator core. However, the torque per PM usage is reduced with the Halbach array. And it brings other problems like manufacturing difficulty and relatively lower mechanical reliability [119-120].

The above two RMSS-PM machines and Halbach SS-PM machine are all Vernier machines. Therefore, the power factors are unsatisfactory, which is a common problem for Vernier machines [121-123]. By contrast, TMSS-PM DSM has a higher power factor. Besides, the relatively lower ending winding length of TMSS-PM DSM also brings lower copper loss under the same current density. The main demerit of TMSS-PM DSM is low torque density and associated low efficiency.

2) Hybrid-Excited Machines

The TMSS-PM SRM and the TMSS-PM DSM have the simplest machine structure but the lowest torque density. Between them, the TMSS-PM DSM has higher torque density and efficiency than TMSS-PM SRM. Although they have similar iron core topology, their working principle and associated winding configuration are distinct. The TMSS-PM SRM is driven by trapezoid current and it does not require a separated field excitation winding. The TMSS-PM DSM has both armature winding and an independent excitation winding. The excitation winding can be replaced by the additional zero-sequence current component in armature winding, but more control complexity is required [124-125]. In both machines, the TMSS PM can relieve the stator core saturation so that higher torque capacity can be obtained, especially at high current conditions.

Among all hybrid-excited machines, the TMSS-PM FSM has the highest torque density and power factor, in spite of the highest PM volume, due to the flux concentrating effect [126]. However, the end winding is slightly longer than those of other hybrid-excited machines, because armature winding is wound across a piece of PM sandwiched by two stator teeth. The flux bridge is essential as the flux path of FEC, but it may cause the short circuit in the magnetic path of TMSS PMs.

The skewed and dual-layer SS-PM machines have similar machine structures and working principles. The TMSS PM (or tangential component of skewed PM) is used to provide a constant biased flux path in the stator core to relieve the saturation caused

by excitation current under the relieving-dc-saturation effect. The RMSS PM (or radial component of skewed PM) is used to provide the additional torque under flux modulation effect. According to the Pareto frontier, the skewed SS-PM machine has higher torque capability than the dual-layer SS-PM machine. Besides, skewed SS-PM machine has less manufacture difficulty as there is only one piece of PM designed at slot opening.

3) Summary

To date, electrical machines have been widely used in many industrial applications, such as electrical vehicles (EV), hybrid electrical vehicles (HEV), unmanned electrical vehicles (UEV), robot joints, ship propelling systems, railway traction, aircraft, and wind power generation. Among them, the EV, HEV, and wind power generation are the most heated target applications of SS-PM machines.

The machines of EV and HEV require considerable efficiency, a wide speed range, and reliable mechanical strength. The TMSS-PM SRM has wide applications in EV/HEV, aircraft because of its simple structure, good mechanical reliability, and easy control. The TMSS-PM SRM is also more suitable for applications that low cost and high reliability are required, such as water pumps. However, due to the special driving circuit and control strategy, little paper uses the TMSS-PM SRM as a generator. In terms of Hybrid-excited TMSS-PM DSM, it has a similar structure to TMSS-PM SRM, and therefore it also enjoys a simple structure and good mechanical reliability. Due to the difference in driving current, the control of TMSS-PM DSM is more complex than TMSS-PM SRM. However, TMSS-PM DSM has a higher torque density than TMSS-PM SRM, and the flexible DC current provides a good flux regulation ability and associated wide speed range. Therefore, the TMSS-PM DSM has been widely studied in EV, HEV, and wind power generation applications. According to our comparative study, the hybrid-excited TMSS-PM FSM has higher torque production than the hybrid-excited TMSS-PM DSM, and it also has good flux regulation ability. However, due to the existence of the iron bridge, the TMSS-PM FSM faces higher mechanical manufacturing difficulties. As for the dual-layer SS-PM machine and skewed SS-PM machine, there are still only a few references for these types of machines. The skewed SS-PM machine is a promising potential candidate for future research. In terms of PM-excited SS-PM machines, the TMSS-PM DSMs have been studied in many industrial applications like EV, wind power generation, and traction systems. As for the dual-RMSS-PM machine and stator-RMSS-PM machine, they have a very high torque density but high iron loss and low power factor. Therefore, it is more suitable for low-speed and high-torque applications like robotic systems. There are only a few publications about the research on the Halbach RMSS-PM machine. But according to our comparative study, the torque production is even higher than that of the stator-RMSS-PM machine, therefore it can also be used in a robotic system, where low speed and high torque are required.

Based on the above results and discussions, a comprehensive performance evaluation of the above-mentioned machines is presented in Table 4. More "√" refers to better machine performance. The conclusions are summarized as follow.

1. The RMSS PMs usually have a higher torque contribution than the TMSS PMs in the SS-PM machines. This is because the flux from RMSS PM passing through the air gap contributes to the torque production directly and the magnetic resistance in the whole magnetic path is relatively small, while the flux leakage from TMSS PM is larger than that from the RMSS-PM design and the magnetic resistance is also large in the whole magnetic path.

2. For RMSS-PM machines, the dual-RMSS-PM machine has a higher torque density and PM utilization factor than the stator-RMSS-PM machine, which is due to the bidirectional flux modulation effect in the dual-RMSS-PM machine. However, there are heat dissipation and centrifugal force problems in rotor PM design.

3. Halbach SS-PM machine has a higher torque density than the stator-RMSS-PM machine because the flux is concentrated to the stator core by the two TMSS PM. However, the torque per PM value of the Halbach SS-PM machine is lower than that of the stator-RMSS-PM machine.

4. Among all the above TMSS-PM machines, the TMSS-FSM has the highest torque and efficiency because of flux concentration effect [126].

5. The TMSS PM can effectively improve the torque capability of the TMSS-PM machine when a biased flux is built in the stator core due to the relieving-dc-saturation effect. The torque improvement of TMSS PM is more significant under high electric load conditions.

Table 4
Summary of SS-PM machine performance.

	TMSS-PM SRM (Hybrid-excited)	TMSS-PM DSM (PM-excited)	TMSS-PM DSM (Hybrid-excited)	TMSS-PM FSM (Hybrid-excited)	Stator-RMSS -PM machine (PM-excited)	Dual-RMSS -PM machine (PM-excited)	Halbach SS -PM machine (PM-excited)	Dual-layer SS -PM machine (Hybrid-excited)	Skewed SS -PM machine (Hybrid-excited)
Torque density	√	√√√	√√	√√√	√√√√	√√√√√	√√√√	√√	√√√
Torque per PM usage	√	√	√√√	√	√√√√	√√√√√	√√√√	√	√√
Power factor	/	√√√√	√	√√√√√	√	√√√	√√	√√√	√√√√
Efficiency	√	√√√√	√√	√√√	√√√√	√√√√√	√√√√√	√√√	√√√

VII. Future Challenges and Trend

Generally speaking, the SS-PM machines are promising candidates and potential solutions in various industries, like electrical vehicles, wind power generation, robots, aerospace, due to their novelty and good machine performance. However, there are some problems and challenges of SS-PM machines left for future study. The torque capacity can be largely limited by the iron core saturation, especially for the machines with biased flux under high current conditions. One possible solution is to adopt TMSS PM having opposite magnetization direction with the biased excitation field. The core saturation can be relieved, higher excitation current can be applied, and wider speed range can be obtained.

To date, the RMSS PM machines and TMSS PM machines have been well investigated in recent decades, but there are relatively fewer publications focusing on CMSS PM machines. According to the results of recent publications and our comparative study, the RMSS PMs usually have a higher torque contribution than TMSS PMs. Under flux modulation effect, although the RMSS PM

machines can achieve a relatively high torque density, the low power factor is a challenging problem for future study. As for TMSS PM machines, the TMSS PMs are usually designed with the DC field current to relieve the stator core saturation. Therefore, in spite of relatively lower torque density, the flux regulation ability can be improved by TMSS PMs. The CMSS PM machines can be seen as a new idea and machine category, which can inherit the advantages from both RMSS PM and TMSS PM machines. In spite of the strong repulsive force between PMs in the same slot, which causes high manufacturing difficulty, especially in Halbach SS-PM machines and Dual-layer SS-PM machines, a good potential solution is to use skewed SS PM to replace the original design.

VIII. Conclusion

This paper presents an overview of the state of the art of SS-PM machines with the emphasis on the basic working principle, machine topology, and electromagnetic performance. The machines are classified into three parts according to the magnetization of SS PMs, namely, TMSS-PM machines, RMSS-PM machines, and CMSS-PM machines. The working principle of each category is introduced based on typical structures. Recent research on topology innovation is discussed. The comprehensive performances of all categories are summarized and evaluated. The following conclusions can be drawn from previous comparative study.

1. The RMSS PMs usually have a higher torque contribution than the TMSS PMs. The main reason is that nearly all the flux of RMSS PM can enter the air gap directly, which produces an effective flux in the armature winding and associated torque production. The stator-RMSS-PM machine and dual-RMSS-PM machine are typical examples of the above statement, whose torque productions are much higher than that of the TMSS-PM machine in the comparative study. Therefore, they are suitable for low-speed and high-torque applications like robotic systems. However, the main limitation of RMSS PM is that the stator core adjacent to RMSS PMs is easy to saturate because of the leakage flux of RMSS PM.

2. The TMSS PMs are usually designed with DC field current, such as TMSS-PM SRM, DSM, and FSM. The common feature of them is that the magnetization of TMSS PM is intentionally designed opposite to that of DC excitation current, so that the stator core can be relieved. Therefore, a higher excitation current can be applied, and torque density can be improved to some extent, especially at high load conditions. Besides, as the vibration range of excitation current can be enlarged by the TMSS PM, a wide speed range can be obtained. Therefore, they are suitable for wide-speed-range applications like EV, HEV, and wind power generation.

3. In terms of the CMSS-PM machine, it can be seen as a special machine category, which combines the features of TMSS-PM and RMSS-PM machines. Therefore, CMSS PM is a promising candidate for future research as a tradeoff between TMSS PM and RMSS PM. However, the operation principle, machine performance, and target application of different CMSS PM machines can be divisive. For Halbach SS-PM machine, it has the highest torque density among the stator PM machines in our comparative study. However, the torque per PM usage is not satisfactory and the repelling forces among the PMs in the same slot opening restrict its

application. Therefore, Halbach SS PM is suitable when very high torque density is required but the cost is high accordingly. For dual-layer and skewed PM machines, they can be seen as the combination of a hybrid-excited TMSS-PM machine and the stator-RMSS-PM machine. Therefore, the relieving-dc-saturation effect of TMSS PM and torque enhancement of RMSS PM can be achieved simultaneously.

ACKNOWLEDGMENTS

This work was supported by the National Natural Science Foundation of China under Project 52077187 and in part by the Research Grant Council of the Hong Kong Government under Project PolyU 152143/18E and PolyU 152109/20E.

REFERENCES

[1] James. F, The Correspondence of Michael Faraday, Volume 1: 1811-1831. IET Digital Library; 1991.
[2] M. A. Rahman, "History of interior permanent magnet motors [History]," IEEE Ind. Appl. Mag., vol. 19, no. 1, pp. 10-15, Jan.-Feb. 2013.
[3] H. Yang, H. Lin, and Z. Q. Zhu, "Recent advances in variable flux memory machines for traction applications: a review," CES Trans. Elect. Mach. Syst., vol. 2, no. 1, pp. 34–50, Mar. 2018.
[4] T. Wang, F. Wang, H. Bai and J. Xing, "Optimization design of rotor structure for high speed permanent magnet machines," 2007 International Conference on Electrical Machines and Systems (ICEMS), 2007, pp. 1438-1442.
[5] Z. Q. Zhu, H. Hua, D. Wu, J. T. Shi and Z. Z. Wu, "Comparative study of partitioned stator machines with different PM excitation stators," IEEE Trans. Ind. Appl., vol. 52, no. 1, pp. 199-208, Jan.-Feb. 2016.
[6] S. E. Rauch and L. J. Johnson, "Design principles of flux-switch alternators [includes discussion]," Trans. Am. Inst. Electr. Eng., 2, Appl. ind., vol. 74, no. 3, pp. 1261-1268, Jan. 1955.
[7] A. Ghaffarpour and M. Mirsalim, "Analysis of an E-core permanent magnet switched reluctance motor," 2021 29th Iranian Conference on Electrical Engineering (ICEE), 2021, pp. 236-240.
[8] K. Nakamura, T. Ono, H. Goto, T. Watanabe and O. Ichinokura, "A novel switched reluctance motor with wound-cores put on stator and rotor poles," IEEE Trans. Magn., vol. 41, no. 10, pp. 3919-3921, Oct. 2005.
[9] Z. Yang, F. Shang, I. P. Brown and M. Krishnamurthy, "Comparative study of interior permanent magnet, induction, and switched reluctance motor drives for EV and HEV applications," IEEE Trans. Transp. Electrification, vol. 1, no. 3, pp. 245-254, Oct. 2015.
[10] F. L. M. dos Santos, J. Anthonis, F. Naclerio, J. J. C. Gyselinck, H. Van der Auweraer and L. C. S. Góes, "Multiphysics nvh modeling: simulation of a switched reluctance motor for an electric vehicle," IEEE Trans. Ind. Electron., vol. 61, no. 1, pp. 469-476, Jan. 2014.
[11] Y. Liao, F. Liang and T. A. Lipo, "A novel permanent magnet motor with doubly salient structure," IEEE Trans. Ind. Appl., vol. 31, no. 5, pp. 1069-1078, Sept.-Oct. 1995.
[12] S. Niu, X. Zhao, X. Zhang and T. Sheng, "A Novel Axial-Flux-Complementary Doubly Salient Machine With Boosted PM Utilization for Cost-Effective Direct-Drive Applications," IEEE Access, vol. 7, pp. 145970-145977, 2019.
[13] X. Y. Ma, G. J. Li, G. W. Jewell, Z. Q. Zhu and H. L. Zhan, "Performance comparison of doubly salient reluctance machine topologies supplied by sinewave currents," IEEE Trans. Ind. Electron., vol. 63, no. 7, pp. 4086-4096, July 2016.
[14] M. Cheng, K. T. Chau and C. C. Chan, "Design and analysis of a new doubly salient permanent magnet motor," IEEE Trans. Magn., vol. 37, no. 4, pp. 3012-3020, July 2001.
[15] E. Hoang, A. H. Ben-Ahmed, and J. Lucidarme, "Switching flux permanent magnet polyphased machines," Proc. Eur. Conf. Power Electron. Appl., 1997, pp. 903–908
[16] C. Hwang, P. Li and C. Liu, "Design and analysis of a novel hybrid excited linear flux switching permanent magnet motor," IEEE Trans. Magn., vol. 48, no. 11, pp. 2969-2972, Nov. 2012.
[17] G. Zhang, W. Hua, M. Cheng, J. Liao, K. Wang and J. Zhang, "Investigation of an improved hybrid-excitation flux-switching brushless machine for HEV/EV applications," IEEE Trans. Ind. Appl., vol. 51, no. 5, pp. 3791-3799, Sept.-Oct. 2015.
[18] G. J. Li and Z. Q. Zhu, "Hybrid Excitation Switched Flux Permanent Magnet Machines with Hybrid Magnets," 8th IET International Conference on Power Electronics, Machines and Drives (PEMD 2016), 2016.
[19] R. P. Deodhar, S. Andersson, I. Boldea, and T. J. E. Miller, "The flux reversal machine: A new brushless doubly-salient permanent-magnet machine," Conf. Rec. IEEE IAS Annu. Meeting, 1996, pp. 786–793.
[20] H. Yang, H. Lin, Z. Q. Zhu, S. Lyu and Y. Liu, "Design and analysis of novel asymmetric-stator-pole flux reversal PM machine," IEEE Trans. Ind. Electron., vol. 67, no. 1, pp. 101-114, Jan. 2020.
[21] Y. Gao, R. Qu, D. Li, J. Li and G. Zhou, "Consequent-pole flux-reversal permanent-magnet machine for electric vehicle propulsion," IEEE Trans. Appl. Supercond., vol. 26, no. 4, pp. 1-5, June 2016, Art no. 5200105.
[22] H. Yang, Z. Q. Zhu, H. Lin, H. Li and S. Lyu, "Analysis of consequent-pole flux reversal permanent magnet machine with biased flux modulation theory," IEEE Trans. Ind. Electron., vol. 67, no. 3, pp. 2107-2121, March 2020.
[23] T. H. Kim and J. Lee, "A study of the design for the flux reversal machine," IEEE Trans. Magn., vol. 40, no. 4, pp. 2053-2055, July 2004.
[24] K. T. Chau, C. C. Chan and C. Liu, "Overview of permanent-magnet brushless drives for electric and hybrid electric vehicles," IEEE Trans. Ind. Electron., vol. 55, no. 6, pp. 2246-2257, June 2008.
[25] I. A. A. Afinowi, Z. Q. Zhu, Y. Guan, J. Mipo and P. Farah, "A novel brushless ac doubly salient stator slot permanent magnet machine," IEEE Trans. Energy Convers., vol. 31, no. 1, pp. 283-292, March 2016.
[26] F. Wang, L. Zhou, J. Wang, Y. Xiao, J. Zhou and L. Shentu, "A novel dual-stator permanent magnet Vernier machine with magnets in rotor and both stators," 2018 21st International Conference on Electrical Machines and Systems (ICEMS), 2018, pp. 197-201.
[27] X. Zhao, "Emerging hybrid reluctance motor drives for electric propulsion," 2020 8th International Conference on Power Electronics Systems and Applications (PESA), 2020, pp. 1-4.

[28] S. Ullah, S. P. McDonald, R. Martin, M. Benarous and G. J. Atkinson, "A permanent magnet assist, segmented rotor, switched reluctance drive for fault tolerant aerospace applications," IEEE Trans. Ind. Appl., vol. 55, no. 1, pp. 298-305, Jan.-Feb. 2019.
[29] Y. Shen, Q. Lu and X. Huang, "Analysis of a novel linear doubly salient slot permanent magnet motor," IEEE Trans. Magn., vol. 53, no. 11, pp. 1-4, Nov. 2017, Art no. 8109904.
[30] J. Yin, L. Quan, X. Zhu, Z. Xiang and H. Zhou, "The performance of a hybrid excitation flux switching motor with ferrite magnets for EVs," 2014 IEEE Conference and Expo Transportation Electrification Asia-Pacific (ITEC Asia-Pacific), 2014, pp. 1-4.
[31] M. Tanujaya, D. Lee and J. Ahn, "Characteristic analysis of a novel 6/5 c-core type three-phase switched reluctance motor," 2011 International Conference on Electrical Machines and Systems, 2011, pp. 1-6.
[32] Y. Hasegawa, K. Nakamura and O. Ichinokura, "A novel switched reluctance motor with the auxiliary windings and permanent magnets," IEEE Trans Magn., vol. 48, no. 11, pp. 3855-3858, Nov. 2012.
[33] J. F. Gieras, "PM synchronous generators with hybrid excitation systems and voltage control capabilities: A review," 2012 XXth International Conference on Electrical Machines, 2012, pp. 2573-2579.
[34] J. B. Bartolo, M. Degano, J. Espina and C. Gerada, "Design and initial testing of a high-speed 45-kw switched reluctance drive for aerospace application," IEEE Trans. Ind. Electron., vol. 64, no. 2, pp. 988-997, Feb. 2017.
[35] P. Andrada, B. Blanqué, E. Martínez and M. Torrent, "A novel type of hybrid reluctance motor drive," IEEE Trans. Ind. Electron., vol. 61, no. 8, pp. 4337-4345, Aug. 2014.
[36] P. Andrada, B. Blanqué, E. Martínez and M. Torrent, "New hybrid reluctance motor drive," 2012 XXth International Conference on Electrical Machines, 2012, pp. 2689-2694.
[37] W. Ding, S. Yang, Y. Hu, S. Li, T. Wang and Z. Yin, "Design consideration and evaluation of a 12/8 high-torque modular-stator hybrid excitation switched reluctance machine for EV applications," IEEE Trans. Ind. Electron., vol. 64, no. 12, pp. 9221-9232, Dec. 2017.
[38] M. A. J. Kondelaji and M. Mirsalim, "Double-stator PM-assisted modular variable reluctance motor for EV applications," 2018 9th Annual Power Electronics, Drives Systems and Technologies Conference (PEDSTC), 2018, pp. 236-240.
[39] K. Nakamura, K. Murota and O. Ichinokura, "Characteristics of a novel switched reluctance motor having permanent magnets between the stator pole-tips," 2007 European Conference on Power Electronics and Applications, 2007, pp. 1-5.
[40] J. Zhu, K. W. E. Cheng and X. Xue, "Design and analysis of a new enhanced torque hybrid switched reluctance motor," IEEE Trans. Energy Convers., vol. 33, no. 4, pp. 1965-1977, Dec. 2018.
[41] E. F. Farahani, M. A. J. Kondelaji and M. Mirsalim, "A new exterior-rotor multiple teeth switched reluctance motor with embedded permanent magnets for torque enhancement," IEEE Trans. Magn., vol. 56, no. 2, pp. 1-5, Feb. 2020, Art no. 8100405.
[42] S. Ullah, S. P. McDonald, R. Martin and G. J. Atkinson, "A permanent magnet assisted switched reluctance machine for more electric aircraft," 2016 XXII International Conference on Electrical Machines (ICEM), 2016, pp. 79-85.
[43] S. P. McDonald, G. J. Atkinson, D. J. B. Smith, and S. Ullah, "Overcoming the challenges of drag torque in a dual-lane actuator for an aircraft," Electrical Machines (ICEM), 2014 International Conference on, 2014, pp. 2120-2126.
[44] X. Zhao, S. Niu, X. Zhang and W. Fu, "Design of a new relieving-DC-saturation hybrid reluctance machine for fault-tolerant in-wheel direct drive," IEEE Trans. Ind. Electron., vol. 67, no. 11, pp. 9571-9581.
[45] J. Ou and M. Doppelbauer, "Torque analysis and comparison of the switched reluctance machine and the doubly-salient permanent magnet machine," 2016 18th European Conference on Power Electronics and Applications (EPE'16 ECCE Europe), 2016, pp. 1-11.
[46] Q. Ze, P. Kou, D. Liang and Z. Liang, "Fault-tolerant performances of switched reluctance machine and doubly salient permanent magnet machine in starter/generator system," 2014 17th International Conference on Electrical Machines and Systems (ICEMS), 2014, pp. 3417-3423.
[47] X. Liu and Z. Q. Zhu, "Comparative study of novel variable flux reluctance machines with doubly fed doubly salient machines," IEEE Trans. Magn., vol. 49, no. 7, pp. 3838-3841, July 2013.
[48] M. Amirkhani and M. Mirsalim, "A comprehensive analysis of a complementary-rotor doubly salient permanent magnet motor for high torque applications," 2021 12th Power Electronics, Drive Systems, and Technologies Conference (PEDSTC), 2021, pp. 1-5.
[49] Y. Shen and Q. Lu, "Investigation of novel multi-tooth linear variable flux reluctance machines," IEEE Trans. Magn., vol. 54, no. 11, pp. 1-5, Nov. 2018, Art no. 8107905.
[50] H. Yang, Z. Q. Zhu, Y. Liu, H. Y. Li and J. C. Mipo, "Comparative study of doubly salient machines with/without stator slot permanent magnets," 2017 IEEE International Electric Machines and Drives Conference (IEMDC), 2017, pp. 1-6.
[51] I. A. A. Afinowi, Z. Q. Zhu, Y. Guan, J. C. Mipo and P. Farah, "Hybrid-excited doubly salient synchronous machine with permanent magnets between adjacent salient stator poles," IEEE Trans. Magn., vol. 51, no. 10, pp. 1-9, Oct. 2015, Art no. 8107909.
[52] Z. Q. Zhu, I. A. A. Afinowi, Y. Guan, J. C. Mipo and P. Farah, "Hybrid-excited stator slot permanent magnet machines—influence of stator and rotor pole combinations," IEEE Trans. Magn., vol. 52, no. 2, pp. 1-10, Feb. 2016, Art no. 8100710.
[53] Y. Mao, S. Niu and Q. Wang, "Design and optimization of a slot-PM-assisted doubly-salient machine based on saturation assuaging," Chin. J. Electr. Eng., vol. 7, no. 3, pp. 65-72, Sept. 2021.
[54] Y. J. Zhou and Z. Q. Zhu, "Comparison of wound-field switched-flux machines," IEEE Trans. Ind. Appl., vol. 50, no. 5, pp. 3314-3324, Sept.-Oct. 2014.
[55] M. Zheng, Z. Q. Zhu, S. Cai, H. Y. Li and Y. Liu, "Influence of magnetic saturation and rotor eccentricity on back emf of novel hybrid-excited stator slot opening permanent magnet machine," IEEE Trans. Magn., vol. 54, no. 11, pp. 1-5, Nov. 2018, Art no. 8105905.
[56] M. Zheng, S. Cai and Z. Q. Zhu, "Investigation of a hybrid excited doubly salient machine with permanent magnets located on stator slot openings," IET Electr. Power Appl., vol. 14, no. 9, pp. 1541-1549, Sept. 2020.
[57] Y. Gong, K. T. Chau, J. Z. Jiang, C. Yu and W. Li, "Design of doubly salient permanent magnet motors with minimum torque ripple," IEEE Trans. Magn., vol. 45, no. 10, pp. 4704-4707, Oct. 2009.
[58] J. Jiang, X. Zhang, S. Niu and X. Zhao, "A novel doubly-fed doubly-salient machine with DC-saturation-relieving structure for wind power generation," IET Renew. Power Gener., vol. 15, no. 9, pp. 2042-2051, July 2021.
[59] W. Cui, Y. Gong, J. Jiang and Y. Zhang, "Optimized doubly salient memory motors with symmetric features using transposition design methods," 2011 International Conference on Power Engineering, Energy and Electrical Drives, 2011, pp. 1-7.
[60] Z. Q. Zhu, Z. Azar and G. Ombach, "Influence of additional air gaps between stator segments on cogging torque of permanent-magnet machines having modular stators," IEEE Trans. Magn., vol. 48, no. 6, pp. 2049-2055, June 2012.
[61] Y. Liu, X. Wu, X. Zhang, S. Niu and W. L. x. Chan, "Coupled electromagnetic-thermal optimization of a separate-stator modular machine with biased flux," IEEE Trans. Magn., vol. 55, no. 6, pp. 1-5, June 2019, Art no. 8103405.
[62] M. Zheng, Z. Q. Zhu, S. Cai and S. S. Xue, "A novel modular stator hybrid-excited doubly salient synchronous machine with stator slot permanent magnets," IEEE Trans. Magn., vol. 55, no. 7, pp. 1-9, July 2019, Art no. 8104409.
[63] Z. Li and S. Niu, "Design and analysis of a novel claw-shaped modular stator relieving-DC-saturation doubly salient machine with 3D complementary magnetic circuit," IET Renew. Power Gener..
[64] Z. Li, X. Zhao, S. Niu and W. N. Fu, "Analysis and design of a new relieving-DC-saturation transverse-flux tubular motor with complementary magnetic circuit," IEEE Trans. Magn., vol. 57, no. 6, pp. 1-5, June 2021, Art no. 8203905.

[65] X. Zhao, S. Niu and W. Fu, "Sensitivity analysis and design optimization of a new hybrid-excited dual-PM generator with relieving-DC-saturation structure for stand-alone wind power generation," IEEE Trans. Magn., vol. 56, no. 1, pp. 1-5, Jan. 2020, Art no. 7504105.
[66] X. Zhao, S. Niu, X. Zhang and W. Fu, "A new relieving-DC-saturation hybrid excitation Vernier machine for HEV starter generator application," IEEE Trans. Ind. Electron., vol. 67, no. 8, pp. 6342-6353, Aug. 2020.
[67] S. Wang, S. Niu and W. Fu, "Comparative study of relieving-DC-saturation hybrid excited Vernier machine with different rotor pole designs for wind power generation," IEEE Access, vol. 8, pp. 198900-198911, 2020.
[68] X. Zhao, S. Niu and W. Fu, "A new modular relieving-DC-saturation Vernier reluctance machine excited by zero-sequence current for electric vehicle," IEEE Trans. Magn., vol. 55, no. 7, pp. 1-5, July 2019, Art no. 8104605.
[69] T. Sheng, S. Niu and S. Yang, "A novel design method for the electrical machines with biased DC excitation flux linkage," IEEE Trans. Magn., vol. 53, no. 6, pp. 1-4, June 2017, Art no. 8103604.
[70] Z. Yu, W. Kong and R. Qu, "Minimum copper loss control strategy for DC-biased Vernier reluctance machines based on speed variation," 2020 International Conference on Electrical Machines (ICEM), 2020, pp. 1999-2005.
[71] A. Li, D. Jiang, W. Kong and R. Qu, "Four-leg converter for reluctance machine with DC-biased sinusoidal winding current," IEEE Trans. Power Electron., vol. 34, no. 5, pp. 4569-4580, May 2019.
[72] A. Li, Z. Gao, D. Jiang, W. Kong, S. Jia and R. Qu, "Three-phase four-leg drive for DC-biased sinusoidal current Vernier reluctance machine," 2018 IEEE Applied Power Electronics Conference and Exposition (APEC), 2018, pp. 1236-1241.
[73] T. Sheng and S. Niu, "A novel zero-sequence-current-based dual-stator biased-flux machine," IEEE Trans. Energy Convers., vol. 33, no. 4, pp. 1934-1942, Dec. 2018.
[74] Z. Yu, W. Kong, C. Gan and R. Qu, "Power converter topologies and control strategies for DC-biased Vernier reluctance machines," IEEE Trans. Ind. Electron., vol. 67, no. 6, pp. 4350-4359, June 2020.
[75] S. Jia, P. Sun, D. Liang, X. Dong, Z. Zhu and J. Liu, "Analysis of DC-biased Vernier reluctance machines having distributed windings," IEEE Trans. Magn., vol. 57, no. 7, pp. 1-5, July 2021, Art no. 8106605.
[76] Q. Wang, P. Igic, S. Niu and J. Wang, "A new dual-PM excited doubly salient machine for traction applications," 2020 2nd IEEE International Conference on Industrial Electronics for Sustainable Energy Systems (IESES), 2020, pp. 275-279.
[77] Q. Wang, M. Ordonez, J. Wang, M. A. Saket and R. Shafaei, "A novel dual slot permanent magnet machine with complementary rotors for electric vehicle propulsion," 2019 IEEE 28th International Symposium on Industrial Electronics (ISIE), 2019, pp. 221-225.
[78] S. Wang, X. Zhang, X. Zhao, S. Niu and W. Fu, "A novel slot-PM assisted complementary-rotor doubly-salient machine with enhanced torque performance," IEEE Trans. Ind. Electron.
[79] Z. Q. Zhu, "Switched flux permanent magnet machines — Innovation continues," 2011 International Conference on Electrical Machines and Systems, 2011, pp. 1-10.
[80] J. Shen and W. Fei, "Permanent magnet flux switching machines — topologies, analysis and optimization," 4th International Conference on Power Engineering, Energy and Electrical Drives, 2013, pp. 352-366.
[81] H. Cherif, S. Affi, J. Belhadj, S. Hlioui and M. Gabsi, "Design and performance investigation of small-scale wind turbine system based on hybrid excited flux switching machine," 2019 International Conference on Advanced Systems and Emergent Technologies (IC_ASET), 2019, pp. 375-380.
[82] E. B. Sulaiman and A. M. Arab, "Fundamental study of outer-rotor hybrid excitation flux switching generator for grid connected wind turbine applications," 2015 IEEE Student Conference on Research and DeveloPMent (SCOReD), 2015, pp. 716-720.
[83] H. Zheng, L. Zhou and R. Cao, "Speed control of linear flux-switching permanent magnet motor with segmented secondary for rail transit," 2021 13th International Symposium on Linear Drives for Industry Applications (LDIA), 2021, pp. 1-5.
[84] R. Cao and M. Lu, "Investigation on high temperature superconducting linear flux-switching motors with different mover and stator pole pitch ratios for urban railway transit system," IEEE Trans. Appl. Supercond., vol. 31, no. 5, pp. 1-5, Aug. 2021, Art no. 5202005.
[85] R. Cao, M. Lu, N. Jiang and M. Cheng, "Comparison between linear induction motor and linear flux-switching permanent-magnet motor for railway transportation," IEEE Trans. Ind. Electron., vol. 66, no. 12, pp. 9394-9405, Dec. 2019.
[86] R. Leuzzi, Y. Li and B. Sarlioglu, "Performance evaluation of a hybrid-excited flux-switching PM motor for traction applications," IECON 2016 - 42nd Annual Conference of the IEEE Industrial Electronics Society, 2016, pp. 1846-1851.
[87] W. Hua, M. Cheng and G. Zhang, "A novel hybrid excitation flux-switching motor for hybrid vehicles," IEEE Trans. Magn., vol. 45, no. 10, pp. 4728-4731, Oct. 2009.
[88] R. Cao, X. Zhang and X. Yuan, "A new three-phase hybride excitation flux-switching motor for EV/HEV applications," 2019 IEEE International Electric Machines & Drives Conference (IEMDC), 2019, pp. 1398-1403.
[89] T. Okada, H. Matsumori, T. Kosaka and N. Matsui, "Hybrid excitation flux switching motor with permanent magnet placed at middle of field coil slots employing high filling factor windings," 2018 IEEE Energy Conversion Congress and Exposition (ECCE), 2018, pp. 4268-4274.
[90] N. A. Jafar and E. Sulaiman, "Design analysis of 12S-10P hybrid-excitation flux-switching permanent-magnet machines for hybrid electric vehicle," 2014 IEEE 8th International Power Engineering and Optimization Conference (PEOCO2014), 2014, pp. 308-312.
[91] E. Sulaiman, T. Kosaka and N. Matsui, "High power density design of 6-slot–8-pole hybrid excitation flux switching machine for hybrid electric vehicles," IEEE Trans. Magn., vol. 47, no. 10, pp. 4453-4456, Oct. 2011.
[92] M. Z. Ahmad, E. Sulaiman, F. Khan and Z. A. Haron, "Electromagnetic flux analysis on a new outer-rotor hybrid excitation flux switching machine," 2014 IEEE Asia-Pacific Conference on Applied Electromagnetics (APACE), 2014, pp. 175-178.
[93] Y. Wang and Z. Deng, "Comparison of hybrid excitation topologies for flux-switching machines," IEEE Trans. Magn., vol. 48, no. 9, pp. 2518-2527, Sept. 2012.
[94] R. L. Owen, Z. Q. Zhu and G. W. Jewell, "Hybrid-excited flux-switching permanent-magnet machines with iron flux bridges," IEEE Trans. Magn., vol. 46, no. 6, pp. 1726-1729, June 2010.
[95] W. Hua, G. Zhang and M. Cheng, "Flux-regulation theories and principles of hybrid-excited flux-switching machines," IEEE Trans. Ind. Electron., vol. 62, no. 9, pp. 5359-5369, Sept. 2015.
[96] Z. Q. Zhu, A. S. Thomas, J. T. Chen and G. W. Jewell, "Cogging torque in flux-switching permanent magnet machines," IEEE Trans. Magn., vol. 45, no. 10, pp. 4708-4711, Oct. 2009.
[97] C. T. Liu, C. C. Hwang, P. L. Li, S. S. Hung and P. Wendling, "Design optimization of a double-sided hybrid excited linear flux switching PM motor with low force ripple," IEEE Trans. Magn., vol. 50, no. 11, pp. 1-4, Nov. 2014, Art no. 8102704.
[98] W. Fei, P. C. K. Luk and J. Shen, "Torque analysis of permanent-magnet flux switching machines with rotor step skewing," IEEE Trans. Magn., vol. 48, no. 10, pp. 2664-2673, Oct. 2012.
[99] M. J. Jin, Y. Wang, J. X. Shen, P. C. K. Luk, W. Z. Fei and C. F. Wang, "Cogging torque suppression in a permanent-magnet flux-switching integrated-starter-generator," IET Electr. Power Appl., vol.4, no. 8, pp. 647-656, Sept. 2010.
[100] S. E. Abdollahi and S. Vaez-Zadeh, "Reducing cogging torque in flux switching motors with segmented rotor," IEEE Trans. Magn., vol. 49, no. 10, pp. 5304-5309, Oct. 2013.

[101] J. H. Hu, L. Wang, J. B. Zou and B. Zhao, "Cogging torque reduction of hybrid excitation flux switching motor," 2015 Fifth International Conference on Instrumentation and Measurement, Computer, Communication and Control (IMCCC), 2015, pp. 1889-1892.
[102] T. Sheng, "Design, analyze and control of novel stator-PM electrical machines," Ph.D. thesis, Department of Electrical Engineering, The Hong Kong Polytechnic University, Hong Kong, China, 2018.
[103] X. Zhao and S. Niu, "Design and optimization of a novel slot-PM-assisted variable flux reluctance generator for hybrid electric vehicles," IEEE Trans. Energy Convers., vol. 33, no. 4, pp. 2102-2111, Dec. 2018.
[104] Q. Wang, S. Niu and L. Yang, "Design optimization and comparative study of novel dual-PM excited machines," IEEE Trans. Ind. Electron., vol. 64, no. 12, pp. 9924-9933, Dec. 2017.
[105] S. Niu, T. Sheng, X. Zhao and X. Zhang, "Operation principle and torque component quantification of short-pitched flux-bidirectional-modulation machine," IEEE Access, vol. 7, pp. 136676-136685, 2019.
[106] S. Niu, S. L. Ho and W. N. Fu, "A novel stator and rotor dual PM Vernier motor with space vector pulse width modulation," IEEE Trans. Magn., vol. 50, no. 2, pp. 805-808, Feb. 2014, Art no. 7019904.
[107] K. Xie, D. Li, R. Qu, Z. Yu, Y. Gao and Y. Pan, "Analysis of a flux reversal machine with quasi-halbach magnets in stator slot opening," IEEE Trans. Ind. Appl., vol. 55, no. 2, pp. 1250-1260, March-April 2019.
[108] K. Xie, D. Li, R. Qu and Y. Gao, "A Novel Permanent Magnet Vernier Machine With Halbach Array Magnets in Stator Slot Opening," IEEE Trans. Magn., vol. 53, no. 6, pp. 1-5, June 2017, Art no. 7207005.
[109] X. Zhao, S. Niu, X. Zhang and W. Fu, "Flux-modulated relieving-DC-saturation hybrid reluctance machine with synthetic slot-PM excitation for electric vehicle in-wheel propulsion," IEEE Trans. Ind. Electron., vol. 68, no. 7, pp. 6075-6086, July 2021.
[110] S. Wang, S. Niu, X. Zhao and W. Fu, "Novel DC-saturation-relieving hybrid reluctance machine with skewed permanent magnets for electric vehicle propulsion," IEEE Trans. Magn.
[111] Q. Wang and S. Niu, "Overview of flux-controllable machines: electrically excited machines, hybrid excited machines and memory machines," Renew. sustain. energy rev., vol. 68, no. 1, pp. 475-491.
[112] M. Zheng, Z. Q. Zhu, S. Cai, H. Y. Li and Y. Liu, "Influence of stator and rotor pole number combinations on the electromagnetic performance of stator slot-openinging PM hybrid-excited machine," IEEE Trans. Magn., vol. 55, no. 5, pp. 1-10, May 2019, Art no. 8101210.
[113] Y. V. Zubkov, Y. A. Makarichev and Y. N. Ivannikov, "Comparison of surface-mounted permanent magnet and interior-mounted permanent magnet starters for gas turbine engines electrical start," 2019 International Conference on Electrotechnical Complexes and Systems (ICOECS), 2019, pp. 1-5.
[114] D. Ngo, M. Hsieh and T. A. Huynh, "Torque Enhancement for a Novel Flux Intensifying PMa-SynRM Using Surface-Inset Permanent Magnet," IEEE Trans. Magn., vol. 55, no. 7, pp. 1-8, July 2019, Art no. 8106108.
[115] Z. Kolondzovski, A. Arkkio, J. Larjola and P. Sallinen, "Power limits of high-speed permanent-magnet electrical machines for compressor applications," IEEE Trans. Energy Convers., vol. 26, no. 1, pp. 73-82, March 2011.
[116] W. Zhao, M. Cheng, W. Hua, H. Jia and R. Cao, "Back-emf harmonic analysis and fault-tolerant control of flux-switching permanent-magnet machine with redundancy," IEEE Trans. Ind. Electron., vol. 58, no. 5, pp. 1926-1935, May 2011.
[117] W. Zhao, M. Cheng, X. Zhu, W. Hua and X. Kong, "Analysis of fault-tolerant performance of a doubly salient permanent-magnet motor drive using transient cosimulation method," IEEE Trans. Ind. Electron., vol. 55, no. 4, pp. 1739-1748, April 2008.
[118] R. Cao, C. Mi and M. Cheng, "Quantitative comparison of flux-switching permanent-magnet motors with interior permanent magnet motor for EV, HEV, and PHEV applications," IEEE Trans. Magn., vol. 48, no. 8, pp. 2374-2384, Aug. 2012.
[119] A. Meyer, J. von Lindenfels, A. Mayr and J. Franke, "Manufacturing imperfections in electric motor production with focus on halbach array permanent magnet rotor assembly," 2018 8th International Electric Drives Production Conference (EDPC), 2018, pp. 1-7.
[120] I. Martinez-Ocaña, N. J. Baker, B. C. Mecrow, C. Gan, S. Brockway and C. Hilton, "Manufacture and testing of an in-wheel halbach array motor for automotive traction," The 10th International Conference on Power Electronics, Machines and Drives (PEMD 2020), 2020, pp. 56-61.
[121] D. Li, R. Qu and T. A. Lipo, "High-power-factor Vernier permanent-magnet machines," IEEE Trans. Ind. Appl., vol. 50, no. 6, pp. 3664-3674, Nov.-Dec. 2014.
[122] T. W. Ching, K. T. Chau and W. Li, "Power factor improvement of a linear Vernier permanent-magnet machine using auxiliary DC field excitation," IEEE Trans. Magn., vol. 52, no. 7, pp. 1-4, July 2016, Art no. 8204804.
[123] D. Li, "Research on Magnetic Field Modulation Permanent Magnet Machines," Ph.D. thesis, School of Electrical and Electronic Engineering, Huazhong University of Science and Technology, Wuhan, China, 2015.
[124] Y. Shen and Q. Lu, "A Novel linear hybrid-excited slot permanent magnet machine with DC-biased sinusoidal current," 2019 22nd International Conference on Electrical Machines and Systems (ICEMS), 2019, pp. 1-5.
[125] S. Jia, R. Qu, J. Li, D. Li and R. Zhang, "Stator/rotor slot and winding pole pair combinations of DC biased sinusoidal Vernier reluctance machines," 2016 XXII International Conference on Electrical Machines (ICEM), 2016, pp. 904-910.
[126] M. Cheng, W. Hua, J. Zhang and W. Zhao, "Overview of stator-permanent magnet brushless machines," IEEE Trans. Ind. Electron., vol. 58, no. 11, pp. 5087-5101, Nov. 2011.

Manuscript Title: Overview of Stator Slot-opening Permanent Magnet Machines

ID: TTE-Reg-2022-03-0270.R1

Paper Type: Regular paper

Response to Associate Editor

Please address all the reviewers' comments and modify the paper accordingly. The authors should provide more comprehensive analysis and detailed results for the presented designs. Also, the conclusion section should be more extensive .

Our response:

We thank the Editors and Reviewers for their time and efforts in reviewing our manuscript. We have addressed the remained comments from reviewers and made all necessary changes to the revised version. The changes in the revised manuscript are typeset in “red” color.

Reply to Reviewer 1:

1. **Reviewer's comment:**

Please provide illustrations of the optimized machine topologies that are developed and studied in Section VI. Also, it will be interesting for the reader to see the flux density distribution and the iron losses distribution of each topology. The authors comment the iron losses and the saturation of each machine category. So, this revision will support their work.

Response-1:

Thank you for your advice. To provide a clear illustration of the optimized machines, the **detailed design parameters** of each optimized machine are attached in the **Appendix** in the response letter.

For the reviewer's convenience, we present the schematic topology, the flux density distribution, and the iron loss distribution of each optimized machine in Fig. 58-Fig.66. The total iron losses of each machine under rotor speed of 2000 rpm are presented in Fig. 67.

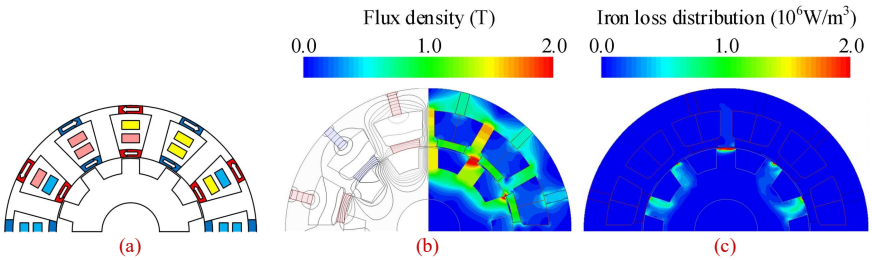

Fig. 58. PM-excited TMSS-PM DSM. (a) Schematic topology. (b) Flux density distribution. (c) Iron loss distribution.

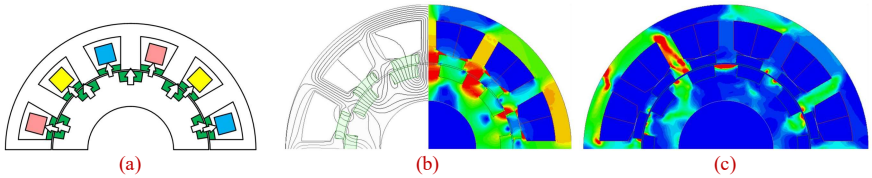

Fig. 59. Dual-RMSS-PM machine. (a) Schematic topology. (b) Flux density distribution. (c) Iron loss distribution.

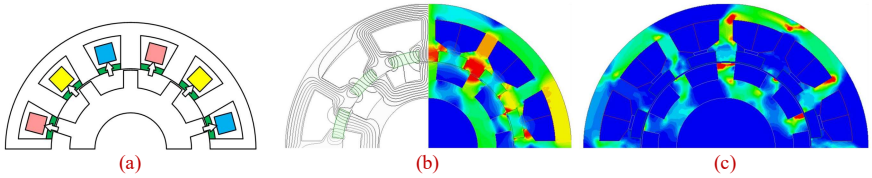

Fig. 60. Stator-RMSS-PM machine. (a) Schematic topology. (b) Flux density distribution. (c) Iron loss distribution.

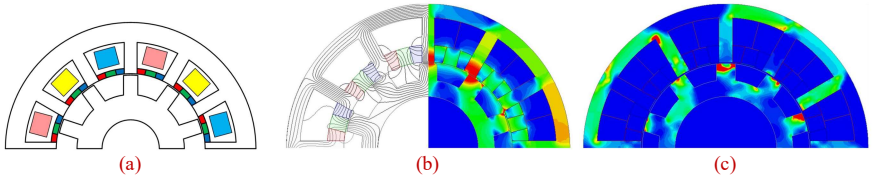

Fig. 61. Halbach SS-PM machine. (a) Schematic topology. (b) Flux density distribution. (c) Iron loss distribution

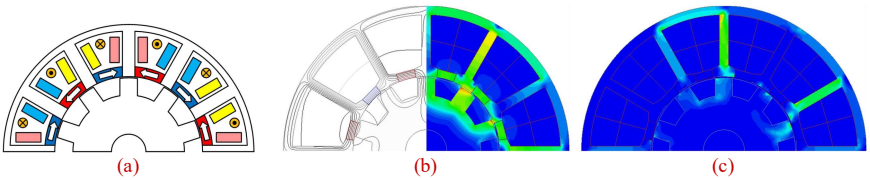

Fig. 62. Hybrid excited TMSS-PM DSM. (a) Schematic topology. (b) Flux density distribution. (c) Iron loss distribution

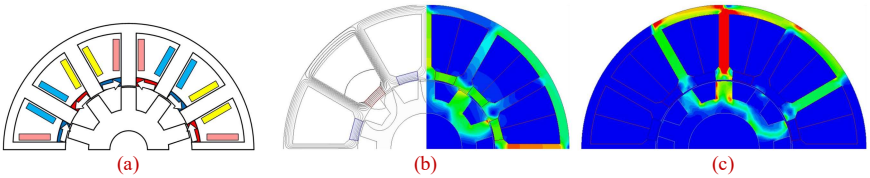

Fig. 63. TMSS-PM SRM. (a) Schematic topology. (b) Flux density distribution. (c) Iron loss distribution

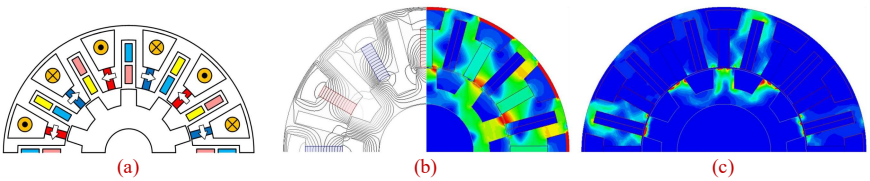

Fig. 64. TMSS-PM FSM. (a) Schematic topology. (b) Flux density distribution. (c) Iron loss distribution

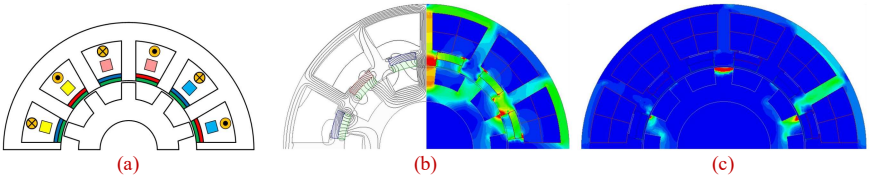

Fig. 65. Dual-layer SS-PM machine. (a) Schematic topology. (b) Flux density distribution. (c) Iron loss distribution

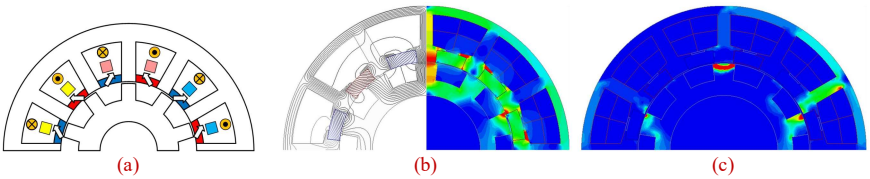

Fig. 66. Skewed SS-PM machine. (a) Schematic topology. (b) Flux density distribution. (c) Iron loss distribution.

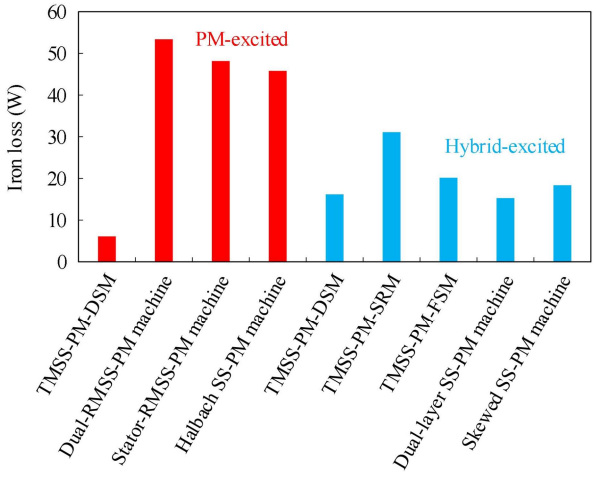

Fig. 67. Iron loss of the optimized machines under rotor speed of 2000 rpm.

It can be found that the dual-RMSS-PM machine, stator-RMSS-PM machine, and Halbach SS-PM machine have significantly higher iron loss than the other machines. This is because they do not have TMSS PM for stator core saturation relieving. By contrast, the stator core of hybrid-excited SS-PM machines can be relieved, and thus lower iron loss can be obtained. However, as is analyzed in Section III, the TMSS PM can only relive the stator core saturation, therefore, the iron loss in the rotor of the TMSS-PM machine is still very high. The iron loss in the stator core is much lower than those of the dual-RMSS-PM machine, stator-RMSS-PM machine, and Halbach SS-PM machine. This can be validated by the iron loss distribution. The only exception is the TMSS-PM SRM (shown in Fig. 63), where the iron loss is still high even with the relieving-DC-saturation effect of TMSS-PM. The reason is that the TMSS-PM SRM is driven by trapezoid current. There is a rapid change in the armature current when the rotor tooth passes by the corresponding stator tooth. Such rapid change in current brings a rapid change in the stator tooth and associated high iron loss. Therefore, a relatively higher iron loss can be found in TMSS-PM SRM.

Changes Made:

We have updated the manuscript by adding the illustrations of the optimized machine, flux density distribution, and the iron losses distribution. The related comments are also added (See Part B of Section VI)

2. **Reviewer's comment:**

The efficiency of the PM-excited and hybrid-excited SS-PM machines is given in Table 2 and Table 3. The efficiency variation of the final topologies is considerable. It will be interesting for the reader to know how the particular losses of each topology impact the efficiency. Please proceed to losses decoupling and comment the results. This revision could be addressed by providing numerical examples for the cases under study.

Response-2:

Thank you for your suggestion. The loss decoupling information of each topology is added in Tables 5 and 6.

Table 5
Loss decoupling information and efficiency of PM-excited SS-PM machines

Topology	TMSS-PM DSM	Stator-RMSS-PM machine	Dual-RMSS-PM machine	Halbach SS-PM machine
Rated copper loss (W)	50	50	50	50
Rated iron loss (W)	6.10	48.18	53.40	45.81
Efficiency (%)	92.74	94.82	97.14	96.50

Table 6
Loss decoupling information and efficiency of hybrid-excited SS-PM machines

Topology	TMSS-PM SRM	TMSS-PM DSM	TMSS-PM FSM	Dual-layer SS-PM machine	Skewed SS-PM machine
Rated copper loss (W)	50	50	50	50	50
Rated iron loss (W)	31.10	16.17	20.18	15.29	18.37

Efficiency (%)	79.77	84.88	91.98	90.72	91.23

In the comparative study section, all typical machine topologies are optimized under the same copper loss for a fair comparison. The copper loss for all topologies is set to be 50W in this case. According to the results, it can be found that the copper loss is relatively higher than the iron loss in the hybrid-excited machines. This is because the iron loss has been suppressed by the relieving-DC-saturation effect of TMSS PM. By contrast, for the PM-excited machines, the iron loss is comparable to the copper loss, except for the TMSS-PM DSM. The main reason for the low iron loss of TMSS-PM DSM is that the TMSS-PM DSM lacks a flux path when the rotor tooth is at the unaligned position with the stator tooth, which leads to a limited stator core flux vibration range and associated low iron loss.

Changes Made:

We have updated the manuscript by adding the loss decoupling information (See Part B of Section VI)

3. **Reviewer's comment:**

The length of Section VII has to be larger. The authors have to comment more sufficiently the future challenges and trends. The authors should discuss more the ideas for future research, the potential limitations of the existing manufacturing technology with respect of the specific machines type.

Response-3:

Thank you for your comments. To date, the RMSS PM machines and TMSS PM machines have been well investigated in recent decades, but there are relatively fewer publications focusing on CMSS PM machines. According to the results of recent publications and our comparative study, the RMSS PMs usually have a higher torque contribution than TMSS PMs. Under flux modulation effect, the RMSS PM machines can achieve a relatively high torque density but low power factor. As for TMSS PM machines, the TMSS PMs are usually designed with the DC field current to relieve the stator core saturation. Therefore, in spite of relatively lower torque density, the flux regulation ability can be improved by TMSS PMs. The CMSS PM machines can be seen as a new idea and machine category, which can inherit the advantages from both RMSS PM and TMSS PM machines. In spite of the strong repulsive force between PMs in the same slot, which causes high manufacturing difficulty, especially in Halbach SS-PM machines and Dual-layer SS-PM machines, a good potential solution is to use skewed SS PM to replace the original design. For example, as is shown in Fig. 68, by replacing the PMs with different magnetization directions with skewed PM, the manufacturing difficulty can be largely reduced.

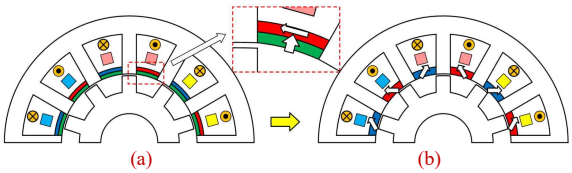

Fig. 68. The modification of CMSS PM machines. (a) Dual-layer SS-PM machine [109]. (b) Skewed SS-PM machine [110].

Apart from the above example, by combining existing TMSS PM machines and RMSS PM machines, there are various novel structures with skewed SS PM machines that can be studied for future work. For example, as is shown in Fig. 69, the first machine is an existing TMSS PM machine proposed in [55], and the second machine is a typical RMSS PM machine [102]. By combining the two machines, a novel structure can be generated with two working fields.

However, as the winding pattern of the original two machines can be different, how to design an appropriate armature winding to utilize the two working fields is left for future challenges. To design an appropriate slot pole combination so that the main working harmonics of the two fields have the same corresponding winding pattern. For example, as is presented in Fig (a), the pole pair number of DC and TMSS PM is 6, and the rotor teeth number is 11, under flux modulation effect, the pole pair number of the main working harmonic is 5. As for the RMSS PM, the pole pair number of equivalent MMF is 18, under flux modulation effect, the pole pair number of the main working harmonic is 7. In this design, there are only 6 slots left for armature winding, thus it can be seen as a 6-slot machine when designing the armature winding. The 5-pole-pair and 7-pole-pair air-gap harmonic have the same winding pattern for a 6-slot machine. **Therefore, the two working fields can be utilized at the same time.**

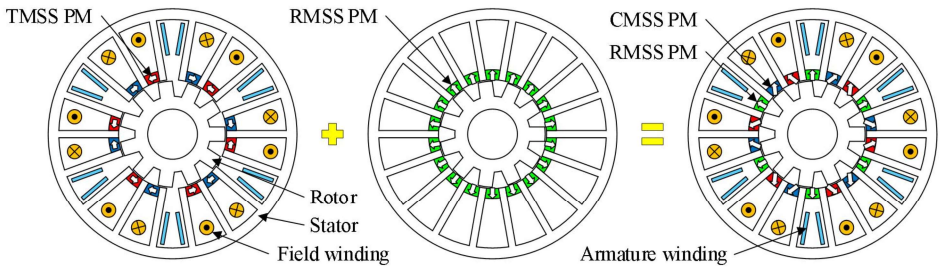

Fig. 69. Hints for new CMSS PM machines with skewed PM. (a) Existing TMSS PM machine [55]. (b) Typical RMSS PM machine [102]. (c) CMSS PM machine.

The above-mentioned CMSS PM machine is presented only as an example to show the reviewer how new CMSS PM machines with skewed PM can be generated. Therefore, the specific topology of this CMSS PM machine is not shown in the manuscript. By combining various existing TMSS PM machines with RMSS PM machines, a large number of novel CMSS PM machines can be studied and proposed for future research.

Changes Made:

We have updated the manuscript by rewriting Section VII and adding the relevant discussions.

4. **Reviewer's comment:**

The authors should discuss more the application field of the studied machine topologies. It would be very interesting for the reader to find out at which type of applications each machine topology is applied to. Is there a machine type that is more preferable by engineers when a specific application (or load profile) is considered? It is clear that the authors have studies a large number of already

published research works. So, it would be easy to proceed to a quantitative and qualitative analysis about this issue.

Response-4:

Thank you for your suggestion. To date, electrical machines have been widely used in many industrial applications, such as electrical vehicles (EV), hybrid electrical vehicles (HEV), unmanned electrical vehicles (UEV), robot joints, ship propelling systems, railway traction, aircraft, and wind power generation. Among them, the EV, HEV and wind power generation are the most heated target applications of SS-PM machines. There are relatively fewer publications on SS-PM machines in the other industrial applications.

In terms of which type of applications each machine topology is applied to, we have checked many recently-published SS-PM machines papers with specified target applications. And the results are summarized as follows. Some publications have not specified their target applications, which is not recorded in the following table.

Table 7
RECENT PUBLICATIONS WITH SS-PM MACHINES AND ASSOCIATED TARGET APPLICATION

Excitation source	Machine type	EV/HEV	Wind power generation	Aircraft	Traction application	Robotic system
Hybrid-excited	TMSS-PM SRM	[36-39]	/	[28][42]	/	/
	TMSS-PM DSM	[53][57][66][68]	[63][67]	/	/	/
	TMSS-PM FSM	/	[90-91]	[81]	/	/
	Dual-layer SS-PM machine	/	/	/	[109]	/
	Skewed SS-PM machine	[110]	/	/	/	/
PM-excited	TMSS-PM DSM	[77]	[58]	/	[76]	/
	Stator-RMSS-PM machine	/	/	/	/	[105]
	Dual-RMSS-PM machine	/	/	/	/	[102]
	Halbach SS-PM machine	/	/	/	[107]	/

The machines of EV and HEV require considerable efficiency, a wide speed range, and reliable mechanical strength. According to the table, the TMSS-PM SRM has wide applications in EV/HEV, and aircraft because of its simple structure, good mechanical reliability, and easy control. The TMSS-PM SRM is also more suitable for applications that low cost and high reliability are required, such as water pumps. However, due to the special driving circuit and control strategy, few papers use the TMSS-PM SRM as a generator. In terms of Hybrid-excited TMSS-PM DSM, it has a similar structure to TMSS-PM SRM, and therefore it also enjoys a simple structure and good mechanical reliability. Due to the difference in driving current, the control of TMSS-PM DSM is more complex than TMSS-PM SRM. However, TMSS-PM DSM has a higher torque density than TMSS-PM SRM, and the flexible DC current provides a good flux regulation ability and associated wide speed range. Therefore, the TMSS-PM DSM has been widely studied in EV, HEV and wind power generation applications. According to our comparative study, the hybrid-excited TMSS-PM FSM has higher torque production than the hybrid-excited TMSS-PM DSM, and it also has good flux regulation ability. However, due to the existence of the iron bridge, the TMSS-PM FSM faces higher mechanical manufacturing difficulties. As for the dual-layer SS-PM machine

and skewed SS-PM machine, there are still only a few references for these types of machines. However, as is discussed in **Response-3**, the skewed SS-PM machine is a promising potential candidate for future research. In terms of PM-excited SS-PM machines, the TMSS-PM DSMs have been studied in many industrial applications like EV, wind power generation, and traction systems. As for the dual-RMSS-PM machine and stator-RMSS-PM machine, they have a very high torque density but high iron loss and low power factor. Therefore, it is more suitable for low-speed and high-torque applications like robotic systems. There are only a few publications about the research on the Halbach RMSS-PM machine. But according to our comparative study, the torque production is even higher than that of the stator-RMSS-PM machine, therefore it can also be used in robotic systems, where low speed and high torque are required.

For clear demonstration, the sequence numbers of the references are the same as those in the manuscript. For the reviewer's convenience, we have listed all the related references as follows

Reference:

[28] S. Ullah, S. P. McDonald, R. Martin, M. Benarous and G. J. Atkinson, "A permanent magnet assist, segmented rotor, switched reluctance drive for fault tolerant aerospace applications," IEEE Trans. Ind. Appl., vol. 55, no. 1, pp. 298-305, Jan.-Feb. 2019.

[36] P. Andrada, B. Blanqué, E. Martínez and M. Torrent, "New hybrid reluctance motor drive," 2012 XXth International Conference on Electrical Machines, 2012, pp. 2689-2694.

[37] W. Ding, S. Yang, Y. Hu, S. Li, T. Wang and Z. Yin, "Design consideration and evaluation of a 12/8 high-torque modular-stator hybrid excitation switched reluctance machine for EV applications," IEEE Trans. Ind. Electron., vol. 64, no. 12, pp. 9221-9232, Dec. 2017.

[38] M. A. J. Kondelaji and M. Mirsalim, "Double-stator PM-assisted modular variable reluctance motor for EV applications," 2018 9th Annual Power Electronics, Drives Systems and Technologies Conference (PEDSTC), 2018, pp. 236-240.

[39] K. Nakamura, K. Murota and O. Ichinokura, "Characteristics of a novel switched reluctance motor having permanent magnets between the stator pole-tips," 2007 European Conference on Power Electronics and Applications, 2007, pp. 1-5.

[42] S. Ullah, S. P. McDonald, R. Martin and G. J. Atkinson, "A permanent magnet assisted switched reluctance machine for more electric aircraft," 2016 XXII International Conference on Electrical Machines (ICEM), 2016, pp. 79-85

[53] Y. Mao, S. Niu and Q. Wang, "Design and optimization of a slot-PM-assisted doubly-salient machine based on saturation assuaging," Chin. J. Electr. Eng., vol. 7, no. 3, pp. 65-72, Sept. 2021.

[57] Y. Gong, K. T. Chau, J. Z. Jiang, C. Yu and W. Li, "Design of doubly salient permanent magnet motors with minimum torque ripple," IEEE Trans. Magn., vol. 45, no. 10, pp. 4704-4707, Oct. 2009.

[58] J. Jiang, X. Zhang, S. Niu and X. Zhao, "A novel doubly-fed doubly-salient machine with DC-saturation-relieving structure for wind power generation," IET Renew. Power Gener., vol. 15, no. 9, pp. 2042-2051, July 2021.

[63] Z. Li and S. Niu, " Design and analysis of a novel claw-shaped modular stator relieving-DC-saturation doubly salient machine with 3D complementary magnetic circuit," IET Renew. Power Gener..

[66] X. Zhao, S. Niu, X. Zhang and W. Fu, "A new relieving-DC-saturation hybrid excitation Vernier machine for HEV starter generator application," IEEE Trans. Ind. Electron., vol. 67, no. 8, pp. 6342-6353, Aug. 2020.

[67] S. Wang, S. Niu and W. Fu, "Comparative study of relieving-DC-saturation hybrid excited Vernier machine with different rotor pole designs for wind power generation," IEEE Access, vol. 8, pp. 198900-198911, 2020.

[68] X. Zhao, S. Niu and W. Fu, "A new modular relieving-DC-saturation Vernier reluctance machine excited by zero-sequence current for electric vehicle," IEEE Trans. Magn., vol. 55, no. 7, pp. 1-5, July 2019, Art no. 8104605.

[76] Q. Wang, P. Igic, S. Niu and J. Wang, "A new dual-PM excited doubly salient machine for traction applications," 2020 2nd IEEE International Conference on Industrial Electronics for Sustainable Energy Systems (IESES), 2020, pp. 275-279.

[77] Q. Wang, M. Ordonez, J. Wang, M. A. Saket and R. Shafaei, "A novel dual slot permanent magnet machine with complementary rotors for electric vehicle propulsion," 2019 IEEE 28th International Symposium on Industrial Electronics (ISIE), 2019, pp. 221-225

[81] H. Cherif, S. Affi, J. Belhadj, S. Hlioui and M. Gabsi, "Design and performance investigation of small-scale wind turbine system based on hybrid excited flux switching machine," 2019 International Conference on Advanced Systems and Emergent Technologies (IC_ASET), 2019, pp. 375-380.

[90] N. A. Jafar and E. Sulaiman, "Design analysis of 12S-10P hybrid-excitation flux-switching permanent-magnet machines for hybrid electric vehicle," 2014 IEEE 8th International Power Engineering and Optimization Conference (PEOCO2014), 2014, pp. 308-312

[91] E. Sulaiman, T. Kosaka and N. Matsui, "High power density design of 6-slot–8-pole hybrid excitation flux switching machine for hybrid electric vehicles," IEEE Trans. Magn., vol. 47, no. 10, pp. 4453-4456, Oct. 2011.

[102] T. Sheng, "Design, analyze and control of novel stator-PM electrical machines," Ph.D. thesis, Department of Electrical Engineering, The Hong Kong Polytechnic University, Hong Kong, China, 2018.

[105] S. Niu, T. Sheng, X. Zhao and X. Zhang, "Operation principle and torque component quantification of short-pitched flux-bidirectional-modulation machine," IEEE Access, vol. 7, pp. 136676-136685, 2019.

[107] K. Xie, D. Li, R. Qu, Z. Yu, Y. Gao and Y. Pan, "Analysis of a flux reversal machine with quasi-halbach magnets in stator slot opening," IEEE Trans. Ind. Appl., vol. 55, no. 2, pp. 1250-1260, March-April 2019.

[109] X. Zhao, S. Niu, X. Zhang and W. Fu, "Flux-modulated relieving-DC-saturation hybrid reluctance machine with synthetic slot-PM excitation for electric vehicle in-wheel propulsion," IEEE Trans. Ind. Electron., vol. 68, no. 7, pp. 6075-6086, July 2021

[110] S. Wang, S. Niu, X. Zhao and W. Fu, "Novel DC-saturation-relieving hybrid reluctance machine with skewed permanent magnets for electric vehicle propulsion," IEEE Trans. Magn.

Changes Made:

We have updated the manuscript by adding the discussion about the application of each machine. (See Part C of Section VI)

5. **Reviewer's comment:**

I suggest the Conclusions section to be re-written. Its length has to be larger.

Response-5:

Thank you for your suggestion. In the original manuscript, some conclusions have been summarized based on the comparative study among 9 typical SS-PM machines in Part B of Section VI. We have followed the reviewer's suggestion to add some detailed explanation of the conclusions. The following conclusions are referenceable for the reader's consideration when designing SS-PM machines or developing novel SS-PM structures under different target applications and load profiles.

1. The RMSS PMs usually have a higher torque contribution than the TMSS PMs. The main reason is that nearly all the flux of RMSS PM can enter the air gap directly, which produces an effective flux in the armature winding and associated torque production. The stator-RMSS-PM machine and dual-RMSS-PM machine are typical examples of the above statement, whose torque productions are much higher than that of the TMSS-PM machine in the comparative study. However, the main limitation of RMSS PM is that the stator core adjacent to RMSS PMs is easy to saturate because of the leakage flux of RMSS PM. Therefore, they are suitable for low-speed and high-torque applications like robotic systems.

2. The TMSS PMs are usually designed with DC field current, such as TMSS-PM SRM, DSM, and FSM. The common feature of them is that the magnetization of TMSS PM is intentionally designed opposite to that of DC excitation current so that the stator core can be relieved. Therefore, a higher excitation current can be applied, and torque density can be improved to some extent, especially at high load conditions. Besides, as the vibration range of excitation current can be enlarged by the TMSS-PM machine, a wide speed range can be obtained. Therefore, they are suitable for applications like EV, HEV, and wind power generation.

3. In terms of the CMSS-PM machine, it can be seen as a special machine category, which combines the features of TMSS-PM and RMSS-PM machines. Therefore, CMSS PM is a promising candidate for future research as a tradeoff between TMSS PM and RMSS PM. However, the operation principle, machine performance, and target application of different CMSS PM machines can be divisive. For Halbach SS-PM machine, it has the highest torque density among the stator PM machines in our comparative study. However, the torque per PM usage is not satisfactory and the repelling forces among the PMs in the same slot opening restrict its application. Therefore, Halbach SS PM is suitable when very high torque density is required but the cost is high accordingly. For dual-layer and skewed PM machines, they can be seen as the combination of the hybrid-excited TMSS-PM machine and the stator-RMSS-PM machine, therefore, the relieving-dc-saturation effect of TMSS PM and torque enhancement of RMSS PM can be achieved simultaneously.

Changes Made:

We have updated the manuscript by adding the contents of the conclusion section (See Section VIII).

Reply to Reviewer 2:

1. **Reviewer's comment:**

The stator slot-opening permanent magnet machines (SS-PMM) are classed into three categories, namely, the tangentially magnetized SS-PMM, the radially magnetized SS-PMM, and the compound magnetized SS-PMM. The performance evaluation and comparative study of these machines are presented. This is an overview paper.

Response-6:

Thank you for your effort in reviewing our manuscript. In this manuscript, the TMSS-PM machines, RMSS-PM machine and CMSS-PM machines are introduced and discussed in Section III to Section V, respectively. In Section VI, 9 aforementioned typical structures are selected and a comparative study among them is presented. For fair comparison, all machines are optimized by Genetic Algorithm under the maximum size, airgap length and copper loss. The following conclusions can be drawn from previous comparative study.

1. The RMSS PMs usually have a higher torque contribution than the TMSS PMs. The main reason is that nearly all the flux of RMSS PM can enter the air gap directly, which produces an effective flux in the armature winding and associated torque production. The stator-RMSS-PM machine and dual-RMSS-PM machine are typical examples of the above statement, whose torque productions are much higher than that of the TMSS-PM machine in the comparative study. Therefore, they are suitable for low-speed and high-torque applications like robotic systems. However, the main limitation of RMSS PM is that the stator core adjacent to RMSS PMs is easy to saturate because of the leakage flux of RMSS PM.

2. The TMSS PMs are usually designed with DC field current, such as TMSS-PM SRM, DSM, and FSM. The common feature of them is that the magnetization of TMSS PM is intentionally designed opposite to that of DC excitation current, so that the stator core can be relieved. Therefore, a higher excitation current can be applied, and torque density can be improved to some extent, especially at high load conditions. Besides, as the vibration range of excitation current can be enlarged by the TMSS PM, a wide speed range can be obtained. Therefore, they are suitable for wide-speed-range applications like EV, HEV, and wind power generation.

3. In terms of the CMSS-PM machine, it can be seen as a special machine category, which combines the features of TMSS-PM and RMSS-PM machines. Therefore, CMSS PM is a promising candidate for future research as a tradeoff between TMSS PM and RMSS PM. However, the operation principle, machine performance, and target application of different CMSS PM machines can be divisive. For Halbach SS-PM machine, it has the highest torque density among the stator PM machines in our comparative study. However, the torque per PM usage is not satisfactory and the repelling forces among the PMs in the same slot opening restrict its application. Therefore, Halbach SS PM is suitable when very high torque density is required but the cost is high accordingly. For dual-layer and skewed PM machines, they can be seen as the combination of a hybrid-excited TMSS-PM machine and the stator-RMSS-PM machine. Therefore, the relieving-dc-saturation effect of TMSS PM and torque enhancement of RMSS PM can be achieved simultaneously.

Reply to Reviewer 3:

1. **Reviewer's comment:**

It seems that the main logic in Section III to V is to introduce the operation principle of each machine topology. However, it lacks in-depth comparative analysis among these topologies. Therefore, it has weak reference value for this research field. It is suggested to emphasize the key points in one type of machine topology.

Response-7:

Thanks for your comment. In the original manuscript, from Section III to V, the TMSS-PM machines, RMSS-PM machines, and CMSS-PM machines are introduced, respectively. To give an in-depth comparative comparison between various SS-PM machines, **a quantitative performance evaluation and comparative study of SS-PM machines has been presented in Section VI of the original manuscript.** To give a fair comparison, there are 9 typical SS-PM machines selected from the above sections and optimized by the Genetic Algorithm under the same dimensional size and copper loss. During the optimization, maximizing the average torque and minimizing the torque ripple are set to be the optimization objectives. Based on the optimized models, the electromagnetic performances of different machine topologies are compared and discussed. The schematic structures of the 9 TMSS-PM machines are presented in Fig. 70 and Fig. 71 (Numbered as Fig. 44 and Fig. 45 in the original manuscript). The Pareto frontier of the Genetic algorithm of each model is presented in Fig. 72 (Numbered as Fig. 46 in the original manuscript).

Taking torque ripple less than 10% as the essential condition for real applications, the model with the highest average torque is selected as the optimal design. The detailed design parameters of each optimal model are presented in the Appendix of the response letter. The electromagnetic performances are evaluated in Table 8 (Numbered as Table 2 and Table 3 in the original manuscript)

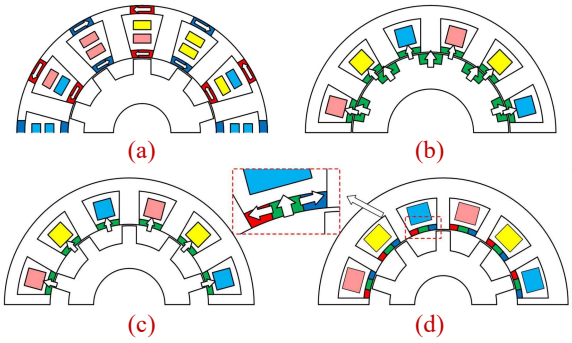

Fig. 70. The PM-excited machines. (a) TMSS-PM DSM.[76] (b) Dual-RMSS-PM machine [105]. (c) Stator-RMSS-PM machine [102]. (d) Halbach SS-PM machine [107].

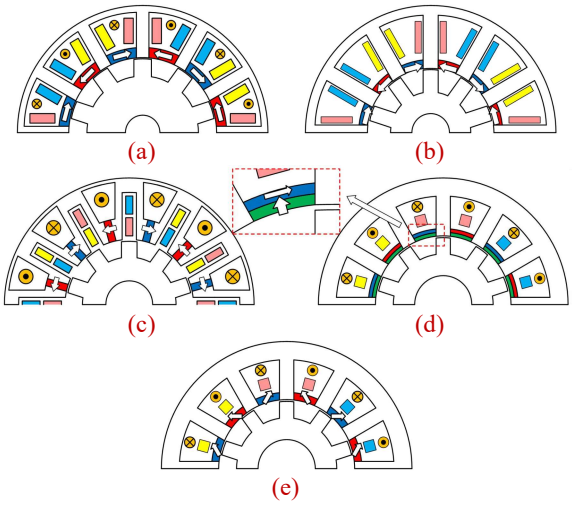

Fig. 71. The hybrid-excited machines. (a) TMSS-PM DSM [51]. (b) TMSS-PM SRM [39]. (c) TMSS-PM FSM [91]. (d) Dual-layer SS-PM machine [109]. (e) Skewed SS-PM machine [110].

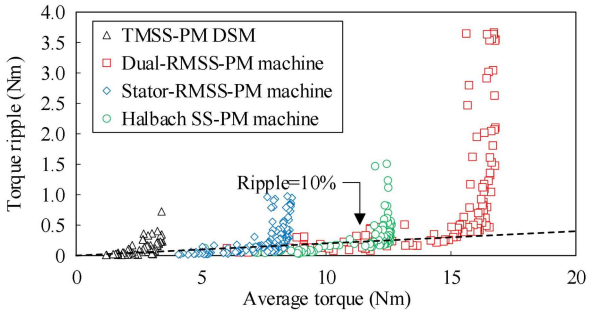

(a)

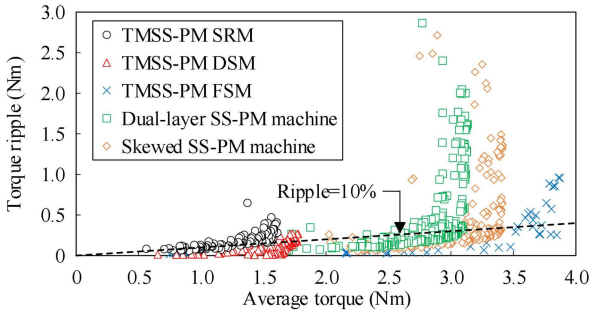

(b)

Fig. 72. The Pareto frontier of each generation in Genetic Algorithm. (a) PM-excited machines. (b) Hybrid-excited machines.

Table 8
Electromagnetic performances of SS-PM machines, IPM and PMa-SynRMs

Excitation type	Hybrid-excited SS-PM machines					PM-excited SS-PM machines			
Topology	TMSS-PM SRM	TMSS-PM DSM	TMSS-PM FSM	Dual-layer SS-PM machine	Skewed SS-PM machine	TMSS-PM DSM	Stator-RMSS-PM machine	Dual-RMSS-PM machine	Halbach SS-PM machine
Torque density (kNm/m^3)	3.89	4.52	9.78	7.76	8.65	8.71	21.85	42.68	32.14
Torque ripple (%)	10.36	10.09	6.90	9.28	9.97	10.26	9.90	8.92	4.06
PM volume (m^3)	1.29×10^{-5}	1.04×10^{-5}	3.12×10^{-5}	2.71×10^{-5}	2.58×10^{-5}	3.07×10^{-5}	2.22×10^{-5}	3.62×10^{-5}	4.31×10^{-5}
Torque per PM usage (kNm/m^3)	118.49	171.25	123.16	112.55	131.80	111.53	387.31	463.42	292.69
power factor	/	0.496	0.935	0.779	0.822	0.839	0.429	0.709	0.647
Efficiency (%)	79.77	84.88	91.98	90.72	91.23	92.74	94.82	97.14	96.50

The further detailed machine performance comparisons, including the **torque-speed characteristics, iron loss, efficiency, power factor, mechanical robustness, manufacturing complexity, power-electronics drive, control methods, and demagnetization risk**, are suggested by **Reviewer 4** and thus they are presented in the **Response 13** in detail.

Changes Made:

We have updated the manuscript by highlighting the comparison between the 9 machines and adding the further comparison contents (See Part C of Section VI).

2. **Reviewer's comment:**

The potential application of stator slot-opening PM machine (SS-PMM) is electrical vehicle. However, this paper doesn't give any comparison between SS-PMM and the existing IPMs or PMa-SynRMs. Therefore, the advantages in torque/power density is not convincing.

Response-8:

Thanks for your comments. We believe the reviewer's concern on advantages in torque/power density of SS-PM machine is referring to the sentence in the abstract: "In the past few decades, the **stator permanent magnet (PM) machines** have attracted much research attention because of their reliable rotor structure, **high power density**, wide speed range, and strong fault-tolerant ability."

Generally speaking, it is admitted that **the stator PM machines usually have relatively lower torque density than the rotor PM machines**, which includes the IPMs and PMa-SynRMs that the reviewer has mentioned. This is because the stator-PM flux is stationary while the rotor-PM flux is rotary. However, as is pointed out in various references, the stator PM machines have irreplaceable advantages over stator PM machines. For example, the rotor PM has to suffer from centrifugal force, which brings challenges to the mechanical strength of the rotor, especially under high-speed conditions [A1-A3]. By comparison, since there is no PM material assigned to the rotor side, the rotor consisting of iron core only can endure much higher centrifugal force than the rotor with PM materials. **Therefore, the rotation speed of stator PM machines can be designed**

much higher than the rotor PM machines. Another main advantage lies in the heat dissipation issue. As is pointed out in various references [A4-A7], the rotor has poorer thermal condition than the stator. Therefore, considering the demagnetization risk of the PM material, the rotor speed of rotor-PM machines would be limited to constrain the iron loss or the excitation current should be limited to constrain the copper loss. Both actions would limit the power density of the rotor PM machines. Therefore, in our original manuscript, **it would be safe to address power density (rather than torque density) as one of the advantages of stator PM machines.**

As is requested by the reviewer, to give a quantitative comparison between various SS-PM machines with IPMs and PMa-SynRMs, in this response letter, we quote the design data of IPMs and PMa-SynRMs from existing references [A8-A9] and compare them with the data of SS-PM machines in our manuscript. The data are listed in Table 9:

Table 9

Electromagnetic performances of SS-PM machines, IPM and PMa-SynRMs

Excitation type	Hybrid-excited SS-PM machines					PM-excited SS-PM machines					
Topology	TMSS-PM SRM	TMSS-PM DSM	TMSS-PM FSM	Dual-layer SS-PM machine	Skewed SS-PM machine	TMSS-PM DSM	Stator-RMS S-PM machine	Dual-RMSS-PM machine	Halbach SS-PM machine	IPM [A8]	PMa -SynRM [A9]
Machine volume (m^3)	3.927×10^{-4}	3.927×10^{-4}	3.927×10^{-4}	3.927×10^{-4}	3.927×10^{-4}	3.927×10^{-4}	3.927×10^{-4}	3.927×10^{-4}	3.927×10^{-4}	2.79×10^{-3}	6.43×10^{-4}
Rated average torque (Nm)	1.5265	1.7743	3.8424	3.049	3.3971	3.42	8.581	16.7616	12.6228	77.3	16
Torque density (kNm/m^3)	3.89	4.52	9.78	7.76	8.65	8.71	21.85	42.68	32.14	27.70	24.87

As is presented in Table 9, the torque density of different SS-PM machines can be distinct. Some SS-PM machines have relatively low torque density while others have high torque density. The dual-RMSS-PM machine has a higher torque density than the IPM and PMa-SynRM because the torque of the Dual-RMSS-PM machine is contributed by both SS PM and rotor PM. The Stator-RMSS-PM machine and Halbach SS-PM machine have comparable torque density with the IPM and PMa-SynRM. However, a relatively higher rotor speed can be applied in the Stator-RMSS-PM machine and Halbach SS-PM machine because the rotor consists of the iron core only. Therefore, they are very promising candidates for high power density applications.

Reference

[A1] T. Wang, F. Wang, H. Bai and J. Xing, "Optimization design of rotor structure for high speed permanent magnet machines," *2007 International Conference on Electrical Machines and Systems (ICEMS)*, 2007, pp. 1438-1442.

[A2] Z. Kolondzovski, A. Arkkio, J. Larjola and P. Sallinen, "Power limits of high-speed permanent-magnet electrical machines for compressor applications," *IEEE Trans. Energy Convers.*, vol. 26, no. 1, pp. 73-82, March 2011.

[A3] W. Zhao, M. Cheng, W. Hua, H. Jia and R. Cao, "Back-emf harmonic analysis and fault-tolerant control of flux-switching permanent-magnet machine with redundancy," *IEEE Trans. Ind. Electron.*, vol. 58, no. 5, pp. 1926-1935, May 2011.

[A4] Z. Q. Zhu, H. Hua, D. Wu, J. T. Shi and Z. Z. Wu, "Comparative study of partitioned stator machines with different PM excitation stators," *IEEE Trans. Ind. Appl.*, vol. 52, no. 1, pp. 199-208, Jan.-Feb. 2016.

[A5] J. Shen and W. Fei, "Permanent magnet flux switching machines — topologies, analysis and optimization," *4th International Conference on Power Engineering, Energy and Electrical Drives*, 2013, pp. 352-366.

[A6] W. Zhao, M. Cheng, X. Zhu, W. Hua and X. Kong, "Analysis of fault-tolerant performance of a doubly salient permanent-magnet motor drive using transient cosimulation method," *IEEE Trans. Ind. Electron.*, vol. 55, no. 4, pp. 1739-1748, April 2008.

[A7] R. Cao, C. Mi and M. Cheng, "Quantitative comparison of flux-switching permanent-magnet motors with interior permanent magnet motor for EV, HEV, and PHEV applications," *IEEE Trans. Magn.*, vol. 48, no. 8, pp. 2374-2384, Aug. 2012.

[A8] Y. V. Zubkov, Y. A. Makarichev and Y. N. Ivannikov, "Comparison of surface-mounted permanent magnet and interior-mounted permanent magnet starters for gas turbine engines electrical start," *2019 International Conference on Electrotechnical Complexes and Systems (ICOECS)*, 2019, pp. 1-5.

[A9] D. Ngo, M. Hsieh and T. A. Huynh, "Torque Enhancement for a Novel Flux Intensifying PMa-SynRM Using Surface-Inset Permanent Magnet," *IEEE Trans. Magn.*, vol. 55, no. 7, pp. 1-8, July 2019, Art no. 8106108.

Changes Made:

We have updated the manuscript by adding the comparison between SS-PM machines and IPMs / PMa-SynRMs and adding related discussion (See Part B of Section VI)

3. **Reviewer's comment:**

In Page 3, Line 42, please delete the irrelevant content。

Response-9:

Thanks for pointing it out. We are sorry for this mistake. We have deleted the irrelevant content.

Changes Made:

We have updated the manuscript by deleting the irrelevant content (See Part A of Section III).

4. **Reviewer's comment:**

Actually, the operation principle of TMSS-PM machine also can be explained based on flux modulation theory. So, why do you put relevant analytical content in Section IV, Page 17, rather than before Section III?

Response-10:

Thanks for your question. In the original manuscript, we have laid our emphasis on the introduction of **the flux from the SS PM** in Sections III and IV. In Section III, there are some TMSS-PM machines whose working principle of SS PM cannot be explained from the air-gap flux modulation theory, **because the flux from SS PM does not go through the air gap** if leakage flux is neglected. The examples of TMSS PM that cannot be explained by the air-gap flux modulation principle are presented in Fig. 73 for the reviewer's convenience. The common feature of these machine topologies is that the TMSS PM is short-circuited in the magnetic circuit by the stator yoke or stator iron bridge. The main purpose of adopting TMSS PM is to relieve the stator

saturation. The flux direction of TMSS PM is intentionally designed to be opposite to that of excitation current, so that stator core saturation can be relieved. Therefore, to clearly present the working principle of TMSS PM to the reader, in the original manuscript, the principle of TMSS PM is explained from the perspective of the magnetic circuit.

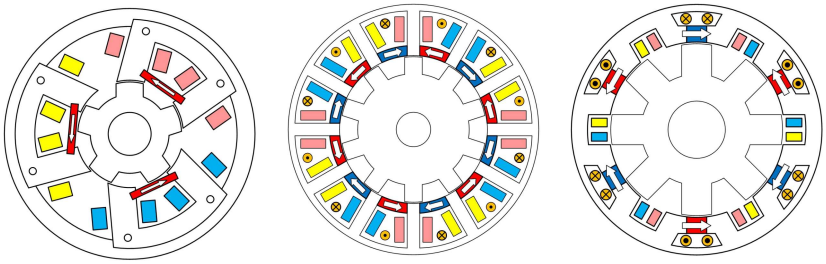

(a) (b) (c)

Fig. 73. Machine topologies where the flux of TMSS PM does not go through air gap. (a) Typical TMSS-PM SRM [35] (b) Typical TMSS-PM DSM [51] (c) TMSS-PM FSM [91].

In Section IV, as the SS PM is radially magnetized, the **flux from RMSS PM is bound to go through the air gap**. Therefore, the working principle of RMSS-PM machines is introduced from the perspective of air-gap flux modulation theory.

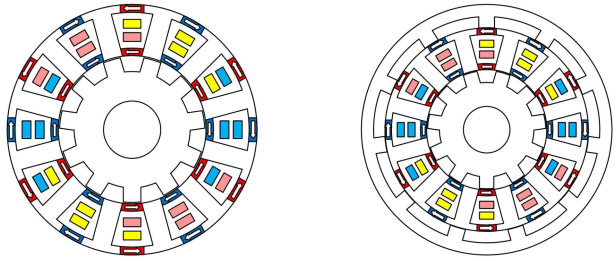

(a) (b)

Fig. 74. The typical topologies where the flux of TMSS PM goes through the air gap. (a) Single rotor topology [76]. (b) Dual rotor topology [77].

However, it is admitted that there are some TMSS-PM machine topologies whose flux of TMSS PM does go through the air gap. The key feature of these topologies is that the flux of TMSS PM is not short-circuited in the magnetic circuit through the stator yoke. Two typical examples are presented in Fig. 74. In the original manuscript, we only explain them from the perspective of the magnetic circuit. Therefore, **in the revised manuscript, we have followed the reviewer's suggestion and added the principle introduction from the perspective of air-gap field modulation theory**. As is shown in Fig. 74, it is obvious that the yoke PM and the TMSS PM have the same air-gap magnetomotive force (MMF) waveform. Thus the introduction of TMSS PM can improve the amplitude of air-gap MMF of the DSM. The air gap flux density from the stator PM (B_{PM}) can be expressed as:

$$B_{PM}(\theta,t)=\sum_{i=1}^{+\infty}\sum_{j=-\infty}^{+\infty}B_{S(i,j)}cos\left[\left(iN_p+jN_r\right)\theta-jN_r\omega_{me}t\right] \quad (1)$$

where θ is the mechanical angular position, $B_{PM}(\theta,t)$ is the air gap flux from TMSS PM and yoke PM, ω_{me} is the rotor mechanical speed, $B_{S(i,j)}$ is the amplitude of air-gap field harmonic, N_r is the

rotor teeth number, and the N_p is the pole pair number of the excitation field. In this typical structure, N_p should satisfy:

$$N_p = N_s / 2 \tag{2}$$

where N_s is the stator slot number. Based on (1), the order number, and rotation speed of each air gap field harmonics can be summarized as:

$$\begin{cases} \theta_{(i,j)} = \left| iN_p + jN_r \right| \\ \omega_{(i,j)} = \dfrac{jN_r\omega_{me}}{\left| iN_p + jN_r \right|} \end{cases} \tag{3}$$

To obtain a higher gearing ratio, the main working harmonic is selected as the case when $i=1$, $j=-1$. The other harmonics with $j=\pm 1$ are also working harmonics, but their contribution is relatively smaller. Therefore, the armature winding pole pair number (P_{aw}) should be designed according to the main working harmonic order as the following equation:

$$P_{aw} = \left| N_{slot} - N_r \right| \tag{4}$$

Changes Made:

We have updated the manuscript by adding the introduction of the flux modulation principle of the PM-excited TMSS PM machines (See Part B of Section III)

5. **Reviewer's comment:**

In Section III, it is suggested to compare the performance between switch reluctance operating type and synchronous operating type (such as DSM), since these two types are similar in topologies.

Response-11:

Thanks for your suggestion. In the original manuscript, we do have mentioned the comparative study between the SRM and DSM at the beginning of Part B of Section III.

"Despite various above-mentioned merits of SRM, SRMs suffer from relatively high torque ripple due to the half-cycle-conducting operation principle [44]. The double salient machine (DSM) is an alternative stator PM machine design to overcome this problem because some comparative studies have pointed out that the DSM has higher torque performance than SRM [45-46]."

Although the SRM and DSM that the references [45-46] have studied are without TMSS PM. Their conclusion is still referenceable that DSM has higher torque production than SRM. This is because the introduction of TMSS PM does not change the reluctance of the magnetic circuit in DSM and SRM, and it also does not change the basic torque generation principle of DSM and SRM. Therefore, it can be predicted that the TMSS-PM DSM has higher torque performance than TMSS-PM SRM.

In Section VI, a comprehensive comparative study among various SS-PM machines is carried out in the original manuscript. The TMSS-PM DSM and TMSS-PM SRM are also included. As is

presented in Fig. 75 (numbered as Fig. 46(b) in the original manuscript), the TMSS-PM DSMs have higher average torque and lower torque ripple than TMSS-PM SRMs. This result agrees with the above-mentioned prediction well.

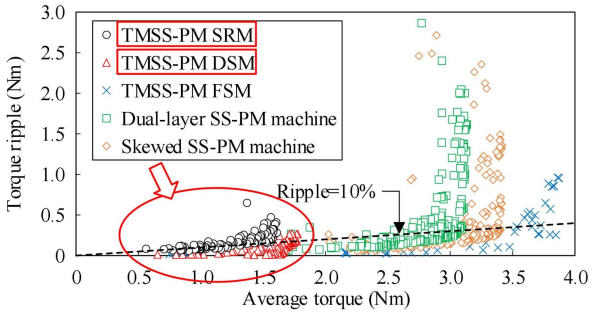

Fig. 75. The Pareto frontier of hybrid-excited machines of each generation in Genetic Algorithm.

Table 10

Electromagnetic performances of hybrid-excited SS-PM machines

Topology	**TMSS-PM SRM**	**TMSS-PM DSM**	TMSS-PM FSM	Dual-layer SS-PM machine	Skewed SS-PM machine
Torque density (kNm/m^3)	**3.89**	**4.52**	9.78	7.76	8.65
Torque ripple (%)	**10.36**	**10.09**	6.90	9.28	9.97
PM volume (m^3)	**1.29×10^{-5}**	**1.04×10^{-5}**	3.12×10^{-5}	2.71×10^{-5}	2.58×10^{-5}
Torque per PM usage (kNm/m^3)	**118.49**	**171.25**	123.16	112.55	131.80
power factor	/	**0.496**	0.935	0.779	0.822
Efficiency (%)	**79.77**	**84.88**	91.98	90.72	91.23

Changes Made:

We have updated the manuscript by highlighting the comparison between the TMSS-PM SRM and TMSS-PM DSM (See Part B of Section III)

6. **Reviewer's comment:**

Please add some prototype figures for some of the machines.

Response-12:

Thanks for your suggestion. We have followed the reviewer's suggestion and added the prototype figures from the corresponding references.

Changes Made:

We have updated the manuscript by adding the prototype figures.

Reply to Reviewer 4:

1. **Reviewer's comment:**

This is a review paper on research works published in the field of PM machines with PM pieces installed in stator slot-opening regions. It is interesting for me as a reader to get detailed information and comprehensive comparisons on the rated and maximum short-duration torque-speed characteristics, efficiency and power-factor maps, reliablity and robustness of the structure, manufacturing cost and complexity, complexity of the power-electronics drive and control methods, demagnetization risk, etc. This is because the most attractive application of the studied topologies is the electric motor of the electric vehicle. Hence, please include these items in your studies in the revised paper.

Response-13:

Thanks for your suggestion. A further comprehensive comparison among the 9 typical structures is presented as follows.

1. Rated and maximum short-duration torque-speed characteristics

In this part, the torque-speed characteristics of the 9 machines are predicted. The DC voltage supply of **PM-excited machines is set to be 350V** while the supply is **100V for hybrid-excited machines**. As the induced voltage is in direct proportion to the number of turns of armature winding, for a fair comparison, the number of turns of armature winding is determined by the following equation.

$$N_t = \begin{cases} \dfrac{A_{slot} k_{sff}}{A_{cond}}, \ for\ single-layer\ winding \\ \dfrac{A_{slot} k_{sff}}{2 A_{cond}}, \ for\ double-layer\ winding \end{cases}$$

where N_t is the number of turns, A_{slot} is the slot area, k_{sff} is the slot filling factor (estimated to be 0.5), A_{cond} is the conductor area (assumed to be 2 mm^2). The **rated copper loss** of all machines are set to be **50W**, and the copper losses assigned to AC and DC current are set to be the same. For the maximum short-duration condition, according to the design experience, the current density can be tripled. Therefore, the copper loss can be set to be 9 times of rated value if the coil resistance is assumed to be unchanged. Thus, the **copper loss of maximum short-duration condition** is set to be **450W** for all machines. The torque-speed characteristics are presented in Fig. 76 and Fig. 77.

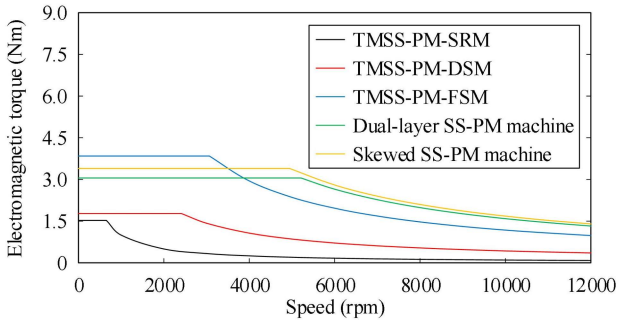

(a)

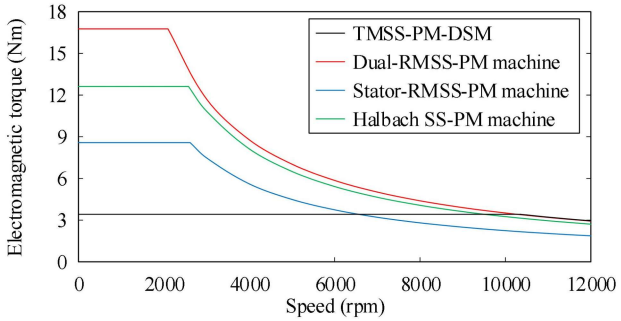

(b)

Fig. 76. Predicted torque-speed characteristics under rated current. (a) Hybrid-excited machines. (b) PM-excited machines.

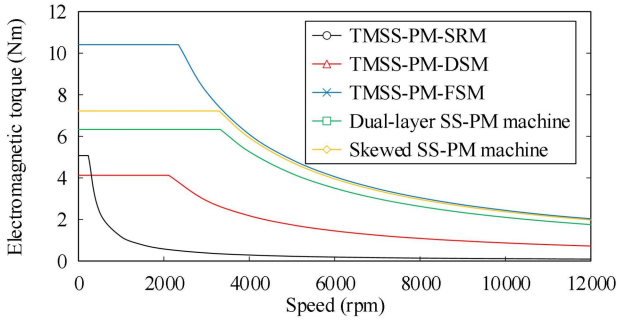

(a)

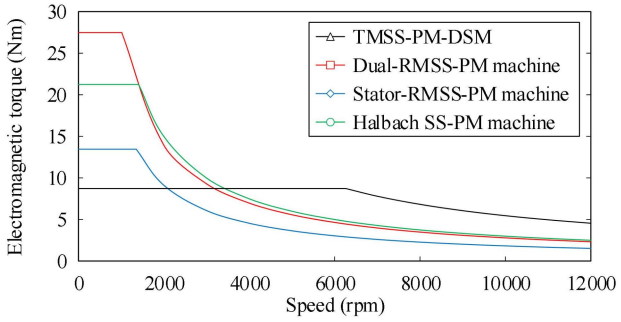

(b)

Fig. 77. Predicted maximum short-duration torque-speed characteristics. (a) Hybrid-excited machines. (b) PM-excited machines.

2. Rated and maximum short-duration iron loss and efficiency characteristics

This part evaluates the iron loss and the associated efficiency under rated and short-duration conditions. The rated and short-duration copper losses are set to be 50W and 450 W, respectively. As is presented in Fig. 78 and Fig. 79, among the hybrid-excited machines, the TMSS-PM SRM, which is driven by trapezoidal wave current, has much higher iron loss than the other machines. This is mainly because the vibration of flux in the stator tooth of TMSS-PM SRM can be very rapid when the driving current is at rising edge or falling edge. In terms of PM-excited machines, the TMSS-PM DSM has a significantly lower iron loss than the other machines. This is because the flux vibration range in the stator core of TMSS-PM DSM is narrower than those of other machines as discussed in Part B of Section III.

As is presented in Fig. 80 and Fig. 81, generally speaking, the efficiency increases as rotation speed at the low-speed region, but declines as the speed at the high-speed region for most machines. All machines show relatively lower efficiency when the copper loss is increased from the rated value to the short-duration value. In hybrid-excited machines, the TMSS-PM FSM has the highest efficiency over a wide speed range because of the highest torque production. By contrast, the efficiency of TMSS-PM SRM is not satisfying, especially at the high-speed region, because of the lowest torque and high iron loss. In PM-excited machines, TMSS-PM DSM has the lowest efficiency because of the lowest torque production, but the efficiency in the high-speed region exceeds the others because of the lowest iron loss.

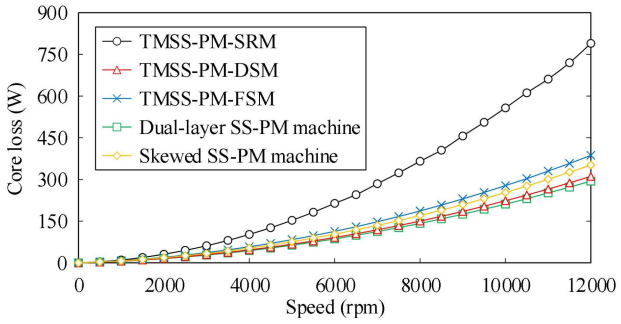

(a)

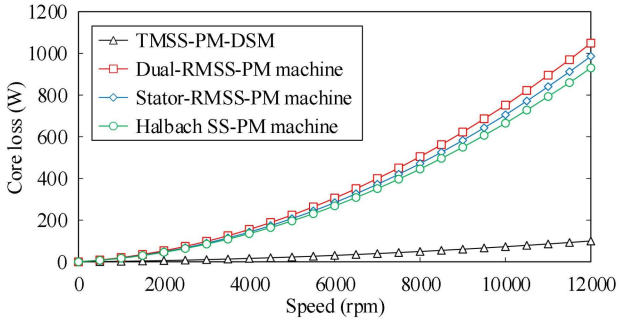

(b)

Fig. 78. iron loss under rated current. (a) Hybrid-excited machines. (b) PM-excited machines.

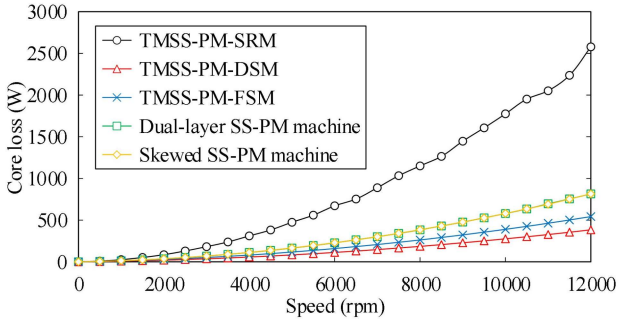

(a)

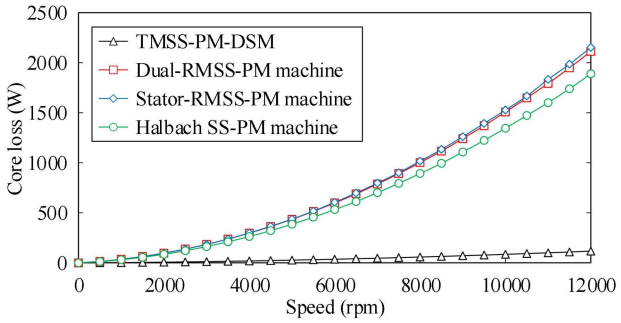

(b)

Fig. 79. Iron loss under short-duration current. (a) Hybrid-excited machines. (b) PM-excited machines.

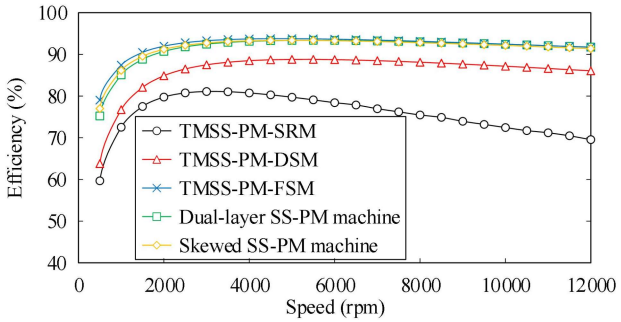

(a)

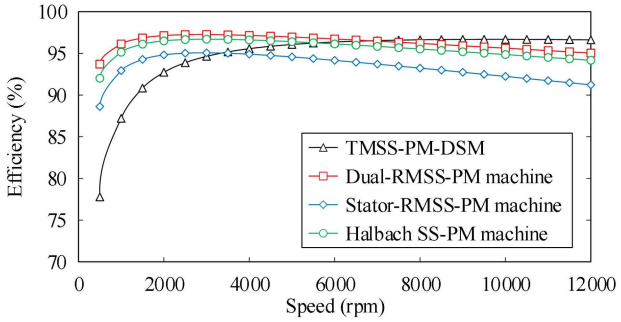

(b)

Fig. 80. Efficiency under rated current. (a) Hybrid-excited machines. (b) PM-excited machines.

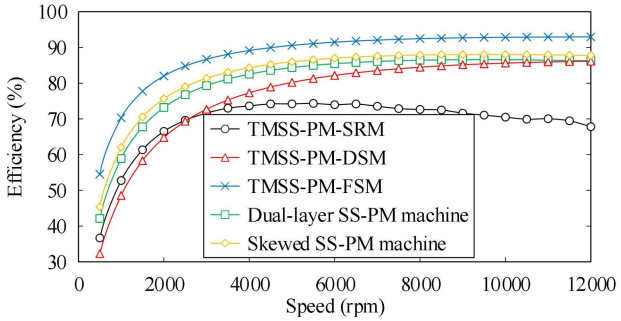

(a)

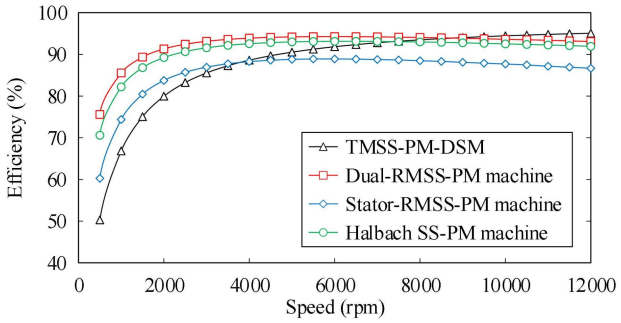

(b)

Fig. 81. Efficiency under short-duration current. (a) Hybrid-excited machines. (b) PM-excited machines.

3. Power factor

The power factors under various excitation conditions for 9 machines are presented in Fig. 82. In hybrid-excited machines, the TMSS-PM FSM has the highest power factor. The TMSS-PM SRM is not included in this part because of its trapezoid driving current. In PM-excited machines, the dual-RMSS-PM machine, stator-RMSS-PM machine, and Halbach SS-PM machine, which are Vernier machines, show a very low power factor under all current excitation. This is a common disadvantage of the Vernier machine.

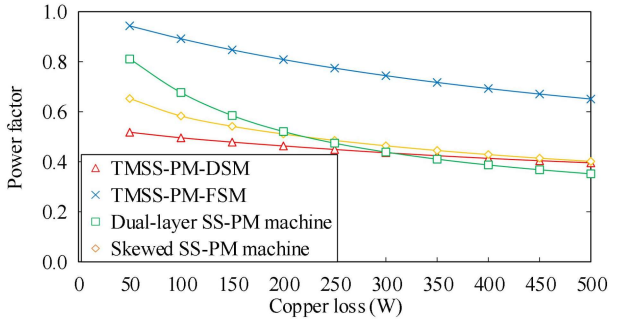

(a)

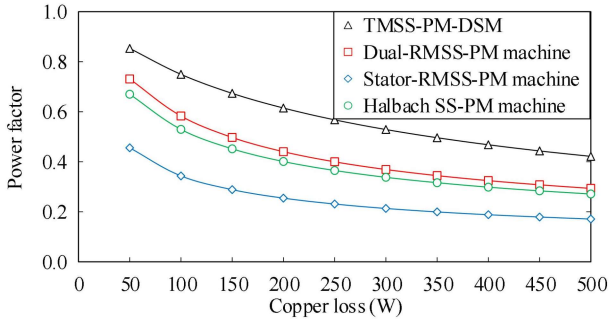

(b)

Fig. 82. Power factor under various current excitation. (a) Hybrid-excited machines. (b) PM-excited machines.

4. Structure robustness and manufacturing complexity

This part discusses the structure robustness, the manufacturing complexity and associated cost. For the reviewer's convenience, the topologies of the 9 typical structures are presented in Fig. 83 and Fig. 84 (Numbered as Fig. 44 and Fig. 45 in the manuscript).

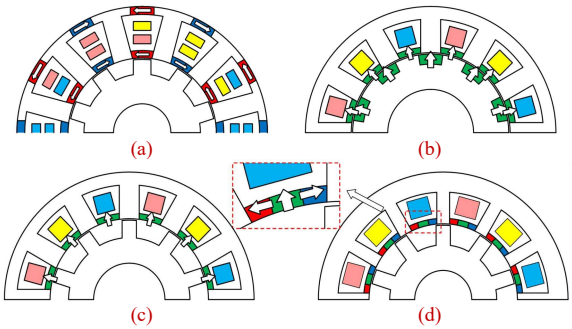

Fig. 83. The PM-excited machines. (a) TMSS-PM DSM.[76] (b) Dual-RMSS-PM machine [105]. (c) Stator-RMSS-PM machine [102]. (d) Halbach SS-PM machine [107].

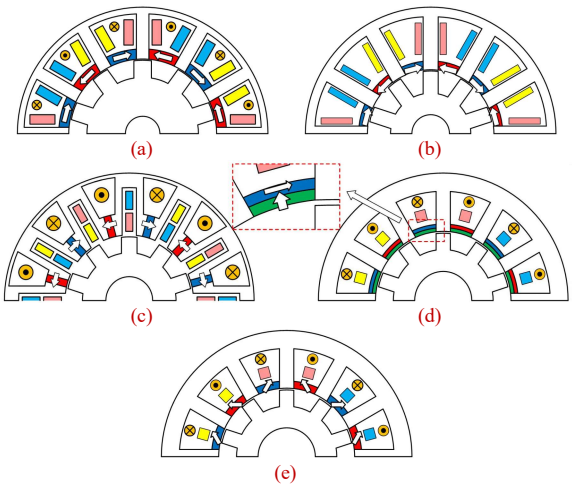

Fig. 84. The hybrid-excited machines. (a) TMSS-PM DSM [51]. (b) TMSS-PM SRM [39]. (c) TMSS-PM FSM [91]. (d) Dual-layer SS-PM machine [109]. (e) Skewed SS-PM machine [110].

a) In terms of rotor mechanical robustness, most machines enjoy simple structure and high rotor mechanical robustness because no PMs are assigned on the rotor side. Therefore, a higher rotor

speed can be applied to these machines to obtain a high output power. However, there is an exception (Dual-RMSS-PM machine) among these machines. The PMs are designed on both rotor and stator sides, and therefore, the rotor PM suffers from centrifugal force and poor heat dissipation conditions.

b) In terms of stator core mechanical robustness, the iron core of TMSS-PM DSM is separated into pieces by the yoke PMs. However, in practical manufacturing, the iron core bridges (whose thickness is usually set as 1mm) are usually designed beside the yoke PM to integrate the stator core into one piece. The purpose of integrating the stator cores is to improve the assembly precision of the stator core. However, these narrow iron core bridges lead to leakage flux. Another problem is that the strength of the iron bridge may not be reliable when stamping the iron core. Although using electrical discharge machining (EDM) is another approach to manufacturing the iron core, it may lead to a long time and associated high cost. A similar problem can also be found in TMSS-PM FSM because the iron bridges are also used. Nevertheless, as is reviewed in Part C of Section III, the iron bridges can be designed wider than those of TMSS-PM DSM. Therefore, TMSS-PM FSM has lower manufacturing difficulty than TMSS-PM DSM in terms of stator iron bridges.

As for the stator core of the other machines, they are similar to that of conventional rotor-PM open-slot synchronous machines. The main difference lies in the structure of the slot open. In conventional design, the slot wedges are usually assigned at the slot opens to hold the windings in place. The slot wedge is indispensable in practical manufacturing but has little contribution in the electromagnetic field. In the SS-PM machines, the SS PMs can be used to replace the slot wedge, which improves the space utilization factor. However, the mechanical strength of PM material is poorer than the conventional slot wedge material (such as plastic), which increase the difficulty in manufacturing.

c) In terms of PM mechanical robustness, the Halbach SS-PM machine has the highest manufacturing difficulty because the repelling forces among the PM pieces are very strong. The PM pieces are likely to fracture by the repelling force from the other PM during the manufacturing process. A similar problem can be found in dual-layer SS-PM machines as TMSS PM and RMSS PM are assigned at the same slot open. Using skewed-magnetized SS PM is a good solution to replace the dual-layer SS PM. As for the other RMSS PM machines, although there is repelling force when adhering PMs to the stator core, the repelling force is much lower than that of Halbach SS-PM machines. By contrast, there is little repelling force when adhering PMs of TMSS-PM DSM, TMSS-PM SRM, and TMSS-PM FSM to the stator core, because the SS PM is short-circuited by the stator yoke in the magnetic circuit. Therefore, TMSS-PM DSM, TMSS-PM SRM, and TMSS-PM FSM have the highest PM mechanical robustness.

5. Power-electronics drive and control complexity.

The above-mentioned machines can be classified into three types according to the driving circuit and control method. The first type is the TMSS-PM SRM, where the trapezoid current is applied in the armature winding to drive the machine. Therefore, the TMSS-PM SRM has the simplest control complexity. The second type includes the TMSS-PM DSM, Dual-RMSS-PM machine, Stator-RMSS-PM machine, and Halbach SS-PM machine. The driving circuit and control model is the same as that of conventional rotor-PM machines. The third type includes TMSS-PM DSM,

TMSS-PM FSM, Dual-layer SS-PM machine, and skewed SS-PM machine. Apart from the three-phase armature winding, there is an additional DC field winding in these machines. The purpose of the DC field winding is to flexibly regulate the flux of the machine so that a wide speed range can be applied. However, the additional DC field winding increases the complexity of the driving circuit and control methods.

6. Demagnetization risk

The demagnetization risk of the PM material mainly results from the high temperature. For the stator-PM machines, as is discussed in Part B of Section VI, it is pointed out in several publications that the stator PMs have the better cooling condition than the rotor PMs. Therefore, the SS PM has a lower demagnetization risk than the conventional rotor-PM machines in terms of thermal condition. Among the above 9 typical SS-PM machines, the dual-RMSS-PM machine may face higher PM temperature under the same cooling condition, because the PMs are designed on both stator and rotor sides.

Changes Made:

We have updated the manuscript by adding the comparison results of rated and maximum short-duration torque-speed characteristics, loss, efficiency, power factor, Structure robustness, and manufacturing complexity, power-electronics drive, control complexity, and demagnetization risk (See Part B of Section VI).

2. **Reviewer's comment:**

In my opinion, the authors should suggest some new structures based on the studied structures or present some useful hint for modification of the existing structures for future works.

Response-14:

Thanks for your suggestion. To date, the RMSS PM machines and TMSS PM machines have been well investigated in recent decades, but there are relatively fewer publications focusing on CMSS PM machines. According to the results of recent publications and our comparative study, the RMSS PMs usually have a higher torque contribution than TMSS PMs. Under flux modulation effect, the RMSS PM machines can achieve a relatively high torque density but low power factor. As for TMSS PM machines, the TMSS PMs are usually designed with the DC field current to relieve the stator core saturation. Therefore, in spite of relatively lower torque density, the flux regulation ability can be improved by TMSS PMs. The CMSS PM machines can be seen as a new idea and machine category, which can inherit the advantages from both RMSS PM and TMSS PM machines. In spite of the strong repulsive force between PMs in the same slot, which causes high manufacturing difficulty, especially in Halbach SS-PM machines and Dual-layer SS-PM machines, a good potential solution is to use skewed SS PM to replace the original design. For example, as is shown in Fig. 85, by replacing the PMs with different magnetization directions with skewed PM, the manufacturing difficulty can be largely reduced.

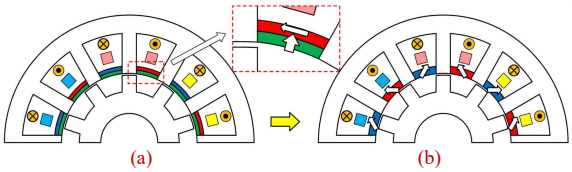

Fig. 85. The modification of CMSS PM machines. (a) Dual-layer SS-PM machine [109]. (b) Skewed SS-PM machine [110].

Apart from the above example, by combining existing TMSS PM machines and RMSS PM machines, there are various novel structures with skewed SS PM machines can be studied for future work. For example, as is shown in Fig. 86, the first machine is an existing TMSS PM machine proposed in [55], and the second machine is a typical RMSS PM machine [102]. By combining the two machines, a novel structure can be generated with two working fields.

However, as the winding pattern of the original two machines can be different, how to design an appropriate armature winding to utilize the two working fields is left for future challenges. To design an appropriate slot pole combination so that the main working harmonics of the two fields have the same corresponding winding pattern. For example, as is presented in Fig (a), the pole pair number of DC and TMSS PM is 6, and the rotor teeth number is 11, under flux modulation effect, the pole pair number of the main working harmonic is 5. As for the RMSS PM, the pole pair number of equivalent MMF is 18, under flux modulation effect, the pole pair number of the main working harmonic is 7. In this design, there are only 6 slots left for armature winding, thus it can be seen as a 6-slot machine when designing the armature winding. The 5-pole-pair and 7-pole-pair air-gap harmonic have the same winding pattern for the 6-slot machine. **Therefore, the two working fields can be utilized at the same time.**

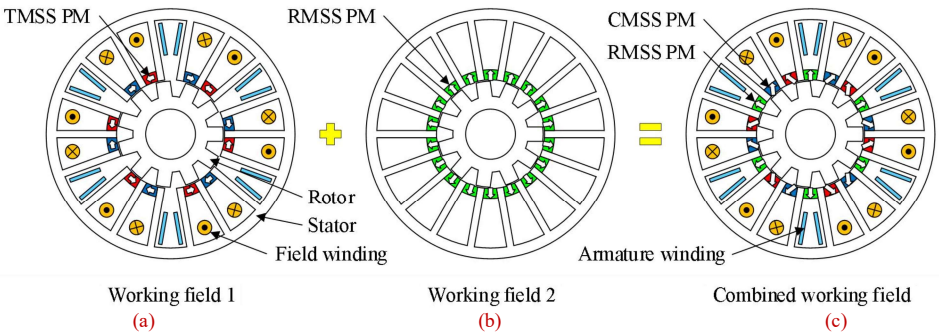

Fig. 86. Hints for new CMSS PM machines with skewed PM. (a) Existing TMSS PM machine [55]. (b) Typical RMSS PM machine [102]. (c) CMSS PM machine.

The above-mentioned CMSS PM machine is presented only as an example to show the reviewer how new CMSS PM machines with skewed PM can be generated. Therefore, the specific topology of this CMSS PM machine is not shown in the manuscript. **By combining various existing TMSS PM machines with RMSS PM machines, a large number of novel CMSS PM machines can be studied and proposed for future research**.

Changes Made:

We have updated the manuscript by rewriting Section VII and adding the relevant discussions (See Section VII).

Appendix

Table 11
Common design parameters.

Item	Unit	Value
Maximum diameter	mm	100
Stack length	mm	50
Air gap length,	mm	0.5
Estimated slot filling factor	/	0.5
Slot number	/	12
Rotor pole number	/	10
Speed	rpm	2000

TMSS-PM SRM:

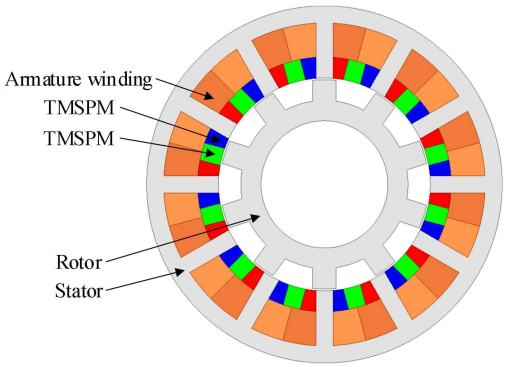

Table 12
Dimensional parameters of TMSS-PM SRM

Item	Unit	Value
Stator yoke thickness	mm	3.2
Stator tooth thickness	mm	3.5
PM central angle	deg	16.2
PM thickness	mm	3.16
Stator inner radius	mm	24
Rotor tooth thickness	mm	5.89
Rotor tooth height	mm	5.97
Rotor yoke thickness	mm	5.12

Hybrid-excited TMSS-PM DSM

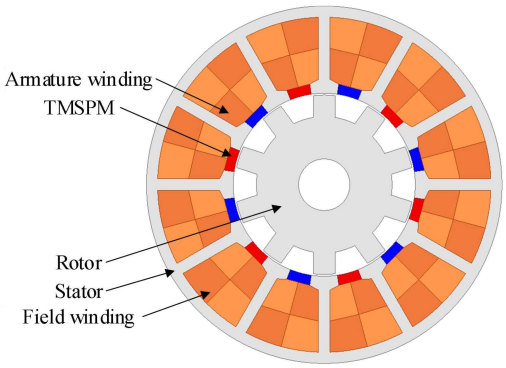

Table 13
Dimensional parameters of Hybrid-excited TMSS-PM DSM

Item	Unit	Value
Stator yoke thickness	mm	3.12
Stator tooth thickness	mm	3.26
PM central angle	deg	13.5
PM thickness	mm	2.85
Stator inner radius	mm	25.6
Rotor tooth thickness	mm	6.14
Rotor tooth height	mm	6.03
Rotor yoke thickness	mm	11.85

TMSS-PM FSM

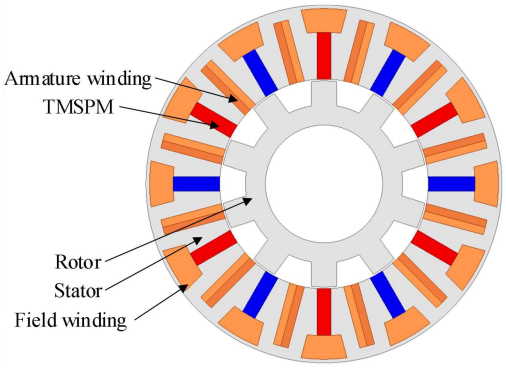

Table 14
Dimensional parameters of TMSS-PM FSM

Item	Unit	Value
Stator yoke thickness	mm	3.09
Stator iron bridge thickness	mm	1
Stator tooth thickness	mm	4.17
PM thickness	mm	4
PM height	mm	13
Stator slot width	mm	4.29
Stator inner radius	mm	29.3
Rotor tooth thickness	mm	7.22
Rotor tooth height	mm	6.74
Rotor yoke thickness	mm	5.6

Dual-layer SS-PM machine

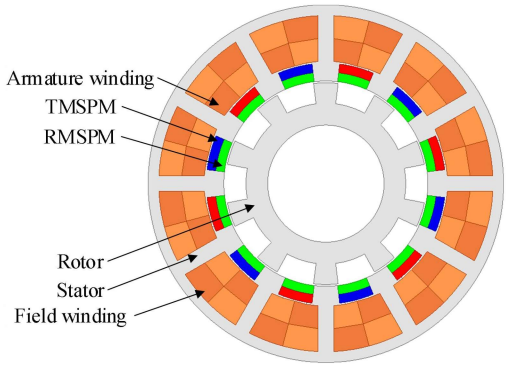

Table 15
Dimensional parameters of Dual-layer SS-PM machine

Item	Unit	Value
Stator yoke thickness	mm	3
Stator tooth thickness	mm	4.39
PM central angle	deg	16.8
RMSS-PM thickness	mm	2.47
TMSS-PM thickness	mm	2.47
Stator inner radius	mm	28.7
Rotor tooth central angle	deg	14.04
Rotor tooth height	mm	5.74
Rotor yoke thickness	mm	6.09

Skewed SS-PM machine

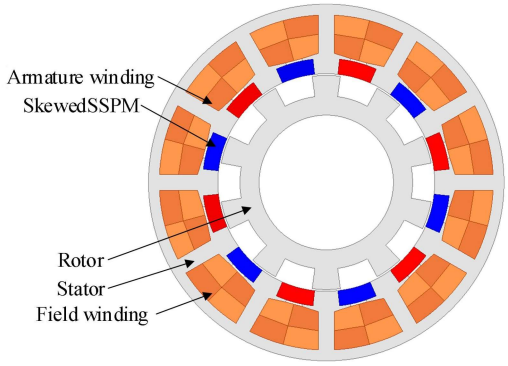

Table 16
Dimensional parameters of Skewed SS-PM machine

Item	Unit	Value
Stator yoke thickness	mm	3.04
Stator tooth thickness	mm	4.45
PM central angle	deg	17.7
RMSS-PM thickness	mm	4.26
Stator inner radius	mm	30.5
Rotor tooth central angle	deg	15.12
Rotor tooth height	mm	5.73
Rotor yoke thickness	mm	5.38

PM-excited TMSS-PM DSM.

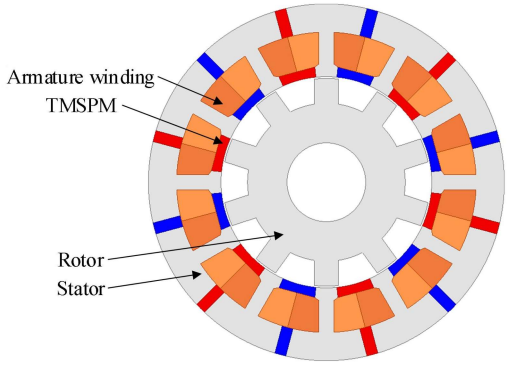

Table 17
Dimensional parameters of PM-excited TMSS-PM DSM.

Item	Unit	Value
Stator yoke thickness	mm	7.91
Stator tooth thickness	mm	4.15
SSPM central angle	deg	18.6
SSPM thickness	mm	2.88
Yoke PM width	mm	3.17
Stator inner radius	mm	29.6
Rotor tooth thickness	mm	6.75
Rotor tooth height	mm	6.96
Rotor yoke thickness	mm	11.09

Dual-RMSS-PM machine

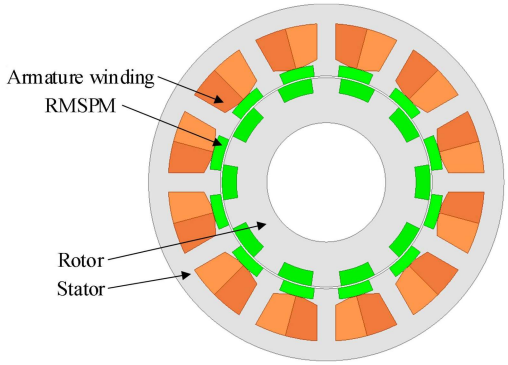

Table 18
Dimensional parameters of Dual-RMSS-PM machine

Item	Unit	Value
Stator yoke thickness	mm	5.52
Stator tooth thickness	mm	5.31
SSPM central angle	deg	17.1
SSPM thickness	mm	3.09
Stator inner radius	mm	29.8
Rotor PM central angle	deg	19.44
Rotor tooth height	mm	4.07
Rotor yoke thickness	mm	8.53

Stator-RMSS-PM machine

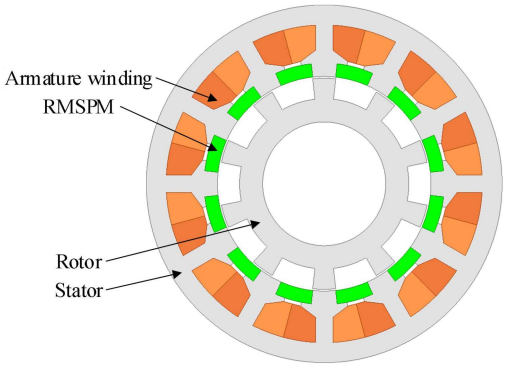

Table 19
Dimensional parameters of Stator-RMSS-PM machine

Item	Unit	Value
Stator yoke thickness	mm	5.57
Stator tooth thickness	mm	4.84
PM central angle	deg	17.7
PM thickness	mm	3.75
Stator inner radius	mm	30
Rotor central angle	deg	12.6
Rotor tooth height	mm	5.72
Rotor yoke thickness	mm	6.48

Halbach SS-PM machine

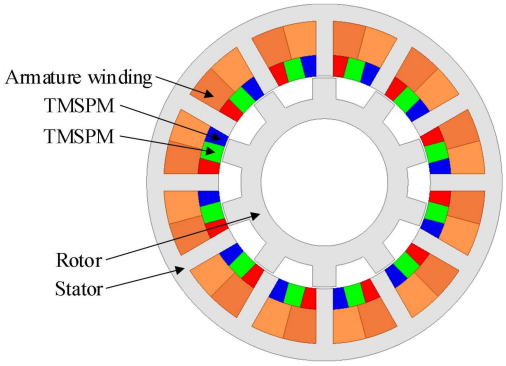

Table 20
Dimensional parameters of Halbach SS-PM machine

Item	Unit	Value
Stator yoke thickness	mm	4.79
Stator tooth thickness	mm	4.82
RMSS PM central angle	deg	9.57
TMSS PM central angle	deg	5.58
PM thickness	mm	5.84
Stator inner radius	mm	29.8
Rotor tooth thickness	mm	6.61
Rotor tooth height	mm	5.79
Rotor yoke thickness	mm	5.69